Journal of Medicinal Chemistry

ACS AuthorChoice

Article

pubs.acs.org/jmc

Terms of Use

Design, Synthesis, and Evaluation of Nonretinoid Retinol Binding Protein 4 Antagonists for the Potential Treatment of Atrophic Age-Related Macular Degeneration and Stargardt Disease

Christopher L. Cioffi,*[,†] Nicoleta Dobri,[‡] Emily E. Freeman,[†] Michael P. Conlon,[†] Ping Chen,[†] Douglas G. Stafford,[†] Daniel M. C. Schwarz,[†] Kathy C. Golden,[†] Lei Zhu,[†] Douglas B. Kitchen,[†] Keith D. Barnes,[†] Boglarka Racz,[‡] Qiong Qin,[‡,○] Enrique Michelotti,[#] Charles L. Cywin,[∞] William H. Martin,[⊥] Paul G. Pearson,[∥] Graham Johnson,[§] and Konstantin Petrukhin*[,‡]

[†]Department of Medicinal Chemistry, Albany Molecular Research, Inc., East Campus, C-Wing, Rensselaer, New York 12144, United States

[‡]Department of Ophthalmology, Columbia University Medical Center, New York, New York 10032, United States

[§]NuPharmAdvise LLC, 3 Lakeside Drive, Sanbornton, New Hampshire 03269, United States

[∥]Pearson Pharma Partners, 31194 La Baya Drive, Westlake Village, California 91361, United States

[⊥]WHM Consulting LLC, 111 Sterling City Road, Lyme, Connecticut 06371, United States

[#]National Institute of Mental Health, National Institutes of Health, Bethesda, Maryland 20892, United States

[∞]National Institute of Neurological Disorders and Stroke, National Institutes of Health, Bethesda, Maryland 20892, United States

S *Supporting Information*

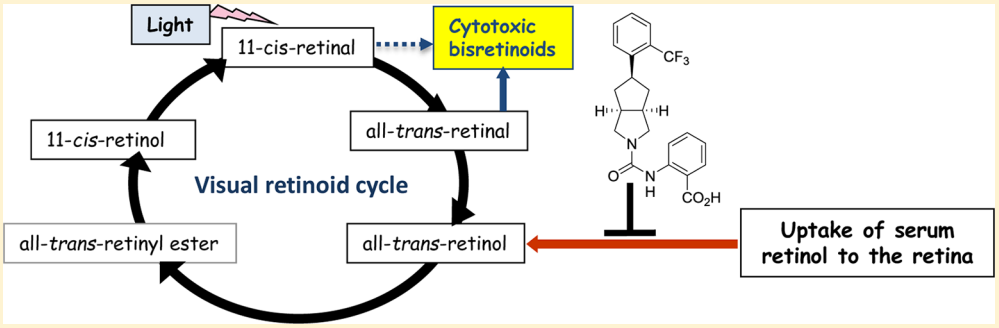

ABSTRACT: Accumulation of lipofuscin in the retina is associated with pathogenesis of atrophic age-related macular degeneration and Stargardt disease. Lipofuscin bisretinoids (exemplified by *N*-retinylidene-*N*-retinylethanolamine) seem to mediate lipofuscin toxicity. Synthesis of lipofuscin bisretinoids depends on the influx of retinol from serum to the retina. Compounds antagonizing the retinol-dependent interaction of retinol-binding protein 4 (RBP4) with transthyretin in the serum would reduce serum RBP4 and retinol and inhibit bisretinoid formation. We recently showed that A1120 (**3**), a potent carboxylic acid based RBP4 antagonist, can significantly reduce lipofuscin bisretinoid formation in the retinas of *Abca4*$^{-/-}$ mice. As part of the NIH Blueprint Neurotherapeutics Network project we undertook the in vitro exploration to identify novel conformationally flexible and constrained RBP4 antagonists with improved potency and metabolic stability. We also demonstrate that upon acute and chronic dosing in rats, **43**, a potent cyclopentyl fused pyrrolidine antagonist, reduced circulating plasma RBP4 protein levels by approximately 60%.

INTRODUCTION

Age-related macular degeneration (AMD) is the leading cause of blindness for individuals aged 60 years or older.[1] An estimated 11 million people in the United States suffer with AMD, and this number is expected to increase to 22 million individuals by 2050 because of the projected demographic expansion of the aging population. Current global direct health care costs associated with AMD are estimated at $255 billion.[2] There are two forms of AMD, dry (atrophic) and wet (neovascular), with the more prevalent dry form accounting for nearly 90% of all diagnosed cases.[3] Intravitreal anti-VEGF therapies have emerged as a standard of care to treat wet AMD; however, there is currently no FDA-approved treatment available for the dry form.[3] Thus, safe and effective treatment of dry AMD remains a critical unmet need.

Atrophic (dry) form of AMD represents a slowly progressing neurodegenerative disorder of the eye in which specialized retinal

Received: July 9, 2014
Published: September 1, 2014

   dx.doi.org/10.1021/jm5010013 | *J. Med. Chem.* 2014, 57, 7731−7757

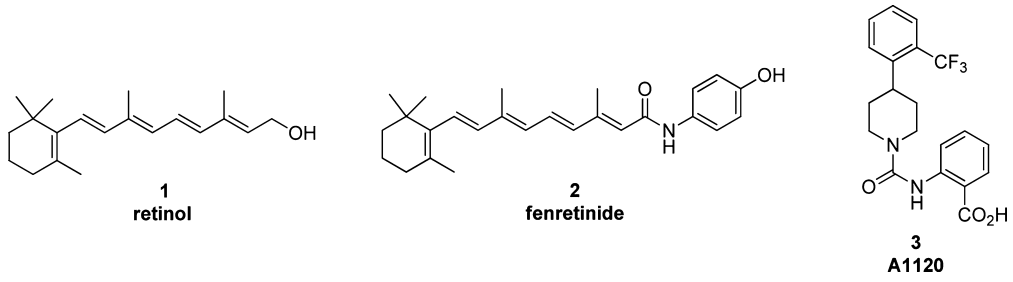

Figure 1. Retinol (**1**), fenretinide (**2**), and A1120 (**3**).

neurons (rod and cone photoreceptors) degenerate in the central part of the retina called macula.[3] Histopathological and clinical data suggest that photoreceptor degeneration in dry AMD is triggered by abnormalities in the retinal pigment epithelium (RPE) that lies beneath photoreceptors and provides critical metabolic support to these light-sensing neuronal cells.[4] Age-dependent accumulation of lipofuscin in the RPE is frequently cited as one of the causes that may potentially contribute to the demise of the RPE in the dry AMD retina.[4b,c,5] Moreover, excessive accumulation of lipofuscin in the retina seems to be the sole causative factor in autosomal recessive Stargardt disease, an untreatable form of inherited macular dystrophy caused by genetic mutations in the *ABCA4* gene. RPE lipofuscin is different from that of other aging tissues, as it contains various bisretinoid fluorophores[5c,6] such as pyridinium bisretinoid *N*-retinide-*N*-retinylidene ethanolamine (A2E).[5c] A2E, which is derived from a nonenzymatic condensation between phosphatidylethanolamine and two molecules of *all-trans* retinal, elicits a myriad of cytotoxic effects such as induction of apoptosis in cultured RPE cells,[5b,7] inhibition of the critical lysosomal transporter,[8] loss of membrane integrity,[9] inhibition of phagocytosis,[5a,10] disruption of mitochondrial function,[10] activation of the complement cascade,[11] and oxidative damage.[12] Given that lipofuscin bisretinoids represent the major cytotoxic component of RPE lipofuscin, it was hypothesized that pharmacological inhibition of bisretinoid formation in the retina may provide a means by which to delay the progression of geographic atrophy in dry AMD and suppress degenerative processes in Stargardt disease.[13] Indeed, there are several classes of pharmacological treatments inhibiting lipofuscin bisretinoid formation in the retina under investigation for the potential treatment of dry AMD and Stargardt's disease.[3,14] Our work focuses on reducing ocular uptake of serum *all-trans* retinol (retinol, vitamin A) (**1**, Figure 1) via inhibition of retinol binding protein 4 (RBP4) as a means by which to reduce the concentration of bisretinoid precursors in the retina and inhibit bisretinoid formation. Retinol is an essential nutrient that plays a critical role in a wide variety of biological functions, including fueling the visual cycle.[15] It is transported to vitamin A dependent tissues as a tertiary complex with RBP4 and transthyretin (TTR).[16] RBP4 is a lipocalin serum protein[17] primarily secreted from the liver[18] and to a lesser extent from kidney and adipose tissue.[19] Because of the relatively low molecular weight of RBP4 (21 kDa), the RBP4-TTR interaction is critical for maintaining serum retinol in circulation as, without complexation with TTR, RBP4-retinol is rapidly cleared from the bloodstream through glomerular filtration.[15] RBP4-TTR complexation is retinol dependent, as *apo*-RBP4 interacts poorly with TTR.[16]

The visual cycle depends on a constant delivery of retinol to the RPE by RBP4. It was suggested that RBP4 ligands antagonizing the retinol-dependent RBP4-TTR interaction in circulation would lead to a dramatic reduction in serum levels of RBP4 via renal elimination of the monomeric protein. As a consequence of this renal RBP4 elimination, serum retinol levels and delivery to the RPE would also be reduced, as would the rate of bisretinoid formation in the retina.[13a] This hypothesis has been preclinically and clinically confirmed with fenretinide (**2**), a synthetic retinoid-based RBP4 antagonist. Fenretinide is known to prevent the binding of *all-trans* retinol to RBP4 and disrupt the retinol-dependent RBP4-TTR interaction in vitro,[20] as well as lower circulating plasma RBP4 levels in vivo.[13a,21] In addition, fenretinide also significantly reduced accumulation of lipofuscin bisretinoids in the $Abca4^{-/-}$ mouse model of enhanced retinal lipofuscinogenesis.[13a] Supporting the therapeutic role of RBP4 in dry AMD, in extended clinical studies, fenretinide was recently confirmed to reduce serum RBP4 in AMD patients.[22] Post hoc analysis of the fenretinide clinical trial data suggests efficacy in reducing the rate of the geographic atrophy growth that was achieved in a subgroup of patients wherein an approximately 70% (or greater) reduction in serum RBP4 levels was realized.[22]

Prior to their application to the treatment of dry AMD and Stargardt disease, RBP4 antagonists were previously being considered for the treatment of diabetes.[19b,c,23] A1120 (**3**), a lead molecule for this indication, was previously reported by a group at Amgen as was its protein-bound crystal structure.[24] This relatively low molecular weight compound features several key structural elements; an *o*-trifluoromethyl arylpiperidine linked via a carbonyl to an unsubstituted anthranilic acid residue. In a study reported elsewhere,[25] we have shown that chronic A1120 administration reduced accumulation of lipofuscin bisretinoids by approximately 50% in the $Abca4^{-/-}$ mouse model. This activity correlated with a 75% reduction in serum RBP4 and 30–50% reduction in certain visual cycle retinoids.[25] However, despite these encouraging preclinical data, A1120 suffers from poor human liver microsomal (HLM) stability (~3% remaining after 30 min incubation), thus posing a significant challenge for further development. Therefore, our aim was to design a novel and potent nonretinoid RBP4 antagonist capable of lowering serum RBP4 levels in vivo with comparable or superior efficacy and improved druglike characteristics that include an improved HLM metabolic profile.

The specific protein movements and molecular interactions that mediate agonist driven RBP4-TTR interaction versus holoenzyme and/or antagonist-bound RBP4-TTR disassociation are of great interest in the design of highly potent and selective RBP4 antagonists. It is for this reason that in our program we measured compound binding affinity to the non-TTR associated RBP4 protein (SPA) as well as determined the RBP4-TTR antagonist potency (HTRF). From evaluation of the reported A1120-bound protein crystal structure, we speculated that variation in both the linkage and relative orientation of the *o*-trifluoromethylphenyl and arylcarboxylic acid fragments might

dx.doi.org/10.1021/jm5010013 | J. Med. Chem. 2014, 57, 7731–7757

further enhance RBP4 antagonist potency as well as permit tuning of the desirable ADME characteristics so as to potentially improve HLM stability (Figure 2). Using computer-assisted drug

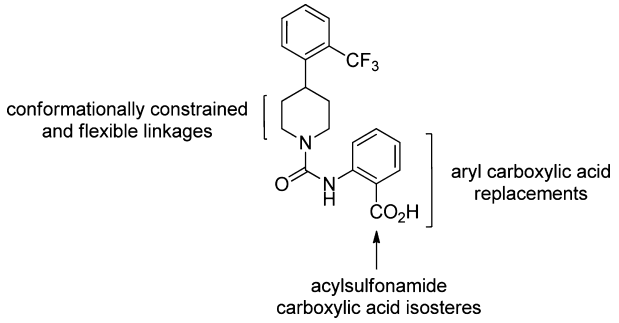

Figure 2. Medicinal chemistry work plan for the identification of novel, nonretinoid RBP4 antagonists.

design based around several RBP4 protein crystal structures, we designed, computationally evaluated, and synthesized illustrative examples of conformationally constrained carboxylic acid based non-retinoid antagonists. In addition, within the context of the original A1120 structural scaffold, we further explored the RBP4 antagonist activity of several acylsulfonamide carboxylic acid isosteres and arylcarboxylic acid replacements. Lastly, acknowledging earlier patent disclosures of conformationally flexible RBP4 antagonists,[26] we also included in our test set several aliphatic analogues bearing an ether-linked ortho-substituted aryl headgroup and terminal urea-linked carboxylic acid.

CHEMISTRY

By employment of the route reported by Swanson and coworkers (Scheme 1),[27] the synthesis of A1120 (**3**) and piperidine core intermediate **7** began with lithium−halogen exchange of 1-bromo-2-(trifluoromethyl)benzene (**4**) followed by 1,2-carbonyl addition of the lithium salt to 1-benzylpiperidin-4-one to give tertiary alcohol **5**. Thionyl chloride induced dehydration of **5** to the intermediary tetrahydropyridine **6** followed by reduction of the olefin with concomitant *N*-benzyl deprotection using ammonium formate and 10% Pd/C to afford **7** upon conversion to the hydrochloride salt. Treatment of **7** with methyl 2-isocyanatobenzoate followed by saponification of the methyl ester provided A1120 (**3**) in good yield. Our initial strategy to generate acylsulfonamide acid isosteres of **3** involved HATU-mediated activation of the carboxylic acid to be followed by acylation with various desired sulfonamides. However, we discovered that treatment of **3** with HATU in the absence of nucleophile yielded acyl β-lactam **8**, which was isolated via column chromatography. Acyl β-lactam **8** ultimately provided a convenient intermediate for the assembly of our desired acylsulfonamides **9**−**11**, as it readily underwent ring-opening to the desired analogues upon treatment with preformed sulfonamide sodium salts.

Highlighted in Scheme 2 are the synthetic routes used to access analogues bearing aliphatic carboxylic acid residues. Piperidine hydrochloride **7** provided a key intermediate for the synthesis of several analogues designed to replace the acylanthranilic acid of **3** with diverse moieties potentially capable of engaging in similar RBP4 binding interactions. Oxoacids **12**−**14** were readily manufactured via acylation of **7** with the corresponding carboxylic acid ester, acid chloride, or anhydride followed by saponification of the pendent ester (if required) to give the desired compound. A racemic mixture of proline-based analogue (±)-**15** was generated by reaction of methyl 1-(chlorocarbonyl)pyrrolidine-2-carboxylate with **7** followed by hydrolysis of the ester to the desired acid.

The synthesis of acyclic phenoxyethylamido ether analogues **20**, **21**, **25**, and **27** is depicted in Scheme 3. S_N2 displacement of bromide **17** with an appropriately substituted phenol followed by TBS deprotection gave hydroxyl aryl ethers **18**. Dess−Martin oxidation to the aldehyde and subsequent reductive amination

Scheme 1[a]

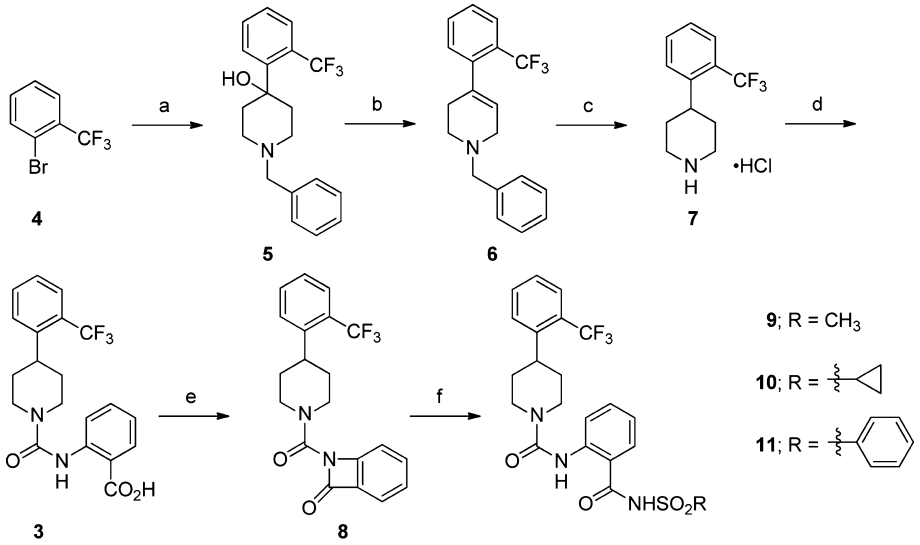

[a]Reagents and conditions: (a) (i) *n*-BuLi, THF, −78 °C, 40 min; (ii) 1-benzylpiperidin-4-one, THF, −78 °C, 74%; (b) $SOCl_2$, 0−20 °C, 2 h, 49%; (c) (i) HCO_2NH_4, 10% Pd/C, CH_3OH, reflux, 21%; (ii) 4.0 M HCl solution in 1,4-dioxane, CH_3CN, 20 °C, 10 min, quantitative; (d) (i) methyl 2-isocyanatobenzoate, CH_2Cl_2, 20 °C, 64 h; (ii) 2 N NaOH, H_2O, THF, CH_3OH, 20 °C, 4 h, 95% over two steps; (e) HATU, DMF, *i*-Pr_2NEt, 20 °C, 2 h, 83%; (f) (i) alkyl- or arylsulfonamide, NaH, DMF, 0−20 °C, 10−15 min; (ii) then addition of **8** as a solution in DMF or THF, 20 °C, 2 h, 18−60%.

dx.doi.org/10.1021/jm5010013 | J. Med. Chem. 2014, 57, 7731−7757

Scheme 2[a]

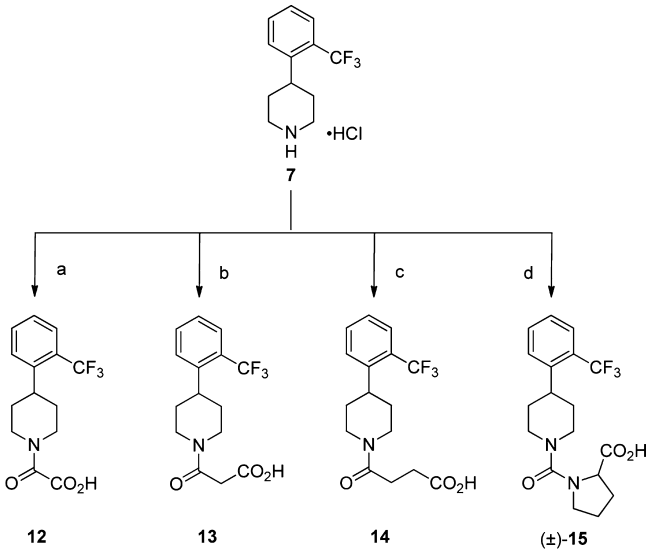

[a]Reagents and conditions: (a) (i) ethyl 2-chloro-2-oxoacetate, Et_3N, CH_2Cl_2, 20 °C 16 h, 94%; (ii) 2 N NaOH, THF, H_2O, CH_3OH, 20 °C, 16 h, 20%; (b) methyl 3-chloro-3-oxopropanoate, Et_3N, CH_2Cl_2, 20 °C 16 h, 71%; (ii) 2 N NaOH, THF, H_2O, CH_3OH, 20 °C, 16 h, 78%; (c) dihydrofuran-2,5-dione, reflux, 4 h, 93%; (d) methyl 1-(chlorocarbonyl)pyrrolidine-2-carboxylate, Et_3N, CH_2Cl_2, 20 °C 6 h, 84%; (ii) 2 N NaOH, THF, H_2O, CH_3OH, 20 °C, 4 h, 91%.

with methylamine afforded phenoxyethylamines **19**. Treatment of intermediate **19** with methyl 2-isocyanatobenzoate followed by saponification of the methyl ester gave the desired carboxylic acid analogues **20** and **21**. The syntheses of analogues **25** and **27** began with Boc protection of 2-chloroethanamine **22** to give carbamate **23**, which was converted to aryl ether **24** via S_N2 displacement with 2-(*tert*-butyl)phenol. Intermediate **24** was converted to analogue **25** via treatment with methyl 2-isocyanatobenzoate followed by hydrolysis of the methyl ester to the desired carboxylic acid. Intermediary carbamate **23** was also used in a similar fashion to generate the 4-fluorophenyl substituted analogue **27**.

The synthesis of various conformationally constrained analogues is depicted in Scheme 4. Similar to the synthesis of A1120, the manufacture of these compounds involved treatment of a core secondary amine with methyl 2-isocyanatobenzoate followed by saponification of the resulting ester to give the desired acids. The synthesis of 3.1.0 bicyclic systems **29** and **30** followed a procedure reported by McHardy and co-workers.[28] 2,6-Diazaspiro[3.3]heptane **31** was synthesized following chemistry reported by Carreira.[29] Lastly, the aryloxy azetidine core used in the synthesis of analogue **33** followed a synthetic route outlined by Pettersson and co-workers.[30] The synthesis of azepine **28**, azetidine **32**, and a racemic mixture of spiroindane (±)-**34** began with the commercially available secondary amine cores.

Construction of the bicyclic {3.3.0}-octahydrocyclopenta[*c*]-pyrrolo analogues **43**, (±)-**45**, and **48** was achieved following routes previously reported by Dart,[31] Lauffer,[32] and Guillemont[33] (Scheme 5). The synthesis began with a $LiAlH_4$ reduction of commercially available dione **35** followed by *N*-Boc protection of the resulting secondary amine to give isoindole **36** in good yield. $NaIO_4$ and $RuO_2{\cdot}H_2O$ facilitated oxidative cleavage of **36** gave ring-opened diacid **37** in good yield. Subsequent Dieckman condensation with concomitant decarboxylation of **37** in acetic anhydride at 120 °C yielded ketone **38** in 55% yield. Deprotonation of **38** with LiHMDS followed by treatment with 1,1,1-trifluoro-*N*-phenyl-*N*-((trifluoromethyl)-sulfonyl)methanesulfonamide provided desired triflate **39**, which underwent smooth conversion to alkene (±)-**40** in the presence of (2-(trifluoromethyl)phenyl)boronic acid under standard Suzuki Pd-catalyzed cross-coupling conditions. Reduction of alkene (±)-**40** via 50 psi of H_2 in the presence of 10% Pd/C in CH_3OH provided exclusively *endo*-product **41**. Boc

Scheme 3[a]

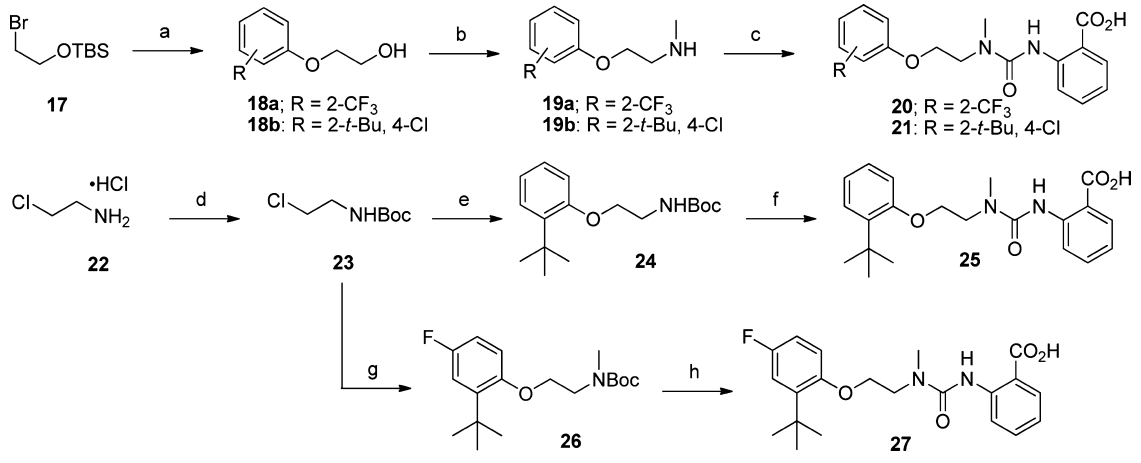

[a]Reagents and conditions: (a) (i) 2-(trifluoromethyl)phenol or 2-(*tert*-butyl)-4-chlorophenol, KI, Cs_2CO_3, DMF, 50 °C, 18 h, 88%; (ii) 4.0 M HCl solution in 1,4-dioxane, 20 °C 3 h; (b) (i) Dess–Martin periodinane, CH_2Cl_2, 20 °C, 18 h, (ii) 2 N solution of methylamine in CH_3OH, 20 °C, 18 h, 2% over three steps; (c) methyl 2-isocyanatobenzoate, CH_2Cl_2, 20 °C, 18 h, 79%; (iii) $LiOH{\cdot}H_2O$, THF, H_2O, CH_3OH, 20 °C, 18 h, 46–57%; (d) Boc_2O, $NaHCO_3$, H_2O, THF, 0–20 °C, 24 h quantitative; (e) 2-(*tert*-butyl)phenol, KI, Cs_2CO_3, DMF, 60 °C, 16 h, 82%; (f) (i) $LiAlH_4$ (1.0 M solution in THF), THF, 60 °C, 16 h, 43%; (ii) methyl 2-isocyanatobenzoate, CH_2Cl_2, 20 °C, 18 h, 46%; (iii) $LiOH{\cdot}H_2O$, THF, H_2O, CH_3OH, 20 °C, 18 h, 79%; (g) (i) CH_3I, LiHMDS (1.0 M solution in THF), THF, 20 °C, 20 min; (ii) 2-(*tert*-butyl)-4-fluorophenol, KI, DMF, 60 °C, 100 h, 25% over two steps; (h) (i) 2 N HCl solution in Et_2O, CH_2Cl_2, 20 °C, 3 h, 93%; (ii) methyl 2-isocyanatobenzoate, CH_2Cl_2, 20 °C, 3 h, 88%; (iii) $LiOH{\cdot}H_2O$, THF, H_2O, CH_3OH, 20 °C, 18 h, 93% over two steps.

dx.doi.org/10.1021/jm5010013 | J. Med. Chem. 2014, 57, 7731–7757

Scheme 4[a]

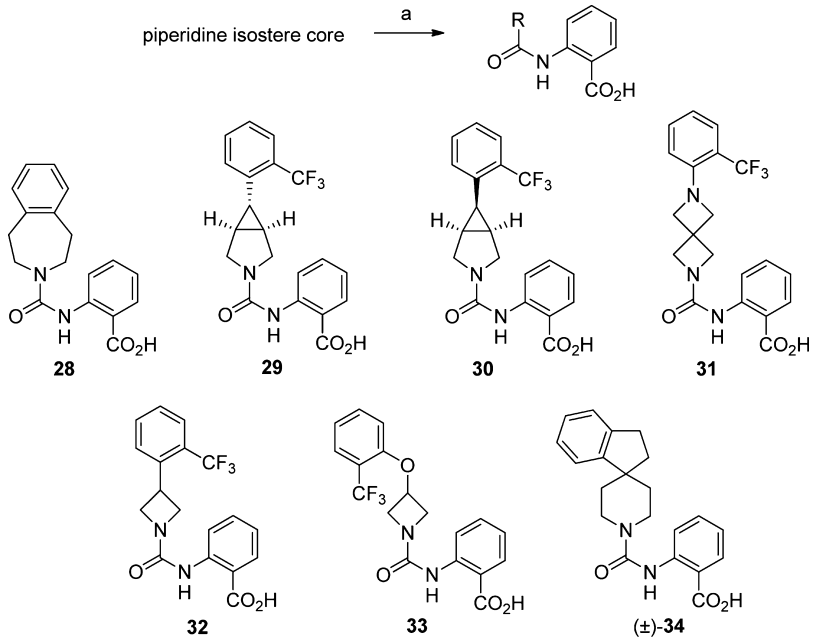

[a]Reagents and conditions: (a) (i) methyl 2-isocyanatobenzoate, CH_2Cl_2, 20 °C, 16 h, 34−94%; (ii) $LiOH·H_2O$, THF, CH_3OH, H_2O, 20 °C, 2−4 h, 34−98%.

Scheme 5[a]

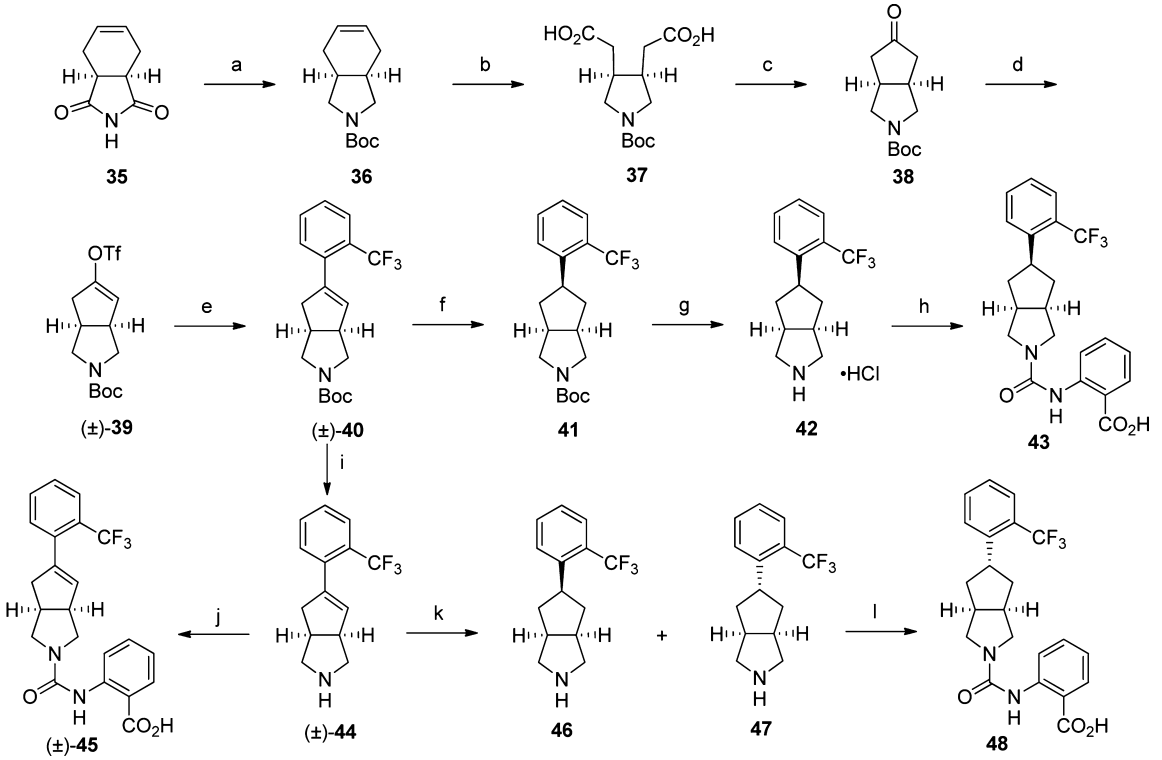

[a]Reagents and conditions: (a) (i) $LiAlH_4$ (1.0 M solution in THF), THF, reflux, 16 h; (ii) Boc_2O, CH_2Cl_2, 20 °C, 2 h, 49% over two steps; (b) (i) $NaIO_4$, $RuO_2·H_2O$, CH_3CN, CCl_4, H_2O, 20 °C, 24 h, 72%; (c) Ac_2O, NaOAc, 120 °C, 3 h, 40%; (d) (i) LiHMDS (1.0 M solution in THF), THF, −78 °C, 30 min; (ii), $PhN(SO_2CF_3)_2$, THF, −78 to 20 °C, 3 h, 44%; (e) (2-(trifluoromethyl)phenyl)boronic acid, $Pd(PPh_3)_4$, 2 M Na_2CO_3, DME, 80 °C, 6 h, 94%; (f) H_2 (40 psi), 10% Pd/C, CH_3OH, 20 °C, 16 h, 85%; (g) 2 M HCl in Et_2O, CH_2Cl_2, 0−20 °C, 24 h, 91%; (h) (i) methyl 2-isocyanatobenzoate, CH_2Cl_2, 20 °C, 16 h; (ii) 2 N NaOH, THF, H_2O, CH_3OH, 16 h, 98% over two steps; (i) (i) TFA, CH_2Cl_2, 0−20 °C, 3 h, quantitative; (j) (i) methyl 2-isocyanatobenzoate, CH_2Cl_2, 20 °C, 16 h; (ii) $LiOH·H_2O$, THF, H_2O, 20 °C, 4 h, 79% over two steps; (k)H_2 (50 psi), 10% Pd/C, CH_3OH, 20 °C, 6 h, 14%; (l) (i) methyl 2-isocyanatobenzoate, CH_2Cl_2, 20 °C, 16 h; (ii) $LiOH·H_2O$, THF, H_2O, 20 °C, 4 h, 98% over two steps.

dx.doi.org/10.1021/jm5010013 | J. Med. Chem. 2014, 57, 7731−7757

Scheme 6[a]

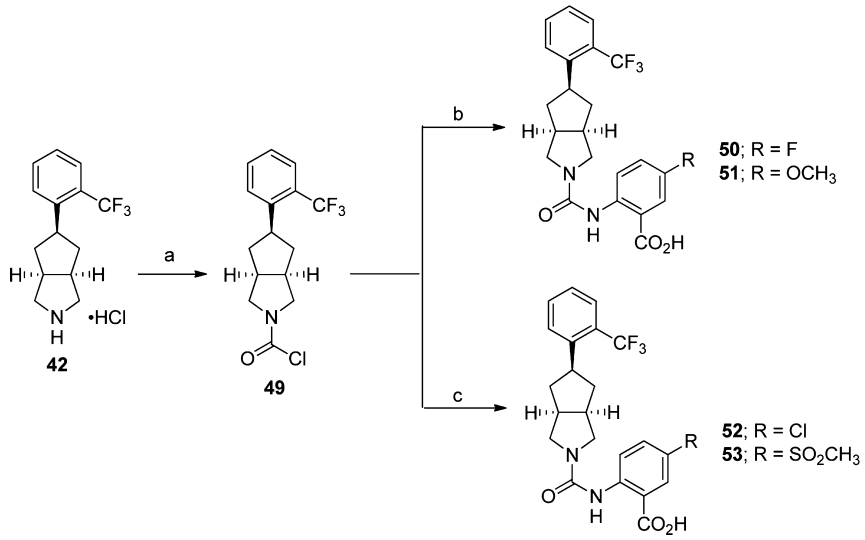

[a]Reagents and conditions: (a) triphosgene, pyridine, CH_2Cl_2, 0−20 °C, 2 h, 53%; (b) (i) **49**, methyl 2-amino-5-substituted benzoate, *i*-Pr_2NEt, THF, reflux, 5−18 h; (ii) LiOH·H_2O, THF, CH_3OH, H_2O, 20 °C, 2−18 h, 12−86%; (c) (i) methyl 2-amino-5-substituted benzoate, NaH, DMF, −10 to 0 °C, 30 min to 1 h, then addition of **49**, 0−20 °C, 5 h, 23−71%.

Scheme 7[a]

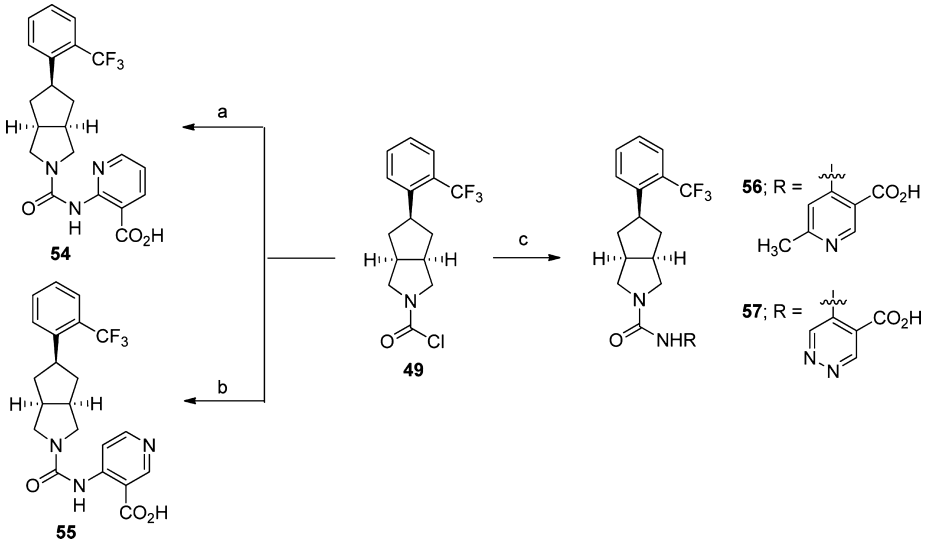

[a]Reagents and conditions: (a) (i) **49**, 7 N NH_3 solution in CH_3OH, 20 °C, 1 h; (ii) 2-chloronicotinate, $Pd(OAc)_2$, BINAP, Cs_2CO_3, toluene, reflux, 2 h, 55% over two steps; (b) (i) **49**, methyl 4-aminonicotinate, *i*-Pr_2NEt, THF, reflux, 4 h, 60%; (ii) LiOH·H_2O, THF, H_2O, CH_3OH, 20 °C, 3 h, quantitative; (c) (i) methyl 4-amino-6-methylnicotinate or methyl 5-aminopyridazine-4-carboxylate, NaH, DMF, 0 °C, 1 h, then addition of **49**, 0−20 °C; (ii) LiOH·H_2O, THF, H_2O, 20 °C, 16 h, 52−86% over two steps.

deprotection of **41** followed by reaction with methyl 2-isocyanatobenzoate and subsequent saponification of the methyl ester afforded desired carboxylic acid analogue **43**. The core geometry of *endo*-isomer **43** was confirmed via a ^{1}H NMR NOESY experiment, which exhibited a positive NOE enhancement between the benzylic and bridging methine hydrogens. Generation of *exo*-product **48** could only be achieved via reduction of des-Boc olefin (±)-**44**, which provided a mixture of *endo*- and *exo*-isomers **46** (free-base of **42**) and **47**, with *endo*-**46** being the major isomer by HPLC (~10:1 *endo*/*exo*). Secondary amines **46** and **47** were separable via reversed phase column chromatography. This result was consistent with the observation reported by Dart and co-workers[31] and could be attributed to reduction readily occurring at the more accessible convex face of the olefin (±)-**44**. The greater degree of selectivity observed for the reduction of *N*-Boc protected intermediate (±)-**40** to yield exclusively *endo*-isomer **41** could be due to further hindrance of hydrogen delivery to the convex face of the olefin by the bulky Boc group. The core geometry of *exo*-isomer **48** was also confirmed via a ^{1}H NMR NOESY experiment, which did not exhibit an NOE enhancement between the benzylic and bridging methine hydrogens.

Related analogues of **43** were accessed via carbamoyl chloride intermediate **49**, which was generated via treatment of amine hydrochloride salt **42** with triphosgene in the presence of pyridine (Scheme 6). Intermediate **49** was reacted with various

dx.doi.org/10.1021/jm5010013 | J. Med. Chem. 2014, 57, 7731−7757

Scheme 8[a]

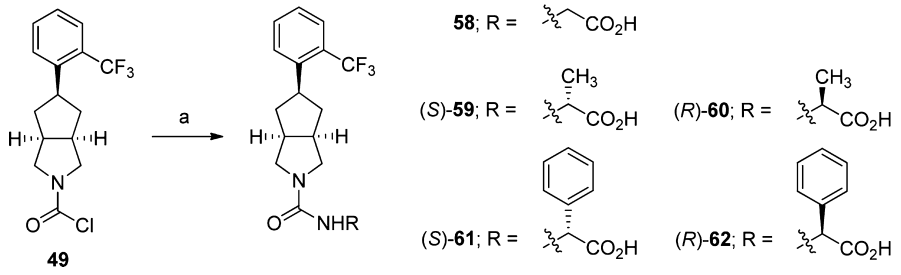

[a]Reagents and conditions: (a) (i) **49**, amino acid methyl ester hydrochloride salts, Et_3N, CH_2Cl_2, 0−20 °C, 16 h; (ii) $LiOH{\cdot}H_2O$, THF, H_2O, 20 °C, 30 min, 43−98% over two steps.

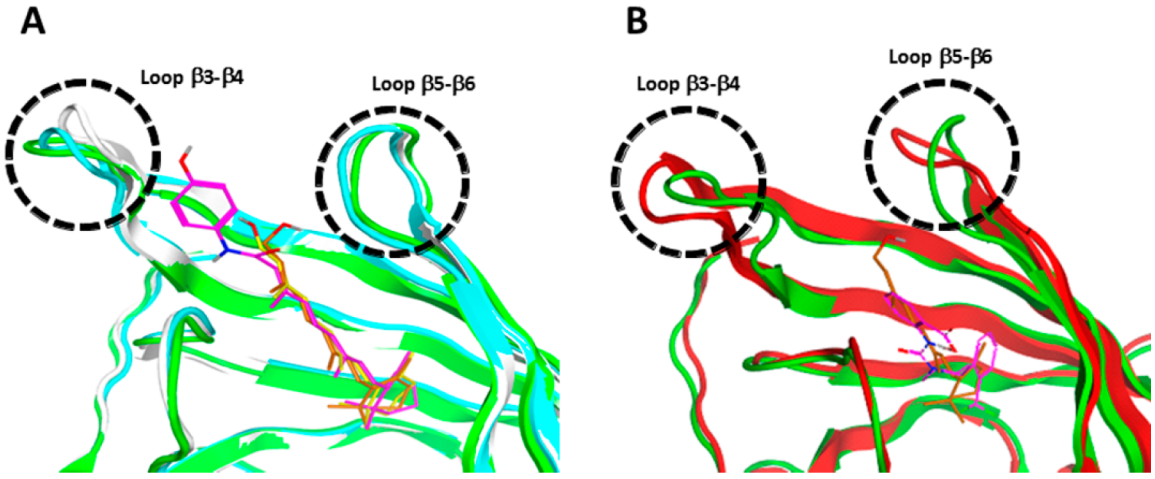

Figure 3. Relative RBP4 loop $\beta3-\beta4$ and $\beta5-\beta6$ conformational changes for agonist and antagonist binding. (A) Comparison of the loop $\beta3-\beta4$ and $\beta5-\beta6$ conformations for retinol and fenretinide binding to RBP4: overlay of protein crystal structures 1rbp (white), 3bsz (green), and 1fel (cyan). Fenretinide is shown as magenta, and retinol is shown as yellow (from 1rbp) and orange (from 3bsz). (B) Comparison of the loop $\beta3-\beta4$ and $\beta5-\beta6$ conformations for retinol and A1120 binding to RBP4: overlay of protein crystal structures 3bsz (green) and 3fmz (red). Retinol is shown as orange, and A1120 is shown as magenta.

methyl 2-amino-5-substituted benzoates, which were subsequently hydrolyzed to the desired carboxylic acid analogues **50**−**53**.

Carbamoyl chloride **49** could also be treated with heteroanthranilic esters to provide the pyridyl and pyridazinyl bicyclic {3.3.0}-octahydrocyclopenta[*c*]pyrrolo analogues **54**−**57** depicted in Scheme 7. Pyridine analogue **54** required an alternative route, which involved a Pd-catalyzed amidation of the primary urea of **49** with 2-chloronicotinate.

The amino acid derived analogues shown in Scheme 8 were also furnished from key carbamoyl chloride intermediate **49** via treatment with the specified amino acid methyl esters followed by hydrolysis to give the desired carboxylic acids.

RESULTS AND DISCUSSION

Computational Docking of Proposed Ligands Using 3fmz X-ray Crystallographic Data. Drawing from the breadth of reported RBP4 X-ray crystallographic data available, we sought to gain better insight into key RBP4 binding interactions and conformational changes for both agonist and antagonist binding states, which would serve to evaluate our nonretinoid antagonist design proposals. With this goal in mind, we analyzed binding differences observed in the reported Protein Data Bank (PDB) high-resolution X-ray crystal structures 1rbp (RBP4 cocrystallized with retinol),[34] 3bsz (the RBP4-TTR complex cocrystallized with retinol),[35] 1fel (RBP4 cocrystallized with fenretinide),[16g] and 3fmz (RBP4 cocrystallized with A1120).[24]

Retinol binds within an internal cavity of RBP4 whereby the polyene chain is encapsulated within a β-barrel core, the β-ionone ring projects into a deep interior hydrophobic pocket, and the terminal hydroxyl group protrudes out of the entrance of the binding cavity toward solvent (Figure 3A).[34] The RBP4 loops $\beta3-\beta4$ (residues 63−68) and $\beta5-\beta6$ (residues 92−99) surround the opening of the binding cavity and present an interaction surface for TTR engagement.[16g,35] Retinol binding to RBP4 induces conformational changes within these loops that facilitate complexation with TTR. The RBP4-TTR complex is further stabilized via an H-bond interaction between the hydroxyl group of retinol and Gly83 of TTR subunit B.[35] Fenretinide also binds within the RBP4 cavity in a similar fashion to retinol; however, it induces a conformational change within RBP4 loop $\beta3-\beta4$ that is unfavorable for RBP4-TTR engagement (Figure 3A).[16g,36] In addition, the fenretinide 4-hydroxyphenylamide is also believed to further disrupt RBP4-TTR complexation by projecting into the RBP4-TTR interaction interface where it presents steric clashes with TTR subunits.[36,37]

A1120 induces significant conformational changes in both RBP4 loops $\beta3-\beta4$ and $\beta5-\beta6$ that are not conducive for complexation with TTR (Figure 3B).[24] The nonretinoid antagonist binds within the β-barrel cavity with the *o*-trifluoromethylphenyl ring projecting into the hydrophobic β-

dx.doi.org/10.1021/jm5010013 | J. Med. Chem. 2014, 57, 7731−7757

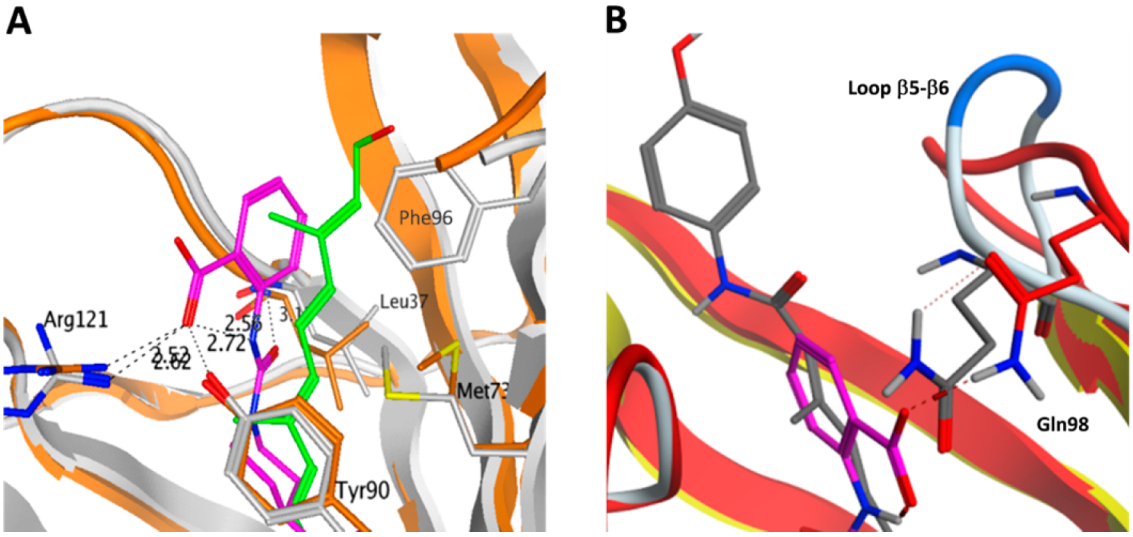

Figure 4. (A) Overlay of protein crystal structures 3bsz (orange) and 3fmz (white). A1120 binding interactions with Arg121, Tyr90, Leu37, and Phe96 are highlighted. Retinol is shown as green, and A1120 is shown as magenta. The $\beta 5$ and $\beta 6$ strands are removed for a better view. Contacting residues are labeled and illustrated in stick format. (B) Comparison of RBP4 loop $\beta 5-\beta 6$ conformational changes between fenretinide (1fel, yellow, white, and blue) and A1120 (3fmz, red) binding. The A1120-Gln98 H-bond interaction is highlighted (Phe96 not shown). Fenretinide is shown as gray, and A1120 is magenta. Contacting residues are labeled and illustrated in stick format.

ionone pocket and the anthranilic carboxylic acid fragment positioned at the opening where it engages in several key binding interactions; the A1120 carboxamidocarbonyl oxygen atom accepts an H-bond from the backbone of Leu37, and the carboxylic acid forms a salt bridge with Arg121 and two H-bonds with Tyr90 and Gln98 (Figure 4A).[24] In addition, a $\pi-\pi$ edge-to-face interaction is observed between the anthranilic carboxylic acid phenyl ring of A1120 and the phenyl ring of Phe96. Of these key binding interactions, it appears that the A1120-Gln98 H-bond and the Phe96 $\pi-\pi$ edge-to-face interaction are potentially playing critical roles in inducing and stabilizing the conformational changes observed within loop $\beta 5-\beta 6$ (Figures 4B).

With these crystallographic data in hand, our medicinal chemistry goals were to design novel, nonretinoid antagonists that would engage in the key aforementioned binding interactions and induce conformational changes in both loops $\beta 3-\beta 4$ and $\beta 5-\beta 6$, thereby leading to disruption of RBP4-TTR complexation. Proposed ligands were initially docked within 3fmz using Standard Precision (SP) mode, and the docking poses were subsequently refined using the Extra Precision (XP) mode of Glide (version 5.8, Schrödinger, LLC.). We aligned the Glide XP refined docking poses of all proposals to the cocrystallized conformation of A1120 and performed molecular mechanics (MM) minimization on these ligands in 3fmz using Impact (version 5.8, Schrödinger, LLC.). These minimized poses and corresponding Glide scores generated were reported as the final docking poses and Glide scores (Glide scores and solvation energies for each analogue are provided in the Supporting Information). Although Glide scores provided some guidance for the triaging of compounds yet to be synthesized, these crude estimates were generally limited with regard to consistently predicting relative levels of RBP4 binding affinity. We found that these scores were useful in prospectively estimating whether a compound would show affinity at RBP4 with potency (IC_{50}) less than 1 μM in the SPA assay. However, detailed SAR analysis showed that, as expected, the scores exhibited a poor correlation with the actual RBP4 SPA assay IC_{50} results observed. In addition, Glide would occasionally provide inconsistent binding modes for some closely structurally related analogues of A1120 (e.g., altered H-bond interactions with either Leu37 or Tyr90). Therefore, focus shifted away from Glide scores and more to the geometric docking of proposed ligands when using the model to triage novel analogue designs prior to synthesis. In this work, our retrospective computational analysis of the RBP4 SPA assay SAR observed for our novel analogues placed emphasis on correlations between the orientation and positioning of our ligands within the RBP4 binding cavity relative to A1120 (geometric docking poses generated) rather than on numeric agreement with the obtained Glide scores.

In Vitro Binding of Compounds to RBP4. Analogue binding affinities for RBP4 were measured using our previously described scintillation proximity assay (SPA).[25] Nonlinear regression analysis conducted following saturation binding of retinol to RBP4 revealed a K_d of 62.5 nM in our assay conditions which is in line with the previously reported 70−190 nM range of values.[16d,38] For compound characterization we measured the competitive displacement of radiolabeled retinol added to the reaction mix at 10 nM which roughly corresponds to the generally recommended $^1/_{10}$ of the K_d concentration of radioligand. The IC_{50} values were calculated from the 12-point compound titrations using a four-parameter logistic equation. Compounds with appreciable RBP4 binding potency (generally, with IC_{50} < 150 nM) were further assessed for the ability to antagonize the retinol-dependent RBP4-TTR interaction using the HTRF assay.

Assessment of Antagonistic Activity in the HTRF RBP4-TTR Interaction Assay. The ability of an analogue to disrupt the retinol-induced interaction of RBP4 with TTR was examined using the previously described HTRF assay[25] that probes retinol-dependent RBP4-TTR interaction. As indicated in the Experimental Section, we used bacterially expressed maltose binding protein (MBP) tagged RBP4 and commercially available TTR labeled directly with Eu^{3+} cryptate along with a d2-conjugated anti-MBP monoclonal antibody in order to implement this assay. Retinol added to the reaction mix at 1 μM concentration stimulates RBP4-TTR interaction which brings

dx.doi.org/10.1021/jm5010013 | J. Med. Chem. 2014, 57, 7731−7757

Table 1. RBP4 SPA Binding Affinity and HTRF Data for Acylsulfonamide and Aliphatic Carboxylic Acid Analogues

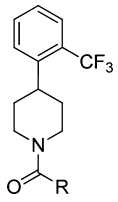

Compound	R	RBP4 SPA[a] IC_{50} (nM)[c]	RBP4 HTRF[b] IC_{50} (μM)[c]
3	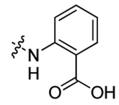	14.8	0.155
9	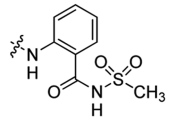	298.5	6.80
10	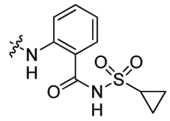	244.4	5.31
11	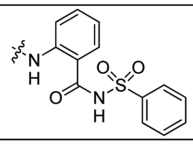	>3000	3.94
12		233.7	3.13
13	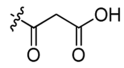	1470	ND
14	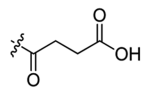	>3000	ND
(±)-15	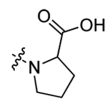	>3000	ND

[a]IC_{50} values for the SPA assay obtained in the presence of a fixed, 10 nM concentration of ^{3}H-retinol. [b]IC_{50} values for the HTRF assay obtained in the presence of 1 μM concentration of retinol. [c]Data represent the mean of at least two independent experiments run in duplicate. ND = not determined.

europium in proximity to the d2 dye with the following fluorescence energy transfer (FRET) to d2. The FRET signal, measured as a 668 nm emission, was normalized using the 620 nm europium emission to compensate for the pipetting and dispensing errors. Following a 12-point dose titration (20 μM to 0.1 nM) the IC_{50} values were calculated using a standard four-parameter logistic nonlinear regression model equation. In order to monitor a correlation between the binding affinity of compounds for RBP4 and their potency as antagonists of the retinol-dependent RBP4-TTR interaction, we tracked a ratio of IC_{50} values in the HTRF and SPA assays. Despite the difference in binding potency, for the majority of analogues, this ratio tended to be within the 5−20 range.

Structure−Activity Relationships. Table 1 summarizes efforts to replace the carboxylic acid moiety of A1120 with an acylsulfonamide appendage. The docking of analogues **9**−**11** within our model indicated favorable geometric alignment within the RBP4 binding cavity and engagement in critical H-bond interactions, with the acylsulfonamide appendages projecting out of the binding cavity toward solvent (Figure 5). However, these analogues exhibited a substantial reduction in potency (20-fold or greater) relative to A1120 in both the SPA and HTRF assays. This loss may be partially attributed to significant binding

dx.doi.org/10.1021/jm5010013 | J. Med. Chem. 2014, 57, 7731−7757

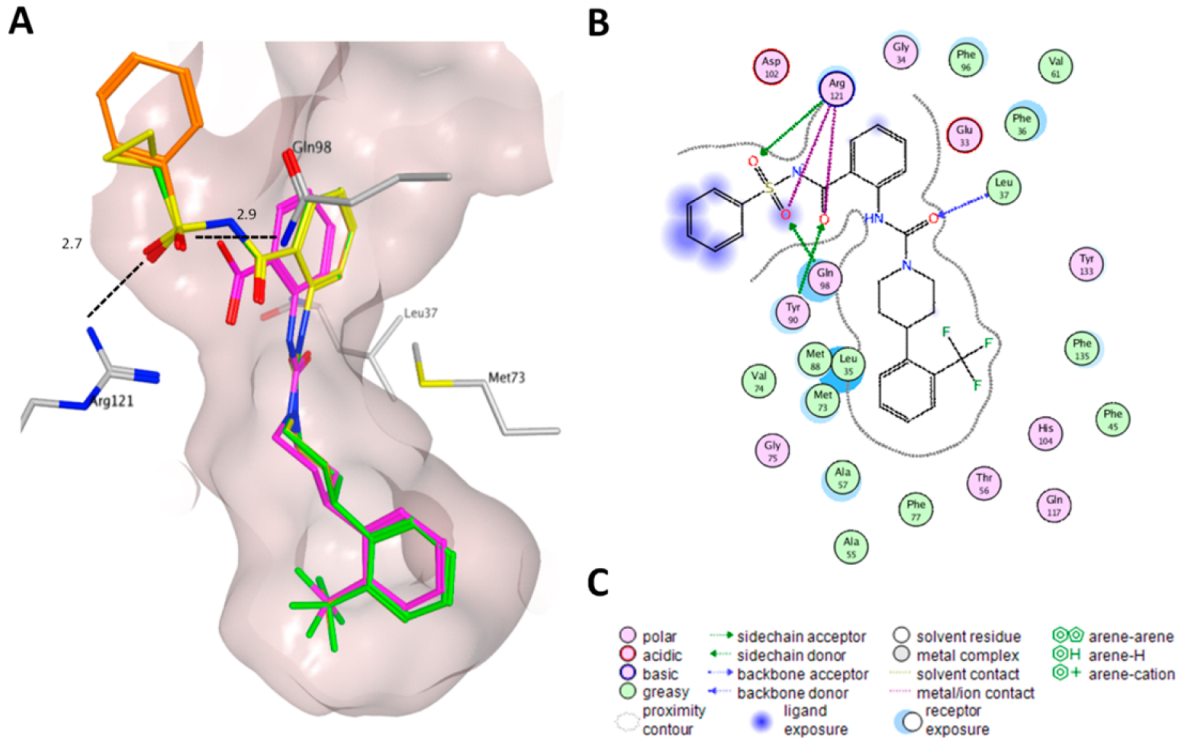

Figure 5. (A) Overlay of Glide docked poses of analogues **9** (green), **10** (yellow), **11** (orange), and A1120 (magenta) within the RBP4 binding cavity using 3fmz. Analogues **9**–**11** are shown extending through the cavity in similar fashion to A1120, with the acylsulfonamide and carboxamido moieties engaging in H-bond interactions with Arg121, Gln98, Tyr90, and Leu37 (both not shown), respectively. Contacting residues are labeled and illustrated in stick format. (B) Ligand interaction diagram of analogue **11**. (C) Legend for the ligand interaction diagram in the binding pose using MOE.

penalties incurred by solvent exposure of the hydrophobic acylsulfonamide residues. Interestingly, the HTRF IC_{50} values improved slightly with increasing size of the acylsulfonamide appendage, which may suggest that the larger moieties could be projecting into the RBP4-TTR interaction interface in a similar fashion as fenretinide, thereby potentially hindering complexation between the two proteins.

To further probe the RBP4-arylcarboxylic acid binding region, we explored the potency effects of replacing the anthranilic acid fragment with aliphatic carboxylic acids. To that end, the acylic oxoacids **12**–**14** and racemic proline analogue (±)-**15** were prepared; however, these compounds also exhibited significantly reduced potency. It is possible that less than optimal positioning of the carboxylic acid within the binding cavity, perhaps in combination with diminished interactions with Phe96, contributed to the weak potency values observed for these analogues. The precipitous drop in RBP4 potency observed for this small sample set of analogues, in addition to the potency results obtained for the aforementioned acysulfonamides, prompted us to explore other changes to the scaffold while keeping the anthranilic carboxylic acid appendage intact.

Acyclic *N*-Methyl-*N*-(2-phenoxyethyl)amido Analogues. Acknowledging the fact that the poor HLM stability observed for A1120 could be due in part to the piperidine ring presenting potential metabolic soft spots for CYP-mediated oxidation, we explored replacing it with alternative scaffolds in an attempt to probe structural changes that could provide suitable RBP4 antagonist activity with an improved metabolic profile. Drawing from the patent literature,[28] a series of analogues were initially prepared whereby the piperidine ring was replaced with an acyclic *N*-methyl-*N*-(2-phenoxyethyl)amido linker in order to impart greater conformational flexibility (Table 2). The

Table 2. RBP4 SPA Binding Affinity and HTRF Data for Acyclic *N*-Methyl-*N*-(2-phenoxyethyl)amido Analogues

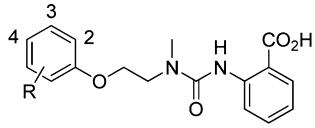

compd	R	RBP4 SPA[a] IC_{50} (nM)[c,d]	RBP4 HTRF[b] IC_{50} (μM)[c]	% remaining HLM[d,e]
3		14.8	0.155	3
20	2-CF_3	1900	2.65	ND
21	2-*tert*-butyl, 4-Cl	>3000	ND	ND
25	2-*tert*-butyl	64.8	0.554	1.1
27	2-*tert*-butyl, 4-F	140.6	ND	3.2

[a]IC_{50} values for the SPA assay obtained in the presence of a fixed, 10 nM concentration of ^{3}H-retinol. [b]IC_{50} values for the HTRF assay obtained in the presence of 1 μM concentration of retinol. [c]Data represent the mean of at least two independent experiments run in duplicate. ND = not determined. [d]Compound concentration was 10 μM, and incubation time was 30 min. [e]HLM = human liver microsomes. ND = not determined.

complementary *o*-trifluoromethylphenyl substituted analogue **20** was found to be significantly less potent than A1120 (~100-fold), presumably because of an entropic penalty incurred by the two additional rotatable bonds of the acyclic linkage. However, the *o*-*tert*-butylphenyl analogue **25** exhibited dramatically improved potency in the SPA and HRTF assays relative to **20** (SPA IC_{50} = 64.8 nM and HTRF IC_{50} = 0.554 μM). This observation may be attributed to partial compensation of the entropic penalty incurred via increased van der Waals contacts between the bulkier and more lipophilic *tert*-butyl group and the hydrophobic surface of the β-ionone pocket within the RBP4

dx.doi.org/10.1021/jm5010013 | J. Med. Chem. 2014, 57, 7731–7757

binding cavity. Our docking model showed a good overlay between **25** and A1120, with its carboxylic acid engaged in the key hydrogen bond interactions with Tyr90, Gln98, Arg121, and Leu37 (Figure 6). Despite the encouraging RBP4 potency

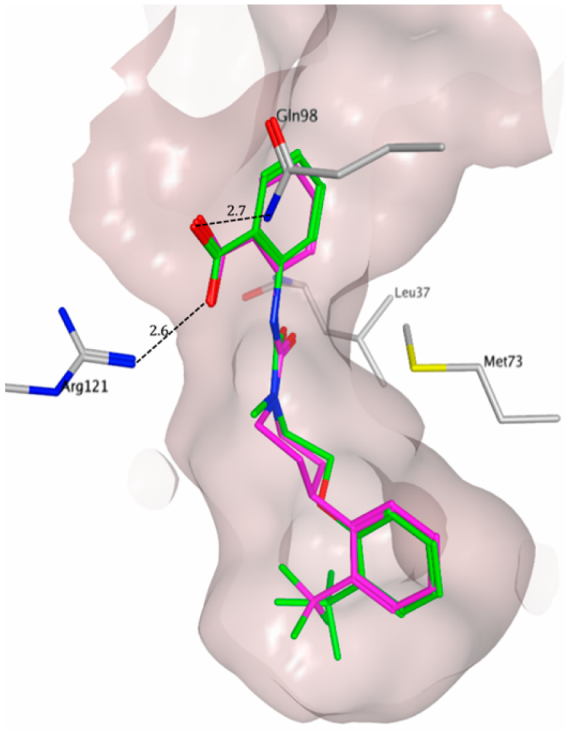

Figure 6. Overlay of minimized bound conformations of RBP4 antagonist **25** (green) and A1120 (magenta) within 3fmz. Analogue **25** is shown extending through the cavity in similar fashion to A1120, with its carboxylic acid engaging in H-bond interactions with Arg121, Gln98, and Tyr90 (not shown) and with carboxamide carbonyl interacting with Leu37 (not shown). Contacting residues are labeled and illustrated in stick format.

observed for antagonist **25**, poor liver microsomal stability across multiple species was identified as a major liability. The observed poor microsomal stability was presumed to be due to extensive CYP-mediated oxidation of the metabolically labile *tert*-butyl group and/or the acyclic linkage. Thus, this series was deprioritized, and the team focused its efforts on analogues with more conformationally restricted core scaffolds that might be less susceptible to CYP-mediated oxidation and not require the presence of the metabolically labile *o*-*tert*-butylphenyl group to achieve favorable RBP4 binding affinity.

Bicyclic {3.3.0}-Octahydrocyclopenta[*c*]pyrrolo Analogues. Additional analogues that contained novel conformationally restricted cores that linked together the *o*-trifluoromethylphenyl and arylcarboxylic acid fragments were investigated (Table 3). In addition to the aforementioned goal of developing a ligand that was less susceptible to CYP-mediated oxidative metabolism, conformationally restricted cores of varying geometry were also explored so as to probe putative bioactive binding conformations that could potentially lead to analogues with enhanced RBP4 binding affinity. Within the set of compounds tested, the bicyclic {3.3.0}-octahydrocyclopenta[*c*]-pyrrolo analogues **43** and (±)-**45** emerged as potent RBP4 antagonists (SPA IC_{50} of 72.7 and 148.5 nM, respectively; HTRF IC_{50} of 0.294 and 0.481 μM, respectively).

Docking analysis of the active *endo*-isomer **43** shows favorable alignment within the RBP4 binding cavity (Figure 7). The bicyclic {3.3.0}-octahydrocyclopenta[*c*]pyrrolo core is shown extending through the β-barrel with the *o*-trifluoromethylphenyl ring extending slightly farther into the hydrophobic β-ionone cavity than A1120, and the anthranilic carboxylic appendage is engaged in key H-bond interactions. Interestingly, *exo*-isomer **48** also exhibited a favorable geometric pose within the model; however the compound was found to be devoid of RBP4 activity (SPA $IC_{50} > 3$ μM). In an attempt to reconcile the discrepancies between the docking experiments and the SPA binding affinities observed for these two geometric isomers, free energy differences associated with minimized bound (docked pose) and unbound ligand conformations were calculated using MacroModel (version 9.9, Schrödinger, LLC.) for both compounds. Indeed, it was determined that the *exo*-isomer **48** adopts a more strained bound geometry relative to *endo*-isomer **43** (~2 kcal/mol greater energy, data not shown) in order to optimize binding interactions with RBP4. While these calculations ignore many other possible effects, they offer a possible explanation for the higher RBP4 binding affinity observed for *endo*-isomer **43**.

In vitro pharmacological evaluation of **43** revealed a desirable profile that included no significant off-target activity at the hERG channel or within a standard screening panel of 55 GPCRs, enzymes, ion channels, and transporters. In addition, **43** exhibited good solubility and metabolic stability, including significantly improved HLM stability (Table 4). The compound did, however, present submicromolar inhibitory activity for CYP2C9 (IC_{50} = 340 nM). Thus, a limited set of follow-up analogues was generated in an attempt to diminish CYP2C9 activity and further improve RBP4 potency. We initially explored the SAR impact of an electron withdrawing or donating group substituted para to the urea on the arylcarboxylic acid phenyl ring (**50**−**53**). Fluorinated analogue **50** presented SPA potency levels comparable to **43** (SPA IC_{50} = 88.8 nM and HTRF IC_{50} = 0.285 μM) with moderate HLM stability; however, CYP2C9 activity did not improve (IC_{50} = 333 nM). Similarly, chlorinated analogue **52** also exhibited undesirable potency at CYP2C9 (IC_{50} = 548 nM) with a concomitant 4-fold diminishment in RBP4 SPA potency relative to **43** (SPA IC_{50} = 328.8 nM and HTRF IC_{50} = 0.340 μM). Substitution with either methoxy (**51**) or methylsulfonyl (**53**) did lead to diminished CYP2C9 activity (IC_{50} of 13 and 8.7 μM, respectively); however, the compounds were also significantly less potent for RBP4. Interestingly, replacing the arylcarboxylic acid phenyl ring of **43** with either a pyridine or pyridazine moiety had a dramatic impact on RBP4 binding affinity for the series. It was initially found that the position of the pyridine nitrogen was critical for RBP4 activity, as the 2-aminopyridyl analogue **54** was essentially devoid of activity while the 4-aminopyridyl analogue **55** exhibited RBP4 potency comparable to A1120 (SPA IC_{50} = 18.7 nM and HTRF IC_{50} = 0.179 μM). Unfortunately, pyridine **55** was found to be a potent CYP3A4 inhibitor (IC_{50} < 46 nM); therefore, we sought to mitigate this liability by introducing a methyl group ortho to the pyridyl nitrogen (**56**). Indeed, analogue **56** exhibited diminished affinity for CYP3A4 (IC_{50} = 1.1 μM). In addition, **56** also exhibited improved activity at CYP2C9 (IC_{50} = 1 μM) relative to **43**, exhibited comparable potency to A1120 in the SPA assay (SPA IC_{50} = 23.9 nM), and was within a 2-fold potency range of A1120 in the HTRF assay (HTRF IC_{50} = 0.235 μM). Lastly, we found that replacing the methylpyridine of **43** with a pyridazine ring (**57**) further improved activity at CYP3A4 (IC_{50} = 12 μM) and CYP2C9 (IC_{50} = 17 μM), provided an overall favorable

dx.doi.org/10.1021/jm5010013 | J. Med. Chem. 2014, 57, 7731−7757

Table 3. RBP4 SPA Binding Affinity and HTRF Data for Conformationally Restricted Analogues

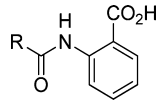

Compound	R	RBP4 SPA[a] IC_{50} (nM)[c]	RBP4 HTRF[b] IC_{50} (μM)[c]
3	---	14.8	0.155
28	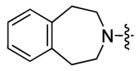	>3000	ND
29	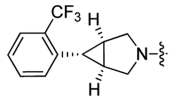	>3000	ND
30	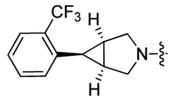	>3000	ND
31	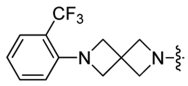	>3000	ND
32	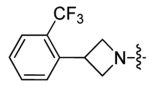	>3000	8.38
33	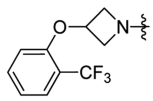	1440	ND
(±)-**34**	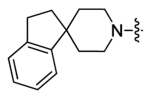	3760	ND
43	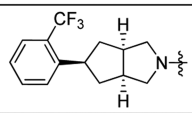	72.7	0.294
(±)-**45**	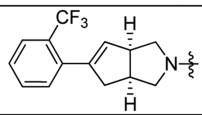	148.5	0.481
48	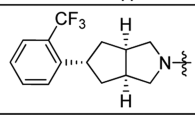	>3000	ND

[a]IC_{50} values for the SPA assay obtained in the presence of a fixed, 10 nM concentration of ^{3}H-retinol. [b]IC_{50} values for the HTRF assay obtained in the presence of 1 μM concentration of retinol. [c]Data represent the mean of at least two independent experiments run in duplicate. ND = not determined.

ADME profile (including excellent HLM stability), and yielded an RBP4 antagonist of comparable potency to A1120 in both the SPA and HTRF assays (SPA IC_{50} = 24.0 nM and HTRF IC_{50} = 0.121 μM).

The superior RBP4 binding affinity of heteroaromatic analogues **55**−**57** relative to **43** and **50**−**53** prompted us to explore our computational model and examine if enhanced π−π edge-to-face interactions with Phe96 could be playing a role in the observed potency trends. We conducted ab initio molecular orbital calculations using a simplified model derived from the docked poses of **43**, **50**, **56**, and **57** to identify changes in the electronic distribution of the aromatic and heteroaromatic rings bearing the carboxylic acid and to generate Phe96 interaction scores for each analogue. As expected, the more polarizable heteroaromatic analogues **56** and **57** presented enhanced Phe96 interaction scores relative to **43** and **50** (Table 5). The enhanced polarization of the ring system is indicated by the ab initio derived partial charges at the point of substitution. The increased

dx.doi.org/10.1021/jm5010013 | J. Med. Chem. 2014, 57, 7731−7757

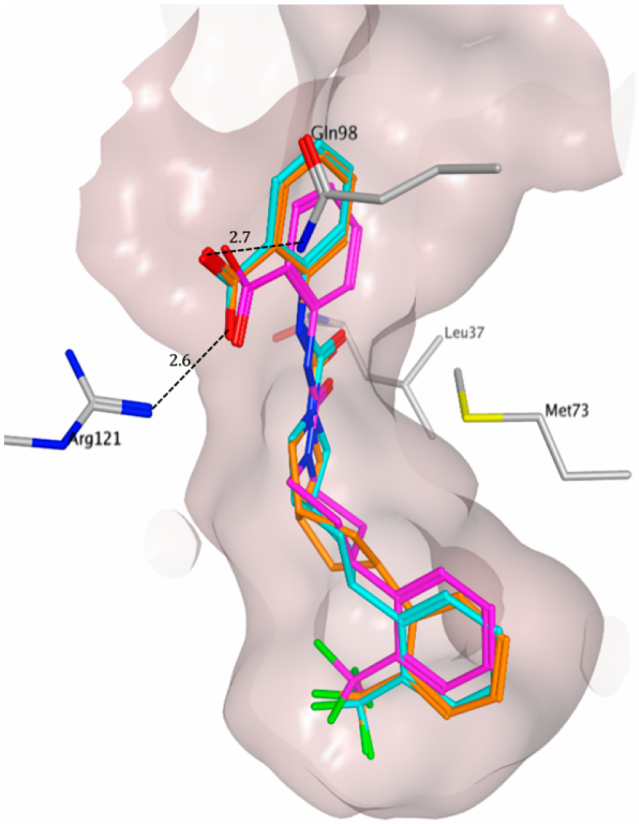

Figure 7. Overlay of minimized bound conformations of *endo*-isomer **43** (cyan), *exo*-isomer **48** (orange), and A1120 (magenta) within 3fmz. Contacting residues are labeled and illustrated in stick format.

negative charge of the π-system of the ligand is expected to interact favorably with the C−H atoms of F96 in the predicted edge-to-face geometry. Increased negative charge and the F96 interaction score roughly parallel the increase in activity. These results could indicate that the $\pi-\pi$ edge-to-face interactions between the heteroaromatic systems of **55**−**57** and Phe96 are stronger relative to the nonheteroaromatic analogues,[39] potentially leading to the enhanced binding affinities and HTRF antagonist activity observed for these analogues.

To further probe the RBP4 arylcarboxylic acid binding region of **43**, we explored a limited set of amino acid based analogues (Table 6). The glycinergic analogue **58** exhibited weak potency in both the SPA and HTRF assays compared to **43**. Interestingly, an enantiopreference for the (*S*)-isomers was observed for chiral analogues **59**−**62**. The eudismic ratio for (*S*)-**59** and its congener (*R*)-**60** was ∼1.7 for the HTRF assay, and the eudismic ratios for (*S*)-**61** and (*R*)-**62** was ∼10 for both the SPA and HTRF assays, respectively. Notably, (*S*)-**61** exhibited the best potency of this series. Our model suggests that the enantiopreference and superior potency of (*S*)-**61** may be partially attributed to optimal positioning of its carboxylic acid to allow for better engagement with Arg121, Tyr90, and Gln98 relative to (*R*)-**62**, as (*R*)-**62** must adopt a higher energy conformation in order for its carboxylic acid to engage in H-bonding interactions with these residues. In addition, the positioning of the phenyl ring of (*S*)-**61** brings it within closer proximity to Phe96 than (*R*)-**62**. This closer proximity to Phe96 could present a stronger $\pi-\pi$ edge-to-face interaction (as evidenced by the F96 interaction scores), which could further contribute to the enantiopreference observed between (*S*)-**61** and (*R*)-**62**. In both compounds, the calculated charges of the closest approaching carbon atoms are 0.10 for (*S*)-**61** and 0.16 for (*R*)-**62**. The more positive charges suggest that the edge-to-face interaction is weaker for both compounds than those in Table 5 but that (*S*)-**61** would more favorably interact than (*R*)-**62**.

The favorable in vitro RBP4 potency and ADME profile of **43** prompted us to evaluate the compound in rodent acute and chronic dosing pharmacokinetic (PK) and pharmacodynamic (PD) experiments. Following iv administration of 0.5 mg/kg, **43** was slowly eliminated from plasma with a mean apparent terminal phase elimination half-life of 10.3 h. The estimated total body clearance of **43** was low (mean, 35.3 mL h^{-1} kg^{-1}), and the estimated apparent volume of distribution at steady state was small (mean, 523 mL/kg). These data are suggestive of a slow rate of metabolism/elimination and limited extravascular distribution of the compound. No unchanged **43** was quantifiable in urine samples collected between 0 and 48 h after iv administration of the compound.

Following po administration of 5 mg/kg as a single dose on day 0, a mean peak plasma concentration of **43** of 3950 ng/mL and an AUC_{INF} of 43 898 h·ng/mL were observed (Table 7). The oral bioavailability of **43** after dosing on day 0, as estimated from AUC_{INF} values, was 31%. For rats given a single daily po dose for 6 consecutive days, plasma concentrations of **43** prior to dosing on day 6 (i.e., approximately 24 h after administration of the previous dose) ranged from 243 to 453 ng/mL. Following dose administration on day 6, mean peak plasma concentrations of **43** and AUC_{INF} were slightly higher than observed on day 0. The estimated oral bioavailability of **43** on day 6 was 44%.

In order to demonstrate the in vivo target engagement, establish the proof of in vivo activity, and document PK−PD correlations, we studied the effect of **43** dosing in rats on the level of plasma RBP4. Aliquots of plasma samples collected during the acute and chronic dosing PK experiments were used to analyze plasma RBP4 concentrations as we previously described.[25] After a single 5 mg/kg oral dose of **43**, a 30−50% decrease in plasma RBP4 was observed (data not shown), while the 7-day oral administration in rats at 5 mg/kg induced an approximately 60% reduction in plasma RBP4 (Figure 8A). Comparison of the dynamics of RBP4 lowering in response to **43** treatment (Figure 8A) with plasma compound levels (Figure 8B) shows a good correlation between the reduction in plasma RBP4 and increase in compound concentration. Given the absolute correlation between RBP4 lowering and bisretinoid reduction in the *Abca4*$^{-/-}$ mouse model of enhanced retinal lipofuscinogenesis, which we and others previously established for the antagonists of the RBP4-TTR interaction from different structural classes,[13a,25] it seems reasonable to expect that **43** and similar analogues with good RBP4 lowering potency will show the desired preclinical efficacy in the *Abca4*$^{-/-}$ mice.

CONCLUSIONS

A1120 is a potent, nonretinoid RBP4 antagonist (SPA IC_{50} = 14.8 nM and HTRF IC_{50} = 155.5 nM) that induces significant lowering of serum RBP4 levels in vivo and has exhibited efficacy in a preclinical rodent model of excessive lipofuscin accumulation in the RPE. Despite its attractive profile, further development of A1120 as a potential therapeutic to treat dry AMD is hampered by the compound's poor HLM stability (∼3% remaining after a 30 min incubation time). Therefore, using A1120 as a template, we sought to explore various structural changes that could provide an novel RBP4 antagonist of comparable potency but with improved HLM stability.

dx.doi.org/10.1021/jm5010013 | *J. Med. Chem.* 2014, 57, 7731−7757

Table 4. SPA Binding Affinity and HTRF Data for Bicyclic {3.3.0}-Octahydrocyclopenta[*c*]pyrrolo RBP4 Antagonists

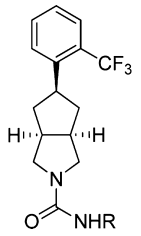

Cmpd.	R	RBP4 SPA[a] IC_{50} (nM)[c]	RBP4 HTRF[b] IC_{50} (μM)[c]	Kinetic Solubility[d] (μM)	LM Stability[e] (% remaining)		CYP Inhibition IC_{50} (μM)[f]			
					H	R	2C9	2C19	2D6	3A4
3	---	14.8	0.155	57	3	85	>100	52	100	>100
43	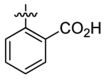	72.7	0.294	55	100	75	0.34	29	>100	28
50	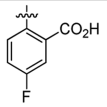	88.8	0.285	55	57	100	0.33	31.0	>100	53
51	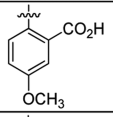	170.3	ND	34	89	72	13	75	>100	8.0
52	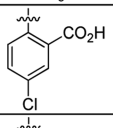	328.8	0.340	60	89	87	0.58	16	>100	50
53	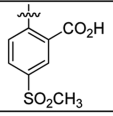	163.1	1.55	>100	100	100	8.7	32	>100	42
54	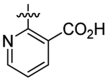	>3000	ND	82	83	81	27	33	>100	>100
55	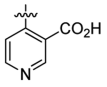	18.7	0.179	29	81	82	5.6	2.1	>100	<0.046
56	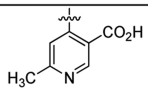	23.9	0.235	93	71	76	1.0	12	>100	1.1
57	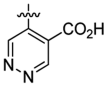	24.0	0.121	>100	97	61	17	6.0	>100	12

[a] IC_{50} values for the SPA assay obtained in the presence of a fixed, 10 nM concentration of ^{3}H-retinol. [b] IC_{50} values for the HTRF assay obtained in the presence of 1 μM concentration of retinol. [c] Data represent the mean of at least two independent experiments run in duplicate. [d] Aqueous kinetic solubility in PBS, pH 7.4. [e] LM = liver microsomes. Compound concentration was 10 μM, and incubation time with the microsomes was 30 min, H = human. R = rat. [f] CYP IC_{50} determined via fluorescence detection and with inhibitors sulfaphenazole (CYP2C9), tranylcypromine (CYP2C19), quinidine (CYP2D6), and ketoconazole (CYP3A4). ND = not determined.

We investigated several modifications, beginning with the acylsulfonamide carboxylic acid isosteres **9**–**11** and the aliphatic carboxylic acids **12**–(±)-**15**. This set of analogues did not yield potent antagonists, and our program quickly shifted focus on modifying the core while keeping the anthranilic acid appendage intact.

Several structural modifications were made to the core, whereby the piperidine ring was replaced with an acyclic and various conformationally constrained motifs. Among the novel

dx.doi.org/10.1021/jm5010013 | J. Med. Chem. 2014, 57, 7731–7757

Table 5. Phe96 (F96) Interaction Score and Partial Charge Comparisons

compd	RBP4 SPA IC_{50} (nM)	partial charge of the aromatic/heteroaromatic ring[a]	F96 interaction score (E_{int})[b]	centroid distance (Å)[c]
43	72.7	−0.26	−2.8	4.88
50	88.8	−0.19	−2.9	4.87
56	23.9	−0.56	−3.6	4.82
57	24.0	−0.36	−3.5	4.90

[a]The aromatic/heteroaromatic ring electronic distribution for each analogue was derived from ab initio molecular orbital calculations performed on simplified docking pose models. [b]The anthranilic motif for each compound was preserved for computational efficiency, and Phe96 was modeled as simply the single amino acid with all other protein atoms removed. E_{int} = interaction energy score. [c]Centroid distance is the distance between the Phe96 CH and the aromatic or heteroaromatic ring of the RBP4 ligand within the RBP4 binding cavity.

RBP4 antagonists identified, the bicyclic {3.3.0}-octahydrocyclopenta[*c*]pyrrolo RBP4 antagonist **43** exhibits potent in vitro RBP4 SPA (IC_{50} = 73 nM) and HTRF (IC_{50} = 294 nM) assay activity that is comparable to A1120. The compound also possesses a favorable ADME profile with excellent HLM stability (100% remaining after a 30 min incubation time) and no limiting off-target pharmacology with the exception of CYP2C9 inhibitory activity (IC_{50} = 340 nM). Furthermore, compound **43** possesses good PK and PD properties, leading to a robust and sustained lowering (>85%) of serum RBP4 levels in both acute and chronic rodent oral dosing studies.

Additional work within the bicyclic {3.3.0}-octahydrocyclopenta[*c*]pyrrolo series led to the discovery of pyridazine **57**, which exhibited potent in vitro RBP4 antagonist activity (SPA IC_{50} = 24 nM and HTRF IC_{50} = 121 nM), favorable ADME profiles, and improved activity at CYP2C9 (IC_{50} = 17 μM). Encouraged by these results, we have continued to focus our efforts within the bicyclic {3.3.0}-octahydrocyclopenta[*c*]-pyrrolo series. Additional refinements have led to RBP4 antagonists possessing exquisite in vitro potency, robust in vivo serum RBP4 lowering capability, and efficacy in the *Abca4*$^{-/-}$ mouse model. These promising data will be reported in due course.

EXPERIMENTAL SECTION

General Chemistry. All reactions were performed under a dry atmosphere of nitrogen unless otherwise specified. Indicated reaction temperatures refer to the reaction bath, while room temperature (rt) is noted as 25 °C. Commercial grade reagents and anhydrous solvents were used as received from vendors, and no attempts were made to purify or dry these components further. 3-(2-(Trifluoromethyl)phenyl)-azetidine hydrochloride was purchased from Small Molecules [CAS number 1203684-79-0]. 2,3,4,5-Tetrahydro-1*H*-benzo[*d*]azepine was purchased from Acros [CAS number 4424-20-8]. *tert*-Butyl 2,6-diazaspiro[3.3]heptane-2-carboxylate hemioxalate was purchased from Alfa [CAS number 1041026-71-4]. 2,3-Dihydrospiro[indene-1,4′-piperidine] hydrochloride was purchased from Matrix Scientific [CAS number 96651-85-3]. Removal of solvents under reduced pressure was accomplished with a Buchi rotary evaporator at approximately 28 mmHg pressure using a Teflon-linked KNF vacuum pump. Thin layer chromatography was performed using 1 in. × 3 in. AnalTech no. 02521 silica gel plates with fluorescent indicator. Visualization of TLC plates was made by observation with short wave UV light (254 nm lamp), 10% phosphomolybdic acid in ethanol or in iodine vapors. Preparative thin layer chromatography was performed using Analtech, 20 cm × 20 cm, 1000 μm preparative TLC plates. Flash column chromatography was carried out using a Teledyne Isco CombiFlash Companion unit with RediSep Rf silica gel columns. If needed, products were purified by reverse phase chromatography, using a Teledyne Isco CombiFlash Companion unit with RediSep Gold C18 reverse phase column. Proton NMR spectra were obtained on either a 300 MHz Bruker nuclear magnetic resonance spectrometer or a 500 MHz Bruker nuclear magnetic resonance spectrometer. Chemical shifts (δ) are reported in parts per million (ppm), and coupling constant (J) values are given in Hz, with the following spectral pattern designations: s, singlet; d, doublet; t, triplet; q, quartet; dd, doublet of doublets; m, multiplet; br, broad. Tetramethylsilane was used as an internal reference. Melting points are uncorrected and were obtained using a MEL-TEMP Electrothermal melting point apparatus. Mass spectroscopic analyses were performed using positive mode electron spray ionization (ESI) on

Table 6. Amino Acid Derived Analogues of Compound 43

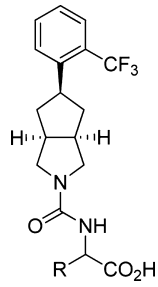

compd	R	RBP4 SPA[a] IC_{50} (nM)[c]	RBP4 HTRF[b] IC_{50} (μM)[c]	F96 interaction score (E_{int})[d]	centroid distance (Å)[e]	partial charge of the aromatic ring[a]
43		72.7	0.294	ND	ND	ND
58	H	1170	6.82	ND	ND	ND
(*S*)-**59**	CH_3	1480	5.26	ND	ND	ND
(*R*)-**60**	CH_3	>3000	9.19	ND	ND	ND
(*S*)-**61**	Ph	124.0	0.829	−1.65	4.19	0.10
(*R*)-**62**	Ph	1320	8.34	−1.04	4.35	0.16

[a]IC_{50} values for the SPA assay obtained in the presence of a fixed, 10 nM concentration of ^{3}H-retinol. [b]IC_{50} values for the HTRF assay obtained in the presence of 1 μM concentration of retinol. [c]Data represent the mean of at least two independent experiments run in duplicate. [d]The anthranilic motif for each compound was preserved for computational efficiency, and Phe96 was modeled as simply the single amino acid with all other protein atoms removed. E_{int} = interaction energy score. [e]Centroid distance is the distance between Phe96 CH and the aromatic or heteroaromatic ring of the RBP4 ligand.

dx.doi.org/10.1021/jm5010013 | *J. Med. Chem.* 2014, 57, 7731−7757

Table 7. Rat PK Parameters Calculated from Plasma Concentrations of 43

	C_{max} [a] (ng/mL)	T_{max} [b] (h)	$t_{1/2\beta}$ [c] (h)	AUC_{last} [d] (h·ng/mL)	AUC_{INF} [e] (h·ng/mL)	Cl[f] (mL h^{-1} kg^{-1})	V_{ss} [g] (mL/kg)
Route = iv; Dose = 0.5 mg/kg							
mean[i]	2945	0.083[k]	10.3	13180	14288	35.3	523
SD	1753	0	7.0	2331	1594	3.9	356
	C_{max} [a] (ng/mL)	T_{max} [b] (h)	$t_{1/2\beta}$ [c] (h)	AUC_{last} [d] (h·ng/mL)	AUC_{INF} [e] (h·ng/mL)		F [h] (%)
Route = po; Dose = 5 mg/kg. Day 0							
mean[i]	3950	2.9	6.2	43606	43898		31
SD	1341	4.4	0.9	2030	2032		
Route = po; Dose = 5 mg/kg. Day 6							
mean[j]	7827	0.33	7.6	62148	62990		44
SD	142	0.14	0.8	5635	6023		

[a]Maximum observed concentration of **43** in plasma. [b]Time of maximum observed concentration of **43** in plasma. [c]Apparent half-life of the terminal phase of elimination of **43** from plasma. [d]Area under the plasma concentration versus time curve from 0 to the last time point **43** was quantifiable in plasma. [e]Area under the plasma concentration versus time curve from 0 to infinity. [f]Total body clearance. [g]Volume of distribution at steady state. [h]Bioavailability: $F = (AUC_{INFpo} \times dose_{iv}) \div AUC_{INFiv} \times dose_{po})$. [i]Dosing groups consisting of three drug naive adult male Sprague–Dawley rats, dosed once on day 0. [j]Dosing group consisting of three drug naive adult male Sprague–Dawley rats, dosed q.d. from day 0 to day 6. [k]Earliest sample collection time point.

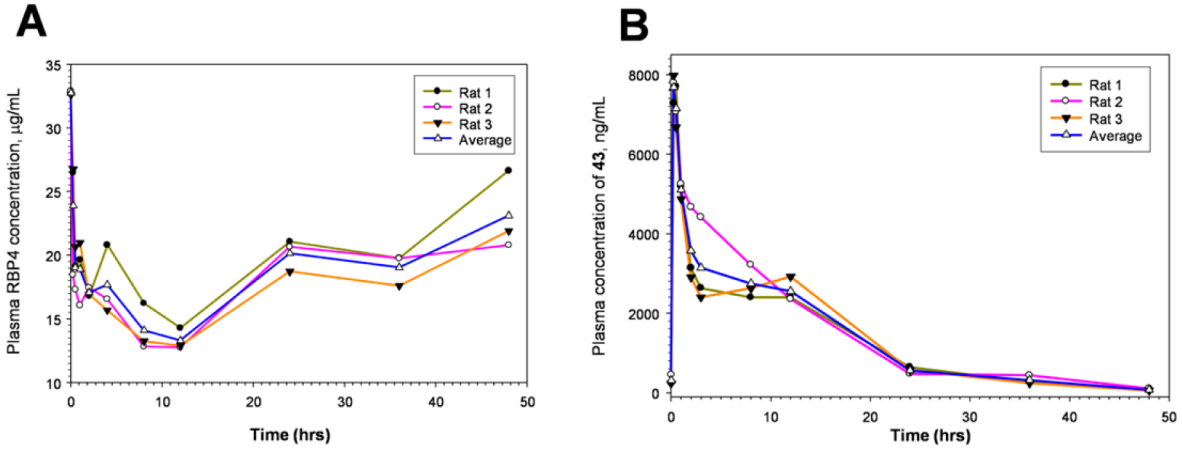

Figure 8. Correlation between the RBP4 (A) and **43** (B) plasma levels after administration of the seventh oral 5 mg/kg dose of **43** in rats.

a Varian ProStar LC–MS 1200L quadrapole mass spectrometer. High pressure liquid chromatography (HPLC) purity analysis was performed using a Varian ProStar HPLC system with a binary solvent system A and B using a gradient elusion [A, H_2O with 0.05% trifluoroacetic acid (TFA); B, CH_3CN with 0.05% TFA] and flow rate of 1 mL/min, with UV detection at 223 nm. All final compounds were purified to ≥95% purity by the Varian ProStar HPLC system using the following methods: (A) Phenomenex C18(2) column (3.0 mm × 250 mm); mobile phase, A = H_2O with 0.05% TFA and B = CH_3CN with 0.05% TFA; gradient, 0–90% B (0.0–20.0 min); (B) Pursuit XRs C18 column (4.6 mm × 250 mm); mobile phase, A = H_2O with 0.05% TFA and B = CH_3CN with 0.05% TFA; gradient, 0–90% B (0.0–15.0 min); (C) SunFire C18 5 μm (4.6 mm × 250 mm), mobile phase, A = H_2O with 0.05% TFA and B = CH_3CN with 0.05% TFA; gradient, 0–100% B (0.0–20.0 min).

***N*-(2-((Methylsulfonyl)carbamoyl)phenyl)-4-(2-(trifluoromethyl)phenyl)piperidine-1-carboxamide (9).** *Step A.* To a solution of 1-bromo-2-(trifluoromethyl)benzene (**4**, 35.0 g, 156 mmol) in THF (350 mL) cooled to −78 °C was slowly added a solution of *n*-BuLi (70.4 mL, 2.5 M in THF, 176 mmol) over a period of 15 min. The mixture was stirred at −78 °C for 40 min, was allowed to warm to 0 °C and then cooled back to −78 °C. To this was added a solution of 1-benzylpiperidin-4-one (22.1 g, 117 mmol) in THF (80 mL) over a period of 10 min. The resulting mixture continued to stir at −78 °C for 2 h. The reaction was carefully quenched with aqueous, saturated NH_4Cl solution (500 mL), and the mixture was extracted with EtOAc (300 mL). The organic extract was washed with H_2O, brine, dried over Na_2SO_4, filtered, and concentrated under reduced pressure. The resulting residue was chromatographed over silica gel (Isco CombiFlash Companion unit, 330 g RediSep column, 0–30% EtOAc in hexanes) to give 1-benzyl-4-(2-(trifluoromethyl)phenyl)piperidin-4-ol (**5**) as a light-yellow oil (29.2 g, 74%): ^{1}H NMR (500 MHz, $CDCl_3$) δ 7.78 (d, J = 1.6 Hz, 1H), 7.59 (m, 1H), 7.47 (m, 1H), 7.36 (m, 5H), 7.31 (m, 2H), 3.58 (s, 2H), 2.80 (m, 2H), 2.55 (m, 2H), 2.27 (m, 2H), 1.88 (m, 2H); ESI MS m/z 336 $[M + H]^+$.

Step B. A 0 °C cooled solution of 1-benzyl-4-(2-(trifluoromethyl)-phenyl)piperidin-4-ol (**5**, 29.2 g, 87.1 mmol) in thionyl chloride (60 mL) stirred for 2 h and was then diluted with CH_2Cl_2 (250 mL). The mixture was carefully poured into a solution of aqueous, saturated $NaHCO_3$ solution (200 mL). The biphasic mixture was separated, and the aqueous layer was further extracted with CH_2Cl_2 (400 mL). The combined organic layers were washed with brine, dried over Na_2SO_4, filtered, and concentrated. The resulting residue was chromatographed over silica gel (Isco CombiFlash Companion unit, 330 g RediSep column, 0–30% EtOAc in hexanes) to give 1-benzyl-4-(2-(trifluoromethyl)phenyl)-1,2,3,6-tetrahydropyridine (**6**) as a light-yellow oil (13.5 g, 49%): ^{1}H NMR (500 MHz, $CDCl_3$) δ 7.63 (d, J = 1.6 Hz, 1H), 7.48 (m, 1H), 7.39 (m, 5H), 7.28 (m, 2H), 5.56 (s, 1H), 0.68 (s, 2H), 3.14 (m, 2H), 2.70 (m, 2H), 2.39 (m, 2H); ESI MS m/z 318 $[M + H]^+$.

Step C. A mixture of 1-benzyl-4-(2-(trifluoromethyl)phenyl)-1,2,3,6-tetrahydropyridine (**6**, 13.6 g, 42.5 mmol), 10% Pd/C (3.0 g), and ammonium formate (26.8 g, 425 mmol) in CH_3OH (800 mL) was heated at reflux for 2 h. The mixture cooled to rt and was filtered over Celite. The filtrate was concentrated and the resulting residue was chromatographed over silica gel (Isco CombiFlash Companion unit, 330 g RediSep column, 0–10% CH_3OH with 1% NH_4OH in CH_2Cl_2)

dx.doi.org/10.1021/jm5010013 | J. Med. Chem. 2014, 57, 7731–7757

to give 4-(2-(trifluoromethyl)phenyl)piperidine as a colorless oil (2.0 g, 21%): ^{1}H NMR (500 MHz, $CDCl_3$) δ 7.61 (d, J = 1.7 Hz, 1H), 7.52 (m, 2H), 7.29 (m, 1H), 3.21 (m, 2H), 3.07 (m, 1H), 2.80 (m, 2H), 2.33 (bs, 1H), 1.77 (m, 4H); ESI MS m/z 230 $[M + H]^+$. To a solution of 4-(2-(trifluoromethyl)phenyl)piperidine (5.6 g, 24.5 mmol) in CH_3CN (30 mL) was added a 4 M solution of HCl in 1,4-dioxane (6.1 mL, 24.5 mmol) at rt. The mixture stirred for 2 h and was then concentrated under reduced pressure to give 4-(2-(trifluoromethyl)phenyl)piperidine hydrochloride (**7**) as a white solid (6.4 g, >99%): ESI MS m/z 230 $[M + H]^+$.

Step D. A mixture of 4-(2-(trifluoromethyl)phenyl)piperidine hydrochloride (**7**, 7.89 g, 29.7 mmol) and methyl 2-isocyanatobenzoate (5.27 g, 29.7 mmol) in CH_2Cl_2 (50 mL) was stirred for 2 h and then chromatographed over silica gel (0−25% EtOAc in hexanes) to give methyl 2-(4-(2-(trifluoromethyl)phenyl)piperidine-1-carboxamido)-benzoate as a white solid (8.27 g, 77%). To a solution of 2-(4-(2-(trifluoromethyl)phenyl)piperidine-1-carboxamido)benzoate (8.0 g, 19.6 mmol) in CH_3OH (50 mL) and THF (50 mL) was added NaOH (2 N, 20 mL). The mixture was stirred at rt for 2 h, was diluted with H_2O (100 mL), and then was acidified to pH 6 with 2 N HCl. The mixture was extracted with CH_2Cl_2 (3 × 150 mL), and the organic extracts were dried over Na_2SO_4, filtered, and concentrated. The residue was chromatographed over silica gel (0−5% CH_3OH in CH_2Cl_2) to give 2-(4-(2-(trifluoromethyl)phenyl)piperidine-1-carboxamido)benzoic acid (A1120) (**3**) as a white solid (7.3 g, 95%). Mp 156−158 °C; ^{1}H NMR (300 MHz, $CDCl_3$) δ 10.68 (s, 1H), 8.59 (d, J = 8.6 Hz, 1H), 8.05 (dd, J = 8.1, 1.6 Hz, 1H), 7.58−7.53 (m, 1H), 7.37 (dd, J = 7.4, 1.6 Hz, 1H), 7.25−7.12 (m, 3H), 7.02−6.96 (m, 1H), 4.40 (m, 2H), 3.50−3.40 (m, 1H), 3.06−2.97 (m, 2H), 1.90−1.80 (m, 4H); ESI MS m/z 393 $[M + H]^+$; HPLC 98.5% purity (AUC), t_R = 12.5 min (method A).

Step E. To a solution of 2-(4-(2-(trifluoromethyl)phenyl)piperidine-1-carboxamido)benzoic acid (**3**, 0.711 g, 1.81 mmol) and *i*-Pr_2NEt (1.41 mL, 8.15 mmol) in DMF (12.7 mL) was added HATU (1.03 g, 2.72 mmol). The mixture stirred at rt for 1.5 h and was then diluted with aqueous saturated NH_4Cl (40 mL). The aqueous mixture was extracted with CH_2Cl_2 (4 × 30 mL), and the combined organic extracts were concentrated under reduced pressure. The resulting residue was chromatographed over silica gel (Isco CombiFlash Companion unit, 40 g RediSep column, 0−25% EtOAc in hexanes) to give 7-(4-(2-(trifluoromethyl)phenyl)piperidine-1-carbonyl)-7-azabicyclo[4.2.0]-octa-1(6),2,4-trien-8-one (**8**) as a white solid (0.565 g, 83%): mp 127−130 °C; ^{1}H NMR (500 MHz, DMSO-d_6) δ 7.91 (d, J = 7.0 Hz, 1H), 7.73−7.65 (m, 3H), 7.64−7.59 (m, 1H), 7.48−7.38 (m, 1H), 7.23 (d, J = 8.5 Hz, 1H), 7.21−7.17 (m, 1H), 4.53−4.44 (m, 2H), 3.19−3.07 (m, 3H), 1.92−1.80 (m, 2H), 1.79−1.73 (m, 2H); ESI MS m/z 375 $[M + H]^+$.

Step F. To a 0 °C solution of methanesulfonamide (0.057 g, 0.60 mmol) in THF (1.0 mL) was added NaH (60% in mineral oil, 0.024 g, 0.60 mmol), and the resulting solution was stirred at 0 °C for 5 min and for an additional 15 min at rt. A solution of **8** (0.150 g, 0.40 mmol) in THF (2.0 mL) was added, and the resulting solution was stirred at rt for 72 h. The reaction was quenched with H_2O and acidified to pH 4 with 2 N HCl. The resulting precipitate was collected by filtration and washed with H_2O (40 mL) and hexanes (40 mL). The obtained solids were chromatographed over silica gel (Isco CombiFlash Companion unit, 40 g RediSep column, 0−5% CH_3OH in CH_2Cl_2 with 0.05% HOAc) to provide *N*-(2-((methylsulfonyl)carbamoyl)phenyl)-4-(2-(trifluoromethyl)phenyl)piperidine-1-carboxamide (**9**) as a white solid (0.035 g, 18%): mp 220−285 °C; ^{1}H NMR (500 MHz, DMSO-d_6) δ 12.03 (br s, 1H), 9.76 (s, 1H), 7.83 (d, J = 7.5 Hz, 1H), 7.70−7.60 (m, 4H), 7.51−7.46 (m, 1H), 7.44−7.39 (m, 1H), 7.09−7.04 (m, 1H), 4.23 (d, J = 13.0 Hz, 2H), 3.32 (s, 3H), 3.12−3.04 (m, 1H), 2.96 (t, J = 11.5 Hz, 2H), 1.83−1.68 (m, 4H); ESI MS m/z 468 $[M + H]^+$; HPLC >99% purity (AUC), t_R = 14.4 min (method C).

***N*-(2-((Cyclopropylsulfonyl)carbamoyl)phenyl)-4-(2-(trifluoromethyl)phenyl)piperidine-1-carboxamide (10).** Compound **10** was prepared according to a similar procedure described for the synthesis of **9**. Mp 195−208 °C; ^{1}H NMR (500 MHz, DMSO-d_6) δ 12.04 (br s, 1H), 9.96 (br s, 1H), 7.98 (d, J = 8.5 Hz, 1H), 7.73−7.66 (m, 3H), 7.65−7.60 (m, 1H), 7.54−7.48 (m, 1H), 7.44−7.39 (m, 1H), 7.09−7.04 (m, 1H), 4.21 (d, J = 13.0 Hz, 2H), 3.14−3.03 (m, 2H), 2.98 (t, J = 12.0 Hz, 2H), 1.84−1.68 (m, 4H), 1.19−1.04 (m, 4H); ESI MS m/z 494 $[M + H]^+$; HPLC >99% purity (AUC), t_R = 11.4 min (method A).

***N*-(2-((Phenylsulfonyl)carbamoyl)phenyl)-4-(2-(trifluoromethyl)phenyl)piperidine-1-carboxamide (11).** Compound **11** was prepared according to a similar procedure described for the synthesis of **9**. Mp 136−141 °C; ^{1}H NMR (500 MHz, DMSO-d_6) δ 7.99−7.90 (m, 3H), 7.72−7.63 (m, 3H), 7.62−7.58 (m, 1H), 7.56−7.49 (m, 3H), 7.48−7.41 (m, 2H), 7.06−6.99 (m, 1H), 4.15−4.05 (m, 2H), 3.08−2.98 (m, 1H), 2.90−2.81 (m, 2H), 1.67−1.55 (m, 4H); ESI MS m/z 530 $[M + H]^+$; HPLC >99% purity (AUC), t_R = 17.8 min (method C).

2-Oxo-2-(4-(2-(trifluoromethyl)phenyl)piperidin-1-yl)acetic Acid (12). *Step A.* To a solution of 4-(2-(trifluoromethyl)phenyl)-piperidine hydrochloride (**7**, 0.140 g, 0.612 mmol) and Et_3N (0.171 mL, 1.22 mmol) in CH_2Cl_2 (4 mL) was added ethyl 2-chloro-2-oxoacetate (0.100 g, 0.73 mmol) at 0 °C. The mixture stirred at rt for 16 h and was concentrated under reduced pressure. The residue was chromatographed over silica gel (0−25% EtOAc in hexanes) to give ethyl 2-oxo-2-(4-(2-(trifluoromethyl)phenyl)piperidin-1-yl)acetate as a thick oil (0.190 g, 94%): ^{1}H NMR (300 MHz, $CDCl_3$) δ 7.64 (d, J = 7.9 Hz, 1H), 7.54 (t, J = 7.6 Hz, 1H), 7.42 (d, J = 7.8 Hz, 1H), 7.33 (t, J = 7.7 Hz, 1H), 4.72−4.67 (m, 1H), 4.37 (q, J = 7.2 Hz, 2H), 3.83−3.77 (m, 1H), 3.29−3.18 (m, 2H), 2.84−2.75 (m, 1H), 1.92−1.67 (m, 4H), 1.39 (t, J = 7.1 Hz, 3H); ESI MS m/z 330 $[M + H]^+$.

Step B. To a solution of ethyl 2-oxo-2-(4-(2-(trifluoromethyl)-phenyl)piperidin-1-yl)acetate (0.190 g, 0.57 mmol) in CH_3OH (2 mL) and THF (2 mL) was added NaOH (2 N, 2 mL). The mixture was stirred for 16 h, was diluted with H_2O (25 mL), and was acidified to pH 4 with 2 N HCl. The mixture was extracted with CH_2Cl_2 (30 mL), and the organic extracts were dried over Na_2SO_4, filtered, and concentrated. The residue was chromatographed over silica gel (0−15% CH_3OH in CH_2Cl_2) to give 2-oxo-2-(4-(2-(trifluoromethyl)phenyl)piperidin-1-yl)acetic acid (**12**) as a white solid (0.035 g, 20%): mp 193−196 °C; ^{1}H NMR (500 MHz, DMSO-d_6) δ 7.69−7.55 (m, 3H), 7.42 (d, J = 7.6 Hz, 1H), 4.43 (m, 1H), 3.96 (m, 1H), 3.07 (br s, 2H), 2.64 (br s, 1H), 1.69−1.55 (m, 4H); ESI MS m/z 300 $[M - H]^-$; HPLC >99% purity (AUC), t_R = 15.7 min (method C).

3-Oxo-3-(4-(2-(trifluoromethyl)phenyl)piperidin-1-yl)-propanoic Acid (13). *Step A.* To a solution of 4-(2-(trifluoromethyl)-phenyl)piperidine hydrochloride (**7**, 0.130 g, 0.56 mmol) and Et_3N (0.157 mL, 1.13 mmol) in CH_2Cl_2 (10 mL) was added methyl 3-chloro-3-oxopropanoate (0.077 g, 0.567 mmol) at 0 °C. The mixture stirred at rt for 16 h and was concentrated under reduced pressure. The residue was chromatographed over silica gel (0−40% EtOAc in hexanes) to give methyl 3-oxo-3-(4-(2-(trifluoromethyl)phenyl)piperidin-1-yl)-propanoate (0.134 g, 71%): ^{1}H NMR (500 MHz, $CDCl_3$) δ 7.63 (d, J = 7.9 Hz, 1H), 7.53 (t, J = 7.5 Hz, 1H), 7.40 (d, J = 7.8 Hz, 1H), 7.32 (t, J = 7.7 Hz, 1H), 4.85−4.78 (m, 1H), 3.90−3.84 (m, 1H), 3.78 (s, 3H), 3.60−3.49 (m, 2H), 3.28−3.14 (m, 2H), 2.75−2.65 (m, 1H), 1.89−1.64 (m, 4H); ESI MS m/z 330 $[M + H]^+$.

Step B. To a solution of methyl 3-oxo-3-(4-(2-(trifluoromethyl)-phenyl)piperidin-1-yl)propanoate (0.134 g, 0.40 mmol) in CH_3OH (2 mL) and THF (2 mL) was added NaOH (2 N, 2 mL). The mixture was stirred for 16 h, diluted with H_2O (25 mL), and acidified to pH 4 with 2 N HCl. The mixture was extracted with CH_2Cl_2 (30 mL), and the organic extracts were dried over Na_2SO_4 and concentrated to give 3-oxo-3-(4-(2-(trifluoromethyl)phenyl)piperidin-1-yl)propanoic acid (**13**) as a white solid (0.100 g, 78%): mp 112−114 °C; ^{1}H NMR (500 MHz, $CDCl_3$) δ 14.24 (br s, 1H), 7.66 (d, J = 7.8 Hz, 1H), 7.54 (t, J = 7.6 Hz, 1H), 7.38−7.32 (m, 2H), 4.84 (m, 1H), 3.93 (m, 1H), 3.42 (m, 2H), 3.27−3.21 (m, 2H), 2.83−2.77 (m, 1H), 1.99−1.93 (m, 2H), 1.76−1.66 (m, 2H); ESI MS m/z 314 $[M - H]^-$; HPLC >99% purity (AUC), t_R = 15.5 min (method C).

Oxo-4-(4-(2-(trifluoromethyl)phenyl)piperidin-1-yl)butanoic Acid (14). A mixture of 4-(2-(trifluoromethyl)phenyl)piperidine hydrochloride (**7**, 0.100 g, 0.43 mmol) and dihydrofuran-2,5-dione (0.048 g, 0.48 mmol) in CH_2Cl_2 (8 mL) was heated at reflux for 4 h and then cooled to rt and concentrated under reduced pressure. The

dx.doi.org/10.1021/jm5010013 | J. Med. Chem. 2014, 57, 7731−7757

resulting residue was chromatographed over silica gel (0−30% EtOAc in hexanes) to give 4-oxo-4-(4-(2-(trifluoromethyl)phenyl)piperidin-1-yl)butanoic acid (**14**) as a white solid (0.134 g, 93%): mp 138−140 °C; ^{1}H NMR (500 MHz, $CDCl_3$) δ 7.64 (d, J = 7.8 Hz, 1H), 7.52 (t, J = 7.6 Hz, 1H), 7.39 (d, J = 7.8 Hz, 1H), 7.31 (d, J = 7.6 Hz, 1H), 4.81 (m, 1H), 4.01 (m, 1H), 3.22−3.17 (m, 2H), 2.80−2.68 (m, 5H), 1.89 (m, 2H), 1.73−1.65 (m, 2H); ESI MS m/z 330 $[M + H]^+$; HPLC 96.5% purity (AUC), t_R = 15.6 min (method C).

1-(4-(2-(Trifluoromethyl)phenyl)piperidine-1-carbonyl)-pyrrolidine-2-carboxylic Acid (±)-(15). *Step A.* To a solution of 4-(2-(trifluoromethyl)phenyl)piperidine hydrochloride (**7**, 0.080 g, 0.30 mmol) in CH_2Cl_2 was added Et_3N (0.125 mL, 0.90 mmol), followed by methyl 1-(chlorocarbonyl)pyrrolidine-2-carboxylate (0.058 g, 0.30 mmol). The mixture stirred at rt for 6 h, was concentrated, and the resulting residue was chromatographed over silica gel (0−5% CH_3OH in CH_2Cl_2) to give methyl 1-(4-(2-(trifluoromethyl)phenyl)piperidine-1-carbonyl)pyrrolidine-2-carboxylate as a colorless thick oil (0.098 g, 84%): ^{1}H NMR (300 MHz, $CDCl_3$) δ 7.63 (d, J = 7.8 Hz, 1H), 7.49 (m, 2H), 7.29 (m, 1H), 4.60−4.55 (m, 1H), 4.02−3.90 (m, 2H), 3.75 (s, 3H), 3.60−3.44 (m, 2H), 3.12−2.82 (m, 3H), 2.33−2.23 (m, 1H), 2.09−1.64 (m, 7H); ESI MS m/z 385 $[M + H]^+$.

Step B. To a solution of methyl 1-(4-(2-(trifluoromethyl)phenyl)-piperidine-1-carbonyl)pyrrolidine-2-carboxylate (0.098 g, 0.25 mmol) in CH_3OH (2 mL) and THF (2 mL) was added aqueous 2 N NaOH (2 mL). The mixture stirred at rt for 4 h and was then diluted with H_2O and acidified to pH 5with 2 N HCl. The mixture was extracted with EtOAc (3 × 30 mL), and the organic extracts were dried over Na_2SO_4, filtered, and concentrated under reduced pressure. The residue was chromatographed over silica gel (0−10% CH_3OH in CH_2Cl_2) to give 1-(4-(2-(trifluoromethyl)phenyl)piperidine-1-carbonyl)pyrrolidine-2-carboxylic acid (±)-(**15**) as a white solid (0.086 g, 91%): ^{1}H NMR (300 MHz, $CDCl_3$) δ 7.63 (d, J = 7.8 Hz, 1H), 7.51 (t, J = 7.5 Hz, 1H), 7.43 (d, J = 7.6 Hz, 1H), 7.30 (t, J = 7.7 Hz, 1H), 4.54 (m, 1H), 4.01−3.94 (m, 2H), 3.51 (m, 2H), 3.17−2.89 (m, 3H), 2.33−1.66 (m, 8H); ESI MS m/z 327 $[M - CO_2 + H]^+$; HPLC 98.1% purity (AUC), t_R = 17.6 min (method A).

2-(3-Methyl-3-(2-(2-(trifluoromethyl)phenoxy)ethyl)ureido)-benzoic Acid (20). *Step A.* A mixture of (2-bromoethoxy)-*tert*-butyldimethylsilane (4.6 mL, 23.1 mmol), 2-trifluoromethylphenol (2.50 g, 15.4 mmol), KI (0.046 g, 0.27 mmol), and Cs_2CO_3 (10.0 g, 30.8 mmol) in DMF (69 mL) was heated at 50 °C for 18 h. The mixture was allowed to cool to rt and was diluted with H_2O (300 mL) and extracted with EtOAc (4 × 75 mL). The combined organic extracts were washed with a brine (8 × 50 mL) and concentrated under reduced pressure to give *tert*-butyldimethyl(2-(2-(trifluoromethyl)phenoxy)ethoxy)silane as a clear oil (4.34 g, 88%): ^{1}H NMR (300 MHz, $CDCl_3$) δ 7.58−7.53 (m, 1H), 7.50−7.41 (m, 1H), 7.06−6.94 (m, 2H), 4.16−4.10 (m, 2H), 4.01−3.95 (m, 2H), 0.91−0.87 (m, 9H), 0.10−0.05 (m, 6H).

Step B. To a solution of *tert*-butyldimethyl(2-(2-(trifluoromethyl)-phenoxy)ethoxy)silane (4.20 g, 13.1 mmol) in 1,4-dioxane (14 mL) was added HCl (4 M in 1,4-dioxane, 14 mL). The mixture was stirred for 3 h, then concentrated under reduced pressure. The obtained oil was diluted with EtOAc (40 mL), washed with a saturated brine solution (30 mL), a 5% LiCl solution (2 × 30 mL), and concentrated under reduced pressure. The resulting residue was chromatographed over silica gel (Isco CombiFlash Rf unit, 80 g RediSep column, 0−50% EtOAc in hexanes) to give 2-(2-(trifluoromethyl)phenoxy)ethanol (**18a**) as an impure white solid (1.88 g).

Step C. To a 0 °C cooled solution of 2-(2-(trifluoromethyl)phenoxy)-ethanol (**18a**, 0.800 g, 3.88 mmol) in CH_2Cl_2 (25 mL) was added Dess−Martin periodinane (2.50 g, 4.85 mmol). The mixture was stirred at rt for 18 h, then diluted with CH_2Cl_2 (30 mL), washed with H_2O (4 × 30 mL), and concentrated under reduced pressure. The resulting residue was chromatographed over silica gel (Isco CombiFlash Rf unit, 40 g RediSep column, 0−50% EtOAc in hexanes) to give 2-(2-(trifluoromethyl)phenoxy)acetaldehyde a white solid (0.377 g), which was used as is in the next step.

Step D. A solution of 2-(2-(trifluoromethyl)phenoxy)acetaldehyde (0.337 g, 1.65 mmol) in methylamine (2 N in CH_3OH, 8.3 mL, 16.5 mmol) was stirred at rt for 18 h. The mixture was concentrated to under reduced pressure. The obtained residue was dissolved in EtOH (8.3 mL) and $NaBH_4$ (0.062 g, 1.65 mmol). The mixture stirred at rt for 2 h and was concentrated under reduced pressure. The resulting residue was diluted in 2 N NaOH (40 mL) and extracted with EtOAc (3 × 30 mL). The organic extracts were combined and concentrated under reduced pressure. The obtained residue was chromatographed over silica gel (Isco CombiFlash Rf unit, 12 g RediSep column, 0−10% CH_3OH in CH_2Cl_2 with 0.1% NH_4OH) to give *N*-methyl-2-(2-(trifluoromethyl)-phenoxy)ethanamine (**19a**) as a clear oil (0.070 g, 2% for three steps): ^{1}H NMR (300 MHz, $CDCl_3$) δ 7.59−7.52 (m, 1H), 7.51−7.42 (m, 1H), 7.05−6.93 (m, 2H), 4.16 (t, J = 5.1 Hz, 2H), 3.02−2.97 (m, 2H), 2.51 (s, 3H), missing N−H; ESI MS m/z 220 $[M + H]^+$.

Step E. To a solution of *N*-methyl-2-(2-(trifluoromethyl)phenoxy)-ethanamine (**19a**, 0.058 g, 0.26 mmol) and Et_3N (0.027 g, 0.26 mmol) in CH_2Cl_2 (0.9 mL) was added methyl 2-isocyanatobenzoate (0.047 g, 0.26 mmol). The mixture stirred at rt for 2 h and was then diluted with H_2O (30 mL) and extracted with CH_2Cl_2 (3 × 30 mL). The combined organic extracts were concentrated under reduced pressure. The resulting residue was chromatographed over silica gel (Isco CombiFlash Rf unit, 12 g RediSep column, 0−50% EtOAc in hexanes) to give methyl 2-(3-methyl-3-(2-(2-(trifluoromethyl)phenoxy)ethyl)ureido)benzoate as a white solid (84 mg, 79%): ^{1}H NMR (300 MHz, DMSO-d_6) δ 10.41 (s, 1H), 8.43 (dd, J = 8.7, 0.9 Hz, 1H), 7.94 (dd, J = 7.8, 1.5 Hz, 1H), 7.66−7.52 (m, 3H), 7.30 (d, J = 8.7 Hz, 1H), 7.13−7.00 (m, 2H), 4.27 (t, J = 5.4 Hz, 2H), 3.85 (s, 3H), 3.76 (t, J = 5.4 Hz, 2H), 3.13 (s, 3H); ESI MS m/z 397 $[M + H]^+$.

Step F. To a solution of methyl 2-(3-methyl-3-(2-(2-(trifluoromethyl)phenoxy)ethyl)ureido)benzoate (0.084 g, 0.21 mmol) in THF (4.2 mL) and CH_3OH (1.9 mL) was added a solution of $LiOH·H_2O$ (0.089 g, 2.1 mmol) in H_2O (0.98 mL). The mixture stirred at rt for 4 h and was then acidified to pH 5 with 2 N HCl and diluted with H_2O (20 mL). The resulting precipitate was collected by filtration to provide 2-(3-(2-(2-(*tert*-butyl)phenoxy)ethyl)-3-methylureido)benzoic acid (**20**) as a white solid (0.046 g, 57%): mp 171−173 °C; ^{1}H NMR (500 MHz, DMSO-d_6) δ 13.51 (br s, 1H), 10.89 (s, 1H), 8.46 (dd, J = 8.5, 0.5 Hz, 1H), 7.96 (dd, J = 8.0, 1.5 Hz, 1H), 7.64−7.58 (m, 2H), 7.54−7.49 (m, 1H), 7.29 (d, J = 8.5 Hz, 1H), 7.11−7.06 (m, 1H), 7.02−6.97 (m, 1H), 4.27 (t, J = 5.5 Hz, 2H), 3.75 (t, J = 5.5 Hz, 2H), 3.11 (s, 3H); ESI MS m/z 381 $[M - H]^-$; HPLC 99.0% purity (AUC), t_R = 10.1 min (method B).

2-(3-(2-(2-(*tert*-Butyl)-4-chlorophenoxy)ethyl)-3-methylureido)benzoic Acid (21). Compound **21** was prepared according to a similar procedure described for the synthesis of **20**. Mp 166−169 °C; ^{1}H NMR (500 MHz, DMSO-d_6) δ 13.50 (br s, 1H), 10.92 (s, 1H), 8.47 (dd, J = 8.5, 0.5 Hz, 1H), 7.95 (dd, J = 8.0, 1.5 Hz, 1H), 7.55−7.50 (m, 1H), 7.21 (dd, J = 8.5, 2.5 Hz, 1H), 7.31 (d, J = 2.5 Hz, 1H), 7.06−6.98 (m, 2H), 4.16 (t, J = 6.0 Hz, 2H), 3.81 (t, J = 6.0 Hz, 2H), 3.10 (s, 3H), 1.26 (s, 9H); ESI MS m/z 405 $[M + H]^+$; HPLC >99% purity (AUC), t_R = 12.2 min (method B).

2-(3-(2-(2-(*tert*-Butyl)phenoxy)ethyl)-3-methylureido)-benzoic Acid (25). *Step A.* To a −10 °C cooled suspension of 2-chloroethanamine hydrochloride (35.5 g, 0.306 mol) and $NaHCO_3$ (102.8 g, 1.22 mol) in THF (450 mL) and H_2O (450 mL) stirring in a 2 L, three-necked, round-bottomed flask equipped with a thermometer was carefully added a solution of di-*tert*-butyl dicarbonate (73.4 g, 0.336 mol) in THF (40 mL) dropwise over 30 min. The mixture was allowed to warm to rt and stirred for an additional 24 h. The mixture was diluted with H_2O (200 mL) and extracted with EtOAc (3 × 150 mL). The combined organic extracts were washed with H_2O (100 mL), brine (100 mL), dried over Na_2SO_4, filtered, and concentrated under reduced pressure to give *tert*-butyl (2-chloroethyl)carbamate (**23**) as a clear, colorless oil that was used as is in the next step (60.96 g, quantitative%): ^{1}H NMR (500 MHz, $CDCl_3$) δ 4.89 (bs, 1H), 3.60 (m, 2H), 3.46 (m, 2H), 1.45 (s, 9H).

Step B. A 2 L, three-necked, round-bottomed flask equipped with a thermometer, reflux condenser, and mechanical stirrer were charged with *tert*-butyl (2-chloroethyl)carbamate (**23**, 65.28 g, 337 mmol), 2-(*tert*-butyl)phenol (34.0 mL, 222 mmol), KI (0.365 g, 2.20 mmol), Cs_2CO_3 (183 g, 560 mmol), and DMF (700 mL), and the mixture was heated at 60 °C for 16 h. The mixture was allowed to cool to rt and was

dx.doi.org/10.1021/jm5010013 | J. Med. Chem. 2014, 57, 7731−7757

diluted with H_2O (1 L) and extracted with EtOAc (3 × 200 mL). The combined organic extracts were washed with 5% aqueous LiCl solution (3 × 250 mL), brine (250 mL), dried over Na_2SO_4, filtered, and concentrated under reduced pressure. The residue was purified over a plug of silica gel (0−15% EtOAc in hexanes) to give *tert*-butyl (2-(2-(*tert*-butyl)phenoxy)ethyl)carbamate (**24**) as a yellow solid (53.46 g, 82%): ^{1}H NMR (500 MHz, $CDCl_3$) δ 7.28 (m, 1H), 7.16 (m, 1H), 6.92 (m, 1H), 6.83 (m, 1H), 4.83 (bs, 1H), 4.07 (m, 2H), 3.59 (m, 2H), 1.39 (s, 9H).

Step C. To a 0 °C cooled solution of $LiAlH_4$ in THF (1.0 M, 367 mL, 360 mmol) in THF (350 mL) in a 3 L, three-necked, round-bottomed flask equipped with a thermometer was carefully added a solution of *tert*-butyl (2-(2-(*tert*-butyl)phenoxy)ethyl)carbamate (**24**, 43.06 g, 147 mmol) in THF (100 mL). Upon complete addition, the mixture was allowed to warm to rt followed by heating at 60 °C for 16 h. The mixture was allowed to cool back to rt and then further cooled to 0 °C. The mixture was carefully quenched by slow addition of H_2O (15 mL), 15% aqueous NaOH solution (15 mL), followed by additional H_2O (40 mL). The rate of quenching was done carefully so as to maintain an internal temperature below 25 °C. The mixture stirred for 1 h and was filtered through Celite. The aqueous filtrate was extracted with Et_2O (2 × 150 mL), and the organic extracts were combined, dried over Na_2SO_4, filtered, and concentrated under reduced pressure. The residue was purified by flash column chromatography (Isco CombiFlash Rf unit, two 330 g RediSep columns, 0−50% CH_3OH in CH_2Cl_2) to give 2-(2-(*tert*-butyl)phenoxy)-*N*-methylethanamine as an oil (13.4 g). This material was dissolved in Et_2O (250 mL) and treated with a solution of 2 M HCl in Et_2O (85 mL) at 0 °C. The mixture stirred for 10 min at rt and was concentrated under reduced pressure to give 2-(2-(*tert*-butyl)phenoxy)-*N*-methylethanamine hydrochloride as a white solid (15.3 g, 43%): ^{1}H NMR (500 MHz, DMSO-d_6) δ 9.14 (bs, 1H), 7.25 (m, 1H), 7.18 (m, 1H), 7.04 (m, 1H), 6.94 (m, 1H), 4.29 (m, 2H), 3.36 (m, 2H), 2.65 (s, 3H), 1.34 (s, 9H).

Step D. To a solution of 2-(2-(*tert*-butyl)phenoxy)-*N*-methylethanamine hydrochloride (0.066 g, 0.312 mmol) and Et_3N (0.038 g, 0.381 mmol) in CH_2Cl_2 (3.0 mL) was added methyl 2-isocyanatobenzoate (0.062 g, 0.352 mmol), and the mixture was stirred at rt for 18 h. The mixture was diluted with H_2O (30 mL), extracted with CH_2Cl_2 (3 × 30 mL), and the combined organic extracts were concentrated under reduced pressure. The resulting residue was chromatographed over silica gel (0−5% CH_3OH in CH_2Cl_2 with 0.01% NH_4OH) to give methyl 2-(3-(2-(2-(*tert*-butyl)phenoxy)ethyl)-3-methylureido)-benzoate as a white solid (0.057 mg, 46%): ^{1}H NMR (300 MHz, $CDCl_3$) δ 10.74 (s, 1H), 8.60 (dd, J = 9.0, 1.2 Hz, 1H), 8.00 (dd, J = 8.1, 1.8 Hz, 1H), 7.55−7.47 (m, 1H), 7.30−7.26 (m, 1H), 7.20−7.12 (m, 1H), 7.02−6.94 (m, 1H), 6.93−6.86 (m, 2H), 4.23 (t, J = 5.4 Hz, 2H), 3.93−3.87 (m, 5H), 3.27 (s, 3H), 1.38 (s, 9H); ESI MS m/z 385 [M + H]$^+$.

Step E. To a solution of methyl 2-(3-(2-(2-(*tert*-butyl)phenoxy)-ethyl)-3-methylureido)benzoate (0.054 g, 0.142 mmol) in THF (2.7 mL) and CH_3OH (1.3 mL) was added a solution of LiOH·H_2O (0.059 g, 1.41 mmol) in H_2O (0.66 mL), and the mixture stirred at rt for 18 h. The mixture was acidified to pH 5with 2 N HCl, diluted with H_2O (10 mL), and extracted with Et_2O (4 × 20 mL). The combined organic extracts were dried over Na_2SO_4, filtered, and concentrated to provide 2-(3-(2-(2-(*tert*-butyl)phenoxy)ethyl)-3-methylureido)benzoic acid (**25**) as a white solid (0.037 mg, 97%): mp 136−141 °C; ^{1}H NMR (500 MHz, DMSO-d_6) δ 13.50 (s, 1H), 10.93 (s, 1H), 8.48 (dd, J = 8.5, 0.5 Hz, 1H), 7.95 (dd, J = 8.0, 1.5 Hz, 1H), 7.56−7.50 (m, 1H), 7.21−7.13 (m, 2H), 7.02−6.97 (m, 2H), 6.88−6.83 (m, 1H), 4.15 (t, J = 6.00 Hz, 2H), 3.82 (t, J = 6.0 Hz, 2H), 3.11 (s, 3H), 1.28 (s, 9H); ESI MS m/z 371 [M + H]$^+$; HPLC 98.4% purity (AUC), t_R = 14.3 min (method B).

2-(3-(2-(2-(*tert*-Butyl)-4-fluorophenoxy)ethyl)-3-methylureido)benzoic Acid (11). *Step A.* To a solution of *tert*-butyl (2-chloroethyl)carbamate (**23**, 2.61 g, 14.5 mmol) in THF (40 mL) was added CH_3I (9.0 mL, 145 mmol) at rt, followed by dropwise addition of a solution of LiHMDS (1.0 M in THF, 18.9 mL, 18.9 mmol) over 10 min. The reaction mixture stirred at rt for an additional 20 min and was then diluted with H_2O (75 mL) and extracted with Et_2O (4 × 100 mL). The combined organics were washed with a saturated brine solution (2 × 30 mL), dried over Na_2SO_4, filtered, and concentrated under reduced pressure to provide *tert*-butyl (2-chloroethyl)(methyl)carbamate as a yellow oil (2.61 g, 92%): ^{1}H NMR (300 MHz, $CDCl_3$) δ 3.68−3.45 (m, 4H), 2.93 (s, 3H), 1.46 (s, 9H).

Step B. A mixture of *tert*-butyl (2-chloroethyl)(methyl)carbamate (1.72 g, 8.92 mmol), 2-(*tert*-butyl)-4-fluorophenol (1.00 g, 5.94 mmol), KI (18 mg, 0.10 mmol), and Cs_2CO_3 (4.93 g, 15.1 mmol) in DMF (23 mL) was heated at 60 °C for 100 h. The mixture was allowed to cool to rt and was diluted with H_2O (100 mL) and extracted with EtOAc (4 × 80 mL). The combined organic extracts were washed with a saturated brine solution (2 × 50 mL) and concentrated under reduced pressure. The resulting residue was chromatographed over silica gel (Isco CombiFlash Rf unit, 40 g RediSep column, 0−10% EtOAc in hexanes) to give *tert*-butyl (2-(2-(*tert*-butyl)-4-fluorophenoxy)ethyl)(methyl)carbamate (**26**) as an orange oil (0.490 g, 25%): ^{1}H NMR (300 MHz, $CDCl_3$) δ 7.03−6.95 (m, 1H), 6.88−6.73 (m, 2H), 4.07 (t, J = 5.7 Hz, 2H), 3.66 (t, J = 5.7 Hz, 2H), 2.97 (s, 3H), 1.46, (s, 9H), 1.36 (s, 9H).

Step C. To a solution of *tert*-butyl (2-(2-(*tert*-butyl)-4-fluorophenoxy)ethyl)(methyl)carbamate (**26**, 0.490 g, 1.51 mmol) in CH_2Cl_2 (6.0 mL) was added HCl (2 N solution in Et_2O, 6.0 mL), and the mixture stirred at rt for 6 h. The mixture was then diluted with Et_2O (30 mL), and the resulting solids were collected by filtration to give 2-(2-(*tert*-butyl)-4-fluorophenoxy)-*N*-methylethanamine hydrochloride as a white solid (0.185 g, 46%): ^{1}H NMR (300 MHz, DMSO-d_6) δ 8.84 (br s, 2H), 7.08−6.98 (m, 3H), 4.24 (t, J = 5.7 Hz, 2H), 3.43−3.28 (m, 2H, overlaps with H_2O), 2.67 (s, 3H), 1.33 (s, 9H); ESI MS m/z 226 [M + H]$^+$.

Step D. To a solution of 2-(2-(*tert*-butyl)-4-fluorophenoxy)-*N*-methylethanamine hydrochloride (0.085 g, 0.32 mmol) and Et_3N (0.066 g, 0.65 mmol) in CH_2Cl_2 (1.1 mL) was added methyl 2-isocyanatobenzoate (0.064 g, 0.326 mmol). The mixture was stirred at rt for 3 h, was then diluted with H_2O (10 mL), and was extracted with CH_2Cl_2 (4 × 10 mL). The combined organic extracts were concentrated under reduced pressure. The resulting residue was chromatographed over silica gel (Isco CombiFlash Rf unit, 12 g RediSep column, 0−20% EtOAc in hexanes) to give methyl 2-(3-(2-(2-(*tert*-butyl)-4-fluorophenoxy)ethyl)-3-methylureido)benzoate as a white solid (0.116 g, 88%): ^{1}H NMR (300 MHz, $CDCl_3$) δ 10.74 (s, 1H), 8.60 (d, J = 8.7 Hz, 1H), 8.00 (dd, J = 8.1, 1.5 Hz, 1H), 7.55−7.48 (m, 1H), 7.01−6.94 (m, 2H), 6.83−6.78 (m, 2H), 4.18 (t, J = 5.7 Hz, 2H), 3.91−3.84 (m, 5H), 3.26 (s, 3H), 1.36 (s, 9H); ESI MS m/z 403 [M + H]$^+$.

Step E. To a solution of methyl 2-(3-(2-(2-(*tert*-butyl)-4-fluorophenoxy)ethyl)-3-methylureido)benzoate (0.110 g, 0.27 mmol) in THF (5.4 mL) and CH_3OH (2.8 mL) was added a solution of LiOH·H_2O (0.114 g, 2.73 mmol) in H_2O (1.4 mL). The mixture stirred at rt for 18 h, was then acidified to pH 5 with 2 N HCl, and was diluted with H_2O (30 mL). The resulting solids were collected by filtration and washed with H_2O to provide 2-(3-(2-(2-(*tert*-butyl)-4-fluorophenoxy)ethyl)-3-methylureido)benzoic acid (**27**) as a white solid (0.099 g, 93%): mp 145−150 °C; ^{1}H NMR (500 MHz, DMSO-d_6) δ 13.51 (s, 1H), 10.94 (s, 1H), 8.47 (d, J = 8.5 Hz, 1H), 7.95 (dd, J = 8.0, 1.5 Hz, 1H), 7.55−7.49 (m, 1H), 7.03−6.93 (m, 4H), 4.14 (t, J = 5.5 Hz, 2H), 3.80 (t, J = 6.0 Hz, 2H), 3.10 (s, 3H), 1.26 (s, 9H); ESI MS m/z 389 [M + H]$^+$; HPLC >99% purity (AUC), t_R = 11.6 min (method B).

2-(2,3,4,5-Tetrahydro-1*H*-benzo[*d*]azepine-3-carboxamido)-benzoic Acid (28). *Step A.* To a solution of 2,3,4,5-tetrahydro-1*H*-benzo[*d*]azepine (0.110 g, 0.74 mmol) and Et_3N (0.12 mL, 0.82 mmol) in CH_2Cl_2 (2.4 mL) was added methyl 2-isocyanatobenzoate (0.132 mg, 0.74 mmol), and the mixture stirred at rt for 2 h. The mixture was diluted with H_2O (20 mL) and extracted with CH_2Cl_2 (3 × 30 mL). The combined organic extracts were concentrated under reduced pressure, and the resulting residue was chromatographed over silica gel (Isco CombiFlash Rf unit, 12 g RediSep column, 0−25% EtOAc in hexanes) to give methyl 2-(2,3,4,5-tetrahydro-1*H*-benzo[*d*]azepine-3-carboxamido)benzoate as a clear film (0.203 g, 83%): ^{1}H NMR (500 MHz, DMSO-d_6) δ 10.46 (br s, 1H), 8.34 (d, J = 8.0 Hz, 1H), 7.94 (dd, J = 8.0, 1.5 Hz, 1H), 7.58−7.53 (m, 1H), 7.20−7.16 (m, 2H), 7.15−7.10 (m, 2H), 7.06−7.02 (m, 1H), 3.89 (s, 3H), 3.68−3.61 (m, 4H), 3.01−2.94 (m, 4H); ESI MS m/z 325 [M + H]$^+$.

dx.doi.org/10.1021/jm5010013 | J. Med. Chem. 2014, 57, 7731−7757

Step B. To a solution of methyl 2-(2,3,4,5-tetrahydro-1*H*-benzo[*d*]-azepine-3-carboxamido)benzoate (0.197 g, 0.60 mmol) in THF (12.0 mL) and CH_3OH (5.6 mL) was added a solution of $LiOH·H_2O$ (0.255 g, 6.07 mmol) in H_2O (2.8 mL). The mixture stirred at rt for 3 h, was neutralized with 2 N HCl, and was diluted with H_2O (30 mL). The resulting precipitate was collected by filtration to give 2-(2,3,4,5-tetrahydro-1*H*-benzo[*d*]azepine-3-carboxamido)benzoic acid (**28**) as a white solid (0.065 mg, 34%): mp 272−278 °C; ^{1}H NMR (500 MHz, DMSO-d_6) δ 14.18 (br s, 1H), 8.30 (d, J = 8.5 Hz, 1H), 7.92 (d, J = 7.5 Hz, 1H), 7.19−7.08 (m, 5H), 6.79−6.74 (m, 1H), 3.65−3.60 (m, 4H), 2.94−2.88 (m, 4H) missing urea N−H; ESI MS m/z 309 $[M - H]^-$; HPLC >99% purity (AUC), t_R = 14.8 min (method A).

2-((1*R*,5*S*,6*s*)-6-(2-(Trifluoromethyl)phenyl)-3-azabicyclo-[3.1.0]hexane-3-carboxamido)benzoic Acid (29). *Step A.* A mixture of 2-(trifluoromethyl)benzaldehyde (5.0 g, 28.7 mmol) and hydrazine hydrate (1.43 g, 28.7 mmol) in *i*-PrOH (100 mL) was heated at reflux for 1 h. The mixture cooled to rt and was concentrated under reduced pressure providing (*E*)-(2-(trifluoromethyl)benzylidene)-hydrazine, which was a yellow oil that crystallized upon standing (5.1 g, 94%). The material was used as is in the next step.

Step B. To a solution of (*E*)-(2-(trifluoromethyl)benzylidene)-hydrazine (5.0 g, 26.5 mmol) in 1,4-dioxane (200 mL) was added MnO_2 (23.1 g, 256 mmol) portionwise, and the mixture stirred at rt for 3 h. The slurry was filtered through Celite and rinsed with additional 1,4-dioxane (50 mL). To the filtrate was added 1-benzyl-1*H*-pyrrole-2,5-dione (4.92 g, 26.5 mmol), and the mixture was stirred at rt for 48 h. The mixture was concentrated under reduced pressure and the resulting residue was chromatographed over silica gel (Isco CombiFlash Rf unit, 330 g RediSep column, 0−5% EtOAc in hexanes) to give (1*R*,5*S*,6*s*)-3-benzyl-6-(2-(trifluoromethyl)phenyl)-3-azabicyclo[3.1.0]hexane-2,4-dione (1.52 g, 17%) as a white solid: ^{1}H NMR (500 MHz, $CDCl_3$) δ 7.69 (d, J = 7.8 Hz, 1H), 7.52 (m, 1H), 7.49 (m, 1H), 7.40−7.29 (m, 5H), 7.10 (d, J = 7.8 Hz, 1H), 4.58 (s, 2H) 2.90 (m, 1H), 2.82 (m, 2H); ESI MS m/z 346 $[M + H]^+$.

Step C. To a solution of (1*R*,5*S*,6*s*)-3-benzyl-6-(2-(trifluoromethyl)-phenyl)-3-azabicyclo[3.1.0]hexane-2,4-dione (1.24 g, 3.59 mmol) in THF (20 mL) was added $NaBH_4$ (0.339 g, 8.97 mmol), and the mixture stirred at rt for 15 min. To this was added $BF_3·Et_2O$ (1.0 M solution in THF, 5.38 mL, 5.38 mmol) dropwise (gas evolution was observed). The mixture was then heated at 50 °C for 5 h. The mixture was allowed to cool back to rt and was carefully quenched by dropwise addition of H_2O (added until gas evolution no longer occurred). To this was added CH_3OH (60 mL), and the resulting mixture was stirred at reflux for 16 h. The mixture cooled back to rt and was concentrated under reduced pressure. The resulting residue was taken up in H_2O (50 mL) and extracted with EtOAc (3 × 50 mL). The combined organic extracts were concentrated under reduced pressure, and the resulting residue was chromatographed over silica gel (Isco CombiFlash Rf unit, 12 g RediSep column, 0−25% EtOAc in hexanes) to give (1*R*,5*S*,6*s*)-3-benzyl-6-(2-(trifluoromethyl)phenyl)-3-azabicyclo[3.1.0]hexane as a colorless, viscous oil (0.720 g, 64%): ^{1}H NMR (500 MHz, $CDCl_3$) δ 7.64 (d, J = 7.8 Hz, 1H), 7.45 (m, 1H), 7.35−7.35 (m, 4H), 7.29−7.21 (m, 2H), 7.08 (d, J = 7.8 Hz, 1H), 3.67 (s, 2H), 3.14 (d, J = 7.8 Hz, 2H), 2.71 (m, 1H), 2.49 (m, 2H), 1.74 (m, 2H).

Step D. A mixture of (1*R*,5*S*,6*s*)-3-benzyl-6-(2-(trifluoromethyl)-phenyl)-3-azabicyclo[3.1.0]hexane (0.700 g, 2.20 mmol) and 10% Pd/C (0.200 g) in CH_3OH (50 mL) was subjected to a 50 psi atmosphere of H_2 at rt for 4 h using a Parr shaker apparatus. The mixture was filtered through Celite and the filtrate was concentrated under reduced pressure to give (1*R*,5*S*,6*s*)-6-(2-(trifluoromethyl)phenyl)-3-azabicyclo[3.1.0]-hexane as a viscous oil (0.478 g, 95%): ^{1}H NMR (500 MHz, $CDCl_3$) δ 7.61 (d, J = 7.8 Hz, 1H), 7.46 (m, 1H), 7.24 (m, 1H), 7.10 (d, J = 7.8 Hz, 1H), 3.17 (d, J = 7.8 Hz, 2H), 3.02 (m, 2H), 1.93 (m, 1H), 1.74 (m, 2H), 1.68 (bs, 1H).

Step E. To a solution of (1*R*,5*S*,6*s*)-6-(2-(trifluoromethyl)phenyl)-3-azabicyclo[3.1.0]hexane (0.100 g, 0.44 mmol) in CH_2Cl_2 (10 mL) was added methyl 2-isocyanatobenzoate (0.078 g, 0.44 mmol), and the mixture stirred at rt for 2 h. The mixture was diluted with H_2O (20 mL) and extracted with CH_2Cl_2 (3 × 30 mL). The combined organic extracts were concentrated under reduced pressure, and the resulting residue was chromatographed over silica gel (Isco CombiFlash Rf unit, 12 g RediSep column, 0−25% EtOAc in hexanes) to give methyl 2-((1*R*,5*S*,6*s*)-6-(2-(trifluoromethyl)phenyl)-3-azabicyclo[3.1.0]hexane-3-carboxamido)-benzoate as a white solid (0.110 g, 62%): ^{1}H NMR (500 MHz, $CDCl_3$) δ 10..55 (bs, 1H), 8.62 (m, 1H), 8.07 (m, 1H), 7.65 (m, 1H), 7.55−7.43 (m, 2H), 7.25 (m, 1H), 7.11 (m, 1H), 6.95 (m, 1H), 3.97 (m, 5H), 3.72 (m, 2H), 2.19 (m, 1H), 2.09 (m, 2H); ESI MS m/z 403 $[M - H]^-$.

Step F. To a solution of methyl 2-((1*R*,5*S*,6*s*)-6-(2-(trifluoromethyl)-phenyl)-3-azabicyclo[3.1.0]hexane-3-carboxamido)benzoate (0.110 g, 0.27 mmol) in THF (2 mL) and CH_3OH (4 mL) was added 2 N NaOH (2 mL). The mixture was stirred at rt for 3 h and was then acidified to pH 5 with 2 N HCl. The resulting precipitate was collected by filtration to 2-((1*R*,5*S*,6*s*)-6-(2-(trifluoromethyl)phenyl)-3-azabicyclo[3.1.0]hexane-3-carboxamido)benzoic acid (**29**) as a white solid (0.105 g, 98%): mp 205−208 °C; ^{1}H NMR (500 MHz, DMSO-d_6) δ 13.52 (bs, 1H), 10.74 (bs, 1H), 8.49 (m, 1H), 7.97 (m, 1H), 7.70 (m, 1H), 7.61 (m, 1H), 7.55 (m, 1H), 7.42 (m, 1), 7.31 (m, 1H), 6.99 (m, 1H), 3.74 (m, 2H), 3.65 (m, 2H), 2.19 (m, 2H), 1.92 (m, 1H); ESI MS m/z 389 $[M - H]^-$; HPLC 97.3% purity (AUC), t_R = 20.4 min (method A).

2-((1*R*,5*S*,6*r*)-6-(2-(Trifluoromethyl)phenyl)-3-azabicyclo-[3.1.0]hexane-3-carboxamido)benzoic Acid (30). Compound **30** was prepared according to a similar procedure described for the synthesis of **29**. Mp 162−165 °C; ^{1}H NMR (500 MHz, DMSO-d_6) δ 8.06 (m, 1H), 7.87 (m, 1H), 7.65 (m, 1H), 7.49 (m, 2H), 7.32 (m, 2H), 6.85 (m, 1H), 3.70 (m, 1H), 3.50 (m, 2H), 2.31 (m, 1H), 2.11 (m, 2H), N−H missing; ESI MS m/z 389 $[M - H]^-$; HPLC >99% purity (AUC), t_R = 13.2 min (method A).

2-(6-(2-(Trifluoromethyl)phenyl)-2,6-diazaspiro[3.3]-heptane-2-carboxamido)benzoic Acid (31). *Step A.* A mixture of *tert*-butyl 2,6-diazaspiro[3.3]heptane-2-carboxylate hemioxalate (0.200 g, 1.01 mmol), 1-bromo-(2-trifluoromethyl)benzene (0.14 mL, 1.03 mmol), $Pd(dba)_3$ (0.014 g, 0.015 mmol), *rac*-BINAP(0.140 g, 0.225 mmol), and K_2CO_3 (0.340 g, 3.03 mmol) in toluene (5 mL) was heated at 110 °C in a sealed tube for 24 h. The mixture cooled to rt and was diluted with EtOAc (10 mL), filtered through Celite, and the filtrate was concentrated under reduced pressure. The residue was chromatographed over silica gel (Isco CombiFlash Rf unit, 40 g RediSep column, 0−100% EtOAc in hexanes) to provide *tert*-butyl 6-(2-(trifluoromethyl)phenyl)-2,6-diazaspiro[3.3]heptane-2-carboxylate as a tan solid (0.131 g, 38%): ^{1}H NMR (500 MHz, $CDCl_3$) δ 7.50−7.48 (m, 1H), 7.37−7.37 (m, 1H), 6.81−6.78 (m, 1H), 6.48 (d, J = 8.5 Hz, 1H), 4.05−4.10 (m, 8H), 1.44 (s, 9H).

Step B. To a solution of *tert*-butyl 6-(2-(trifluoromethyl)phenyl)-2,6-diazaspiro[3.3]heptane-2-carboxylate (0.131 g, 0.38 mmol) in CH_2Cl_2(2 mL) was added 2 M HCl in Et_2O (2 mL), and the mixture stirred at rt for 4 h. The mixture was concentrated under reduced pressure, and the resulting residue was dissolved in CH_2Cl_2 (4 mL). To this solution were added Et_3N (0.12 mL, 0.86 mmol) and methyl-2-isocyanatobenzoate (80 mg, 0.45 mmol), and the mixture stirred at rt for 24 h. The mixture was washed with saturated aqueous 2 M $NaHCO_3$ solution (10 mL) and extracted with CH_2Cl_2 (2 × 10 mL). The combined organic extracts were dried over Na_2SO_4, filtered, and concentrated under reduced pressure. The resulting residue was chromatographed over silica gel (Isco CombiFlash Rf unit, 24 g RediSep column, 0−50% EtOAc in hexanes) to provide methyl 2-(6-(2-(trifluoromethyl)phenyl)-2,6-diazaspiro[3.3]heptanes-2-carboxamido)-benzoate as an off-white solid (0.080 g, 50%): ^{1}H NMR (500 MHz, $CDCl_3$) δ 8.52 (d, J = 8.5 Hz, 1H), 7.99−7.98 (m, 1H), 7.53−7.44 (m, 2H), 7.36−7.33 (m, 1H), 6.99−6.96 (m, 2H), 6.71 (t, J = 7.5 Hz, 1H), 4.86 (br s, 1H), 3.92 (s, 3H), 3.68 (d, J = 11.35 Hz, 2H), 3.55 (d, J = 11.35 Hz, 2H), 3.47−3.46 (m, 2H), 3.35−3.34 (m, 2H).

Step C. To a mixture of methyl 2-(6-(2-(trifluoromethyl)phenyl)-2,6-diazaspiro[3.3]heptanes-2-carboxamido)benzoate (0.080 g, 0.19 mmol) in CH_3OH (3 mL) and THF (3 mL) was added $LiOH·H_2O$ (0.080 g, 1.91 mmol) in H_2O (10 mL). The mixture was stirred at rt for 3 h followed by acidification to pH 6 with 2 N HCl. The mixture was further diluted with H_2O (10 mL), and the resulting precipitate was collected by filtration. The material was recrystallized from EtOAc and heptanes to provide (**31**) 2-(6-(2-(trifluoromethyl)phenyl)-2,6-diazaspiro[3.3]-heptanes-2-carboxamido)benzoic acid as a white solid (0.049 mg,

dx.doi.org/10.1021/jm5010013 | J. Med. Chem. 2014, 57, 7731−7757

64%): mp 181−184 °C; ^{1}H NMR (500 MHz, DMSO-d_6) δ 11.66 (s, 1H), 7.96 (m, 1H), 7.69−7.66 (m, 1H), 7.45−7.42 (m, 2H), 7.24−7.18 (m, 2H), 6.92−6.90 (m, 1H), 6.72 (t, J = 7.5 Hz, 1H), 6.07−6.05 (m, 1H), 4.31−4.21 (m, 2H), 3.86−3.79 (m, 4H), 3.48−3.45 (m, 2H); ESI MS m/z 404 $[M - H]^-$; HPLC 96.4% purity (AUC), t_R = 14.7 min (method A).

2-(3-(2-(Trifluoromethyl)phenyl)azetidine-1-carboxamido)-benzoic Acid (32). Compound **32** was prepared according to a similar procedure described for the synthesis of **28**. Mp 192−195 °C; ^{1}H NMR (500 MHz, DMSO-d_6) δ 13.52 (br s, 1H), 10.59 (s, 1H), 8.46 (d, J = 8.5 Hz, 1H), 7.97−7.91 (m, 2H), 7.78−7.71 (m, 2H), 7.57−7.48 (m, 2H), 7.04−6.98 (m, 1H), 4.47−4.37 (m, 2H), 4.25−4.17 (m, 1H), 4.15−4.02 (m, 2H); ESI MS m/z 363 $[M - H]^-$; HPLC >99% purity (AUC), t_R = 13.8 min (method B).

2-(3-(2-(Trifluoromethyl)phenoxy)azetidine-1-carboxamido)benzoic Acid (33). *Step A.* To a 0 °C cooled solution of azetidin-3-ol hydrochloride (2.00 g, 18.21 mmol) and Et_3N (3.65 mL, 26.01 mmol) in CH_3OH (18 mL) was added di-*tert*-butyl dicarbonate (2.82 g, 12.9 mmol). The resulting mixture stirred at rt for 18 h. The mixture diluted with CH_2Cl_2 (100 mL) and washed with H_2O (3 × 30 mL). The organic layer was dried over Na_2SO_4, filtered, and concentrated under reduced pressure to give *tert*-butyl 3-hydroxyazetidine-1-carboxylate as a white solid (1.74 g, 78%): ^{1}H NMR (500 MHz, DMSO-d_6) δ5.62−5.58 (m, 1H), 4.39−4.32 (m, 1H), 4.01−3.93 (m, 2H), 3.60−3.51 (m, 2H), 1.36 (m, 9H).

Step B. To a 0 °C cooled solution of *tert*-butyl 3-hydroxyazetidine-1-carboxylate (1.73 g, 9.99 mmol) and Et_3N (1.69 mL, 12.01 mmol) in CH_2Cl_2 (51 mL) was added MsCl (0.85 mL, 11.0 mmol). The mixture continued to stir at 0 °C for 1 h. The mixture was diluted with a saturated brine solution (70 mL) and extracted with CH_2Cl_2 (3 × 40 mL). The combined organic extracts were dried over Na_2SO_4, filtered, and concentrated under reduced pressure to give to give *tert*-butyl 3-((methylsulfonyl)oxy)azetidine-1-carboxylate as a light yellow oil (2.60 g, >99%): ^{1}H NMR (500 MHz, $CDCl_3$) δ 5.22−5.16 (m, 1H), 4.29−4.24 (m, 2H), 4.12−4.07 (m, 2H), 3.06 (s, 3H), 1.44 (s, 9H).

Step C. A mixture of *tert*-butyl 3-((methylsulfonyl)oxy)azetidine-1-carboxylate (2.51 g, 9.99 mmol), 2-trifluoromethylphenol (1.62 g, 9.99 mmol), Cs_2CO_3 (3.57 g, 11.0 mmol) in DMF (90 mL) was heated at 80 °C for 18 h. The mixture was allowed to cool to rt and was diluted with a saturated brine solution (50 mL) and extracted with EtOAc (3 × 50 mL). The combined organic extracts were washed with a saturated brine solution (2 × 50 mL) and concentrated under reduced pressure. The resulting residue was chromatographed over silica gel (Isco CombiFlash Rf unit, 40 g RediSep column, 0−60% EtOAc in hexanes) to give *tert*-butyl 3-(2-(trifluoromethyl)phenoxy)azetidine-1-carboxylate as a clear oil (1.49 mg, 47%): ^{1}H NMR (500 MHz, $CDCl_3$) δ 7.60 (d, J = 7.5 Hz, 1H), 7.60−7.43 (m, 1H), 7.08−7.04 (m, 1H), 6.63 (d, J = 8.0 Hz, 1H), 4.98−4.92 (m, 1H), 4.34−4.29 (m, 2H), 4.08−4.04 (m, 2H), 1.45 (s, 9H); ESI MS m/z 262 $[M - t\text{-Bu}]^+$.

Step D. To a solution of *tert*-butyl 3-(2-(trifluoromethyl)phenoxy)-azetidine-1-carboxylate (0.255 g, 0.80 mmol) in CH_3OH (1.5 mL) was added 2 M HCl in Et_2O (1.5 mL), and the mixture was stirred at rt for 2 h. The mixture was diluted with Et_2O (30 mL) and the resulting precipitate was collected by filtration to give 3-(2-(trifluoromethyl)-phenoxy)azetidine as a white solid (0.182 g, 89%): ^{1}H NMR (500 MHz, DMSO-d_6) δ 9.45 (s, 2H), 7.68 (d, J = 7.5 Hz, 1H), 7.65−7.60 (m, 1H), 7.20−7.17 (m, 1H), 7.04 (d, J = 8.5 Hz, 1H), 5.25−5.20 (m, 1H), 4.50−4.45 (m, 2H), 4.01−3.97 (m, 2H); ESI MS m/z 218 $[M + H]^+$.

Step E. To a mixture of 3-(2-(trifluoromethyl)phenoxy)azetidine hydrochloride (0.080 g, 0.31 mmol) and Et_3N (88 μL, 0.63 mmol) in CH_2Cl_2 (1.0 mL) was added methyl 2-isocyanatobenzoate (0.056 g, 0.31 mmol). The mixture stirred at rt for 18 h followed by dilution with H_2O (5 mL). The mixture was extracted with CH_2Cl_2 (3 × 10 mL), and the combined organic extracts were washed with a saturated brine solution (1 × 10 mL) and concentrated under reduced pressure. The resulting residue was chromatographed over silica gel (Isco CombiFlash Rf unit, 12 g RediSep column, 0−50% EtOAc in hexanes) to give methyl 2-(3-(2-(trifluoromethyl)phenoxy)azetidine-1-carboxamido)benzoate as a white solid (92 mg, 74%): ^{1}H NMR (500 MHz, DMSO-d_6) δ 10.04 (s, 1H), 8.35 (d, J = 8.5 Hz, 1H), 7.93 (dd, J = 8.0, 1.5 Hz, 1H), 7.69−7.64 (m, 2H), 7.59−7.55 (m, 1H), 7.19−7.16 (m, 1H), 7.10−7.04 (m, 2H), 5.27−5.24 (m, 1H), 4.58−4.50 (m, 2H), 3.99−3.93 (m, 2H), 3.86 (s, 3H); ESI MS m/z 395 $[M + H]^+$.

Step F. To a mixture of methyl 2-(3-(2-(trifluoromethyl)phenoxy)-azetidine-1-carboxamido)benzoate (0.090 g, 0.22 mmol) in THF (4.5 mL) and CH_3OH (2.1 mL) was added a solution of $LiOH·H_2O$ (0.095 g, 2.28 mmol) in H_2O (1.1 mL). The mixture stirred at rt for 18 h, followed by neutralization with 2 N HCl, and diluted with additional H_2O (30 mL). The resulting precipitate was collected by filtration to provide 2-(3-(2-(trifluoromethyl)phenoxy)azetidine-1-carboxamido)-benzoic acid (**33**) as a white solid (0.074 g, 85%): mp 186−189 °C; ^{1}H NMR (500 MHz, DMSO-d_6) δ 13.53 (br s, 1H), 10.58 (s, 1H), 8.41 (d, J = 8.5 Hz, 1H), 7.95 (dd, J = 8.0, 1.0 Hz, 1H), 7.69−7.62 (m, 2H), 7.56−7.52 (m, 1H), 7.17 (dd, J = 7.5, 1.0 Hz, 1H), 7.09−7.00 (m, 2H), 5.29−5.22 (m, 1H), 4.56−4.48 (m, 2H), 3.98−3.91 (m, 2H); ESI MS m/z 379 $[M - H]^-$; HPLC >99% purity (AUC), t_R = 15.4 min (method A).

(±)-2-(2,3-Dihydrospiro[indene-1,4′-piperidin]-1′-ylcarboxamido)benzoic Acid (±)-(34). Compound (±)-**34** was prepared according to a similar procedure described for the synthesis of **28**. Mp 166−170 °C; ^{1}H NMR (500 MHz, DMSO-d_6) δ 13.52 (s, 1H), 10.96 (s, 1H), 8.43 (d, J = 8.5 Hz, 1H), 7.95 (dd, J = 8.0, 1.5 Hz, 1H), 7.56−7.50 (m, 1H), 7.23−7.19 (m, 2H), 7.17−7.12 (m, 2H), 7.03−6.99 (m, 1H), 4.11−4.01 (m, 2H), 3.17−3.05 (m, 2H), 2.89 (t, J = 7.5 Hz, 2H), 2.08 (t, J = 7.5 Hz, 2H), 1.81−1.74 (m, 2H), 1.59−1.48 (m, 2H); ESI MS m/z 351 $[M + H]^+$; HPLC >99% purity (AUC), t_R = 16.7 min (method A).

2-((3a*R*,5*r*,6a*S*)-5-(2-(Trifluoromethyl)phenyl)-octahydrocyclopenta[*c*]pyrrole-2-carboxamido)benzoic Acid (43). *Step A.* To a 0 °C cooled solution of $LiAlH_4$ in THF (1.0 M, 800 mL, 800 mmol) in THF (800 mL) was carefully added (3a*R*,7a*S*)-3a,4,7,7a-tetrahydro-1*H*-isoindole-1,3(2*H*)-dione (**35**, 53.7 g, 0.35 mol) portionwise. An exotherm of ∼5 °C occurred upon each addition of **35**. Upon complete addition, the mixture was allowed to warm to rt followed by heating at 70 °C for 16 h. The mixture was allowed to cool back to rt and then further cooled to 0 °C. The reaction was carefully quenched by slow addition of H_2O (30 mL), 15% aqueous NaOH solution (30 mL), followed by another bolus of H_2O (90 mL). The rate of quenching was done carefully so as to maintain an internal temperature below 25 °C. The mixture stirred for 1 h and was filtered through Celite. The aqueous filtrate was extracted with Et_2O (2 × 100 mL), and the organic extracts were combined and concentrated under reduced pressure. The resulting residue was purified using a Kugelrorh distillation apparatus to give (3a*R*,7a*S*)-2,3,3a,4,7,7a-hexahydro-1*H*-isoindole as a clear, colorless oil (19.45 g, 44%): ^{1}H NMR (500 MHz, $CDCl_3$) δ 5.29 (s, 2H), 3.88 (bs, 1H), 3.26 (m, 2H), 2.82 (m, 2H), 2.41−2.19 (m, 4H), 1.96 (m, 2H).

Step B. To a 0 °C cooled solution of (3a*R*,7a*S*)-2,3,3a,4,7,7a-hexahydro-1*H*-isoindole (11.5 g, 93.5 mmol) in CH_2Cl_2 (200 mL) was added Boc_2O (24.5 g, 112 mmol), and the mixture was stirred at rt for 16 h. The mixture was washed with H_2O (100 mL), brine (100 mL), dried over Na_2SO_4, filtered, and concentrated under reduced pressure. The residue was purified by flash column chromatography (Isco CombiFlash Rf unit, 330 g RediSep column, 0−30% EtOAc in hexanes) to give (3a*R*,7a*S*)-*tert*-butyl 3a,4,7,7a-tetrahydro-1*H*-isoindole-2(3*H*)-carboxylate (**36**) as an oil (20.10 g, 49%): ^{1}H NMR (500 MHz, $CDCl_3$) δ 5.64 (s, 2H), 3.39 (m, 2H), 3.20 (m, 2H), 3.15 (m, 2H), 2.23−2.19 (m, 4H), 1.97 (m, 2H), 1.57 (s, 9H).

Step C. To a 0 °C cooled mixture of (3a*R*,7a*S*)-*tert*-butyl 3a,4,7,7a-tetrahydro-1*H*-isoindole-2(3*H*)-carboxylate (**36**, 66.78 g, 224 mmol) in CH_3CN (600 mL), CCl_4 (400 mL), and H_2O (800 mL) was added $NaIO_4$ (192.3 g, 899 mmol) followed by $RuO_2·H_2O$ (1.19 g, 8.94 mmol). The mixture was stirred at rt for 24 h with mechanical stirring and then filtered through Celite. The filter cake was washed with 10% CH_3OH in CH_2Cl_2 (200 mL), and the biphasic mother liquor was separated. The aqueous phase was further extracted with CH_2Cl_2 (3 × 150 mL), and the combined organic extracts were washed with H_2O (100 mL), brine (100 mL), dried over Na_2SO_4, filtered, and concentrated under reduced pressure. The residue was filtered through a plug of silica gel using a CH_3OH/CH_2Cl_2 eluent system (2%−10% CH_3OH in CH_2Cl_2). The filtrate was concentrated under reduced

dx.doi.org/10.1021/jm5010013 | J. Med. Chem. 2014, 57, 7731−7757

pressure to give 2,2′-((3*S*,4*R*)-1-(*tert*-butoxycarbonyl)pyrrolidine-3,4-diyl)diacetic acid (**37**) as a solid (46.75 g, 72%): ^{1}H NMR (500 MHz, DMSO-d_6) δ 12.2 (s, 2H), 3.38 (m, 2H), 3.02 (m, 2H), 2.49 (m, 2H), 2.32 (m, 2H), 2.29 (m, 2H), 1.42 (s, 9H).

Step D. To a suspension of 2,2′-((3*S*,4*R*)-1-(*tert*-butoxycarbonyl)-pyrrolidine-3,4-diyl)diacetic acid (**37**, 6.97 g, 24.31 mmol) in Ac_2O (50 mL) was added NaOAc (1.99 g, 24.31 mmol), and the mixture was heated at 120 °C for 3 h. The mixture cooled to rt and filtered through Celite. The filter cake was washed with Et_2O (5 × 50 mL), and the mother liquor was concentrated under reduced pressure. The resulting residue was purified by flash column chromatography (Isco CombiFlash Rf unit, 120 g RediSep column, 0−30% EtOAc in hexanes) to give (3a*R*,6a*S*)-*tert*-butyl 5-oxohexahydrocyclopenta[*c*]pyrrole-2(1*H*)-carboxylate (**38**) as a white foam (2.17 g, 40%): ^{1}H NMR (500 MHz, $CDCl_3$) δ 3.69 (m, 2H), 3.22 (m, 2H), 2.91 (m, 2H), 2.50 (m, 2H), 2.17 (m, 2H), 1.46 (s, 9H).

Step E. To a −78 °C cooled solution of (3a*R*,6a*S*)-*tert*-butyl 5-oxohexahydrocyclopenta[*c*]pyrrole-2(1*H*)-carboxylate (**38**, 22.35 g, 99.2 mmol) in THF (500 mL) was slowly added a solution of LiHMDS in THF (1.0 M, 129 mL). The mixture continued to stir at −78 °C for 30 min, and then a solution of 1,1,1-trifluoro-*N*-phenyl-*N*-((trifluoromethyl)sulfonyl)methanesulfonamide (49.65 g, 139 mmol) in THF (150 mL) was slowly added. The mixture stirred for an additional 1 h at −78 °C and was then allowed to stir at rt for 2 h. The mixture was concentrated under reduced pressure and the residue was purified by flash column chromatography (Isco CombiFlash Rf unit, 330 g RediSep column, 0−50% EtOAc in hexanes) to give (±)-(3a*S*,6a*S*)-*tert*-butyl 5-(((trifluoromethyl)sulfonyl)oxy)-3,3a,6,6a-tetrahydrocyclopenta[*c*]pyrrole-2(1*H*)-carboxylate ((±)-**39**) as a clear, viscous oil (1.56 g, quantitative): ^{1}H NMR (500 MHz, $CDCl_3$) δ 5.58 (s, 1H), 3.62 (m, 1H), 3.53 (m, 1H), 3.46 (m, 2H), 3.19 (m, 1H), 2.95 (m, 2H), 2.46 (m, 1H), 1.47 (s, 9H).

Step F. To an N_2 degassed mixture of (±)-(3a*S*,6a*S*)-*tert*-butyl 5-(((trifluoromethyl)sulfonyl)oxy)-3,3a,6,6a-tetrahydrocyclopenta[*c*]-pyrrole-2(1*H*)-carboxylate ((±)-**39**, 14.79 g, 41.4 mmol), 2-trifluoromethylphenylboronic acid (19.70 g, 104 mmol), and a 2 M aqueous solution of Na_2CO_3 (250 mL) in DME (500 mL) was added $Pd(PPh_3)_4$ (4.80 g, 4.16 mmol). The mixture was heated at 80 °C for 6 h, then cooled to rt and diluted with H_2O (500 mL). The aqueous mixture was extracted with EtOAc (2 × 200 mL), and the combined organic extracts were washed with H_2O (200 mL), brine (200 mL), dried over Na_2SO_4, filtered, and concentrated under reduced pressure. The residue was purified by flash column chromatography (Isco CombiFlash Rf unit, 330 g RediSep column, 0−10% EtOAc in hexanes) to give (±)-(3a*R*,6a*S*)-*tert*-butyl 5-(2-(trifluoromethyl)phenyl)-3,3a,6,6a-tetrahydrocyclopenta[*c*]pyrrole-2(1*H*)-carboxylate ((±)-**40**) as a clear, viscous oil (13.70 g, 94%): ^{1}H NMR (500 MHz, $CDCl_3$) δ 7.65 (m, 1H), 7.47 (m, 2H), 7.25 (m, 1H), 5.58 (s, 1H), 3.85−3.42 (m, 4H), 3.23 (m, 1H), 2.98 (m, 2H), 2.49 (m, 1H), 1.47 (s, 9H).

Step G. A mixture of (±)-(3a*R*,6a*S*)-*tert*-butyl 5-(2-(trifluoromethyl)-phenyl)-3,3a,6,6a-tetrahydrocyclopenta[*c*]pyrrole-2(1*H*)-carboxylate ((±)-**40**, 8.63 g, 24.41 mmol) and 10% Pd/C (1.57 g, wet, 10% w/w) in CH_3OH (50 mL) was subjected to an atmosphere of H_2 gas (40 psi) using a Parr shaker apparatus at rt for 16 h. The mixture was filtered through Celite, and the filtrate was concentrated under reduced pressure. The resulting residue was purified by flash column chromatography (Isco CombiFlash Rf unit, 40 g RediSep column, 0−30% EtOAc in hexanes) to give (3a*R*,5*r*,6a*S*)-*tert*-butyl 5-(2-(trifluoromethyl)phenyl)hexahydrocyclopenta[*c*]pyrrole-2(1*H*)-carboxylate (**41**) as a clear, viscous oil (0.910 g, 85%): ^{1}H NMR (500 MHz, $CDCl_3$) δ 7.69 (m, 1H), 7.51 (m, 2H), 7.25 (m, 1H), 3.49 (m, 5H), 2.75 (m, 2H), 2.92 (m, 2H), 1.52 (m, 2H), 1.48 (s, 9H).

Step H. To a 0 °C cooled solution of (3a*R*,5*r*,6a*S*)-*tert*-butyl 5-(2-(trifluoromethyl)phenyl)hexahydrocyclopenta[*c*]pyrrole-2(1*H*)-carboxylate (**41**, 7.94 g, 22.32 mmol) in CH_2Cl_2 (60 mL) was added a 2 M HCl solution in Et_2O (60 mL), and the mixture was allowed to stir at rt for 24 h. The mixture was diluted with Et_2O (200 mL) and the precipitated product was filtered to give (3a*R*,5*r*,6a*S*)-5-(2-(trifluoromethyl)phenyl)octahydrocyclopenta[*c*]pyrrole hydrochloride (**42**) as a white solid (5.90 g, 91%): ^{1}H NMR (500 MHz, $CDCl_3$) δ 10.17 (bs, 1H), 8.06 (m, 1H), 7.59 (m, 1H), 7.53 (m, 1H), 7.27 (m, 1H), 3.42 (m, 2H), 3.38 (m, 3H), 3.01 (m, 2H), 2.36 (m, 2H), 1.96 (m, 2H); ESI MS *m*/*z* 256 $[M + H]^+$.

Step I. To a solution of (3a*R*,5*r*,6a*S*)-5-(2-(trifluoromethyl)phenyl)-octahydrocyclopenta[*c*]pyrrole hydrochloride (**42**, 0.640 g, 2.50 mmol) in CH_2Cl_2 (50 mL) was added methyl 2-isocyanatobenzoate (0.442 g, 2.50 mmol), and the mixture was stirred at rt for 16 h. The mixture was concentrated under reduced pressure and the resulting residue was purified by flash column chromatography (Isco CombiFlash Rf unit, 40 g RediSep column, 0−30% EtOAc in hexanes) to give methyl 2-((3a*R*,5*r*,6a*S*)-5-(2-(trifluoromethyl)phenyl)octahydrocyclopenta[*c*]-pyrrole-2-carboxamido)benzoate as a white solid (0.700 g, 64%): ESI MS *m*/*z* 433 $[M + H]^+$.

Step J. To a solution of methyl 2-((3a*R*,5*r*,6a*S*)-5-(2-(trifluoromethyl)phenyl)octahydrocyclopenta[*c*]pyrrole-2-carboxamido)benzoate (0.700 g, 1.61 mmol) in CH_3OH (20 mL) and THF (20 mL) was added aqueous 2 N NaOH (10 mL). The mixture stirred at rt for 16 h and concentrated under reduced pressure. The residue was diluted with H_2O (25 mL) and acidified to pH 5with 2 N HCl, and the resulting precipitate was filtered to give 2-((3a*R*,5*r*,6a*S*)-5-(2-(trifluoromethyl)phenyl)octahydrocyclopenta[*c*]pyrrole-2-carboxamido)benzoic acid (**43**) as a white solid (0.668 g, 98%): mp 157−161 °C; ^{1}H NMR (300 MHz, DMSO-d_6) δ 13.46 (br s, 1H), 10.79 (s, 1H), 8.53 (d, *J* = 8.5 Hz, 1H), 7.96 (dd, *J* = 8.0, 1.5 Hz, 1H), 7.80 (m, 1H), 7.69 (m, 1H), 7.60 (m 1H), 7.48 (m, 1H), 7.36 (m, 1H), 6.99 (m, 1H), 3.65−3.62 (m, 2H), 3.47−3.38 (m, 3H), 2.86 (m, 2H), 2.27−2.22 (m, 2H), 1.66−1.59 (m, 2H); ESI MS *m*/*z* 419 $[M + H]^+$; HPLC 98.7% purity (AUC), t_R = 14.8 min (method A).

2-((3a*S*,6a*R*)-5-(2-(Trifluoromethyl)phenyl)-1,2,3,3a,4,6a-hexahydrocyclopenta[*c*]pyrrole-2-carboxamido)benzoic Acid ((±)-45). *Step A.* To a solution of (±)-(3a*R*,6a*S*)-*tert*-butyl 5-(2-(trifluoromethyl)phenyl)-3,3a,6,6a-tetrahydrocyclopenta[*c*]pyrrole-2(1*H*)-carboxylate ((±)-**40**, 120 mg, 0.34 mmol) in CH_2Cl_2 (3 mL) was added a TFA (3 mL), and the resulting solution was stirred at rt for 3 h. The residue was dissolved in CH_2Cl_2 (25 mL) and washed with saturated aqueous $NaHCO_3$ solution (25 mL), brine (25 mL), dried over Na_2SO_4, filtered, and concentrated under reduced pressure to provide (±)-(3a*S*,6a*R*)-5-(2-(trifluoromethyl)phenyl)-1,2,3,3a,4,6a-hexahydrocyclopenta[*c*]pyrrole ((±)-**44**) as an off-white solid (0.146 mg, >99%): ^{1}H NMR (300 MHz, $CDCl_3$) δ 9.21 (br s, 1H), 8.18 (br s, 1H), 7.67 (d, *J* = 7.8 Hz, 1H), 7.51−7.34 (m, 3H), 5.57 (s, 1H), 3.82 (br s, 1H), 3.62−3.54 (m, 2H), 3.39−3.09 (m, 4H), 2.62−2.56 (m, 1H).

Step B. A solution of (±)-(3a*S*,6a*R*)-5-(2-(trifluoromethyl)phenyl)-1,2,3,3a,4,6a-hexahydrocyclopenta[*c*]pyrrole ((±)-**44**, 159 mg, 0.43 mmol), methyl 2-isocyanatobenzoate (91 mg, 0.51 mmol), and Et_3N (0.14 mL, 1.0 mmol) in CH_2Cl_2 (6 mL) was stirred at rt for 24 h. The mixture was diluted with saturated aqueous $NaHCO_3$ (30 mL) and extracted with CH_2Cl_2 (3 × 10 mL). The combined organic extracts were washed with brine, dried over Na_2SO_4, filtered, and concentrated under reduced pressure. The resulting residue was chromatographed over silica gel (0−100% EtOAc in hexanes) to give (±)-methyl 2-((3a*S*,6a*R*)-5-(2-(trifluoromethyl)phenyl)-1,2,3,3a,4,6a-hexahydrocyclopenta[*c*]pyrrole-2-carboxamido)benzoate as an off-white solid (0.114 g, 62%): ^{1}H NMR (300 MHz, $CDCl_3$) δ 8.66 (dd, *J* = 8.4, 0.9 Hz, 1H), 8.02−7.98 (m, 1H), 7.66−7.64 (m, 1H), 7.54−7.34 (m, 4H), 6.99−6.93 (m, 1H), 5.67 (br s, 1H), 4.02−3.90 (m, 4H), 3.81−3.67 (m, 3H), 3.37−3.31 (m, 1H), 3.16−2.97 (m, 2H), 2.58−2.53 (m, 1H).

Step C. To a stirring solution of (±)-methyl 2-((3a*S*,6a*R*)-5-(2-(trifluoromethyl)phenyl)-1,2,3,3a,4,6a-hexahydrocyclopenta[*c*]pyrrole-2-carboxamido)benzoate (114 mg, 0.26 mmol) in CH_3OH (4 mL) and THF (4 mL) was added a solution of $LiOH·H_2O$ (110 mg, 2.62 mmol) in H_2O (2 mL). The mixture was stirred at rt for 4 h, was diluted with additional H_2O (10 mL), and was acidified to pH 6 with 2 N HCl. The resulting solids were collected by filtration and dried under reduced pressure to provide (±)-2-((3a*S*,6a*R*)-5-(2-(trifluoromethyl)phenyl)-1,2,3,3a,4,6a-hexahydrocyclopenta[*c*]pyrrole-2-carboxamido)benzoic acid ((±)-**45**) as a white solid (0.085 mg, 79%): mp 148−152 °C; ^{1}H NMR (500 MHz, DMSO-d_6) δ 13.50 (bs, 1H), 10.74 (s, 1H), 8.50 (d, *J* = 8.5 Hz, 1H), 7.96 (m, 1H), 7.73 (m, 1H), 7.64 (m, 1H), 7.52 (m, 2H), 7.44 (m, 1H), 7.01 (m, 1H), 5.68 (s, 1H), 3.83−3.79 (m, 1H), 3.64−

dx.doi.org/10.1021/jm5010013 | *J. Med. Chem.* 2014, 57, 7731−7757

3.55 (m, 3H), 3.31−2.96 (m, 3H); ESI MS m/z 415 $[M-H]^-$; HPLC 97.5% purity (AUC), t_R = 13.6 min (method A).

2-((3a*R*,5*s*,6a*S*)-5-(2-(Trifluoromethyl)phenyl)octahydrocyclopenta[*c*]pyrrole-2-carboxamido)benzoic Acid (48). *Step A.* To a solution of (±)-(3a*S*,6a*R*)-5-(2-(trifluoromethyl)phenyl)-1,2,3,3a,4,6a-hexahydrocyclopenta[*c*]pyrrole ((±)-**44**, 0.680 g, 1.92 mmol) in CH_3OH (25 mL) was added Pd/C (10% w/w, Degussa type E101 NE/W, 0.140 g). The mixture was subjected to an atmosphere of H_2 (50 psi) at rt for 6 h and was filtered through Celite. The filtrated was concentrated under reduced pressure, and the resulting residue was purified by reversed phase column chromatography (Isco C18 Reversed phase Gold column, 10−30% CH_3CN in H_2O with 0.05% TFA). The resulting material was dissolved in CH_2Cl_2 and washed with saturated aqueous $NaHCO_3$, dried over Na_2SO_4, filtered, and concentrated under reduced pressure to give (3a*R*,5*s*,6a*S*)-5-(2-(trifluoromethyl)phenyl)octahydrocyclopenta[*c*]pyrrole (**46**) as a white solid (0.070 g, 14%): ^{1}H NMR (300 MHz, $CDCl_3$) δ 7.61 (d, J = 7.8 1H), 7.50 (m, 2H), 7.30−7.24 (m, 1H), 3.54−3.42 (m, 1H), 3.32−3.26 (m, 2H), 2.81−2.68 (m, 2H), 2.51−2.46 (m, 2H), 1.84−1.76 (m, 4H); ESI MS m/z 256 $[M+H]^+$.

Step B. To a solution of (3a*R*,5*s*,6a*S*)-5-(2-(trifluoromethyl)phenyl)-octahydrocyclopenta[*c*]pyrrole (**46**, 0.030 g, 0.12 mmol) in CH_2Cl_2 (2 mL) was added methyl 2-isocyanatobenzoate (0.021 g, 0.12 mmol). The mixture was stirred for 2 h and then chromatographed over silica gel (0−50% EtOAc in hexanes) to give methyl 2-((3a*R*,5*s*,6a*S*)-5-(2-(trifluoromethyl)phenyl)octahydrocyclopenta[*c*]pyrrole-2-carboxamido)benzoate as a white solid (0.052 g, quantitative): ^{1}H NMR (300 MHz, $CDCl_3$) δ 10.53 (s, 1H), 8.67 (m, 1H), 8.01 (dd, J = 8.0, 1.6 Hz, 1H), 7.62−7.46 (m, 4H), 7.28 (m, 1H), 6.99−6.94 (m, 1H), 3.92 (m, 5H), 3.79−3.67 (m, 1H), 3.38−3.33 (m, 2H), 3.07 (m, 2H), 2.11−1.93 (m, 4H); ESI MS m/z 433 $[M+H]^+$.

Step C. To a solution of 2-((3a*R*,5*s*,6a*S*)-5-(2-(trifluoromethyl)-phenyl)octahydrocyclopenta[*c*]pyrrole-2-carboxamido)benzoate (0.052 g, 0.12 mmol) in THF (3 mL) and CH_3OH (1 mL) was added a solution of LiOH·H_2O (0.015g, 0.36 mmol) in H_2O (1 mL). The mixture was stirred at rt for 6 h, was acidified to pH 2 with 2 N HCl, and was poured into H_2O. The mixture was extracted with CH_2Cl_2 (30 mL), and the organic extracts were washed with brine, dried over Na_2SO_4, filtered, and concentrated under reduced pressure. The residue was chromatographed over silica gel (0−10% CH_3OH in CH_2Cl_2) to give 2-((3a*R*,5*s*,6a*S*)-5-(2-(trifluoromethyl)phenyl)octahydrocyclopenta[*c*]-pyrrole-2-carboxamido)benzoic acid (**48**) as a white solid (0.049 g, 98%): mp 172−174 °C; ^{1}H NMR (300 MHz, $CDCl_3$) δ 13.48 (bs, 1H), 10.74 (bs, 1H), 8.51 (d, J = 8.7 Hz, 1H), 7.97 (d, J = 8.1 Hz, 1H), 7.69 (m, 3H), 7.55 (m, 1H), 7.41 (m, 1H), 7.02 (m, 1H), 3.76 (m, 2H), 3.56 (m, 1H), 3.25 (dd, J = 10.8, 4.8 Hz, 2H), 3.04 (m, 2H), 2.01−1.89 (m, 4H); ESI MS m/z 419 $[M+H]^+$. HPLC >99% purity (AUC), t_R = 14.7 min (method A).

5-Fluoro-2-((3a*R*,5*r*,6a*S*)-5-(2-(trifluoromethyl)phenyl)-octahydrocyclopenta[*c*]pyrrole-2-carboxamido)benzoic Acid (50). *Step A.* To a solution of triphosgene (0.148 g, 0.50 mmol) in CH_2Cl_2 (3.0 mL) under N_2, cooled to −78 °C, was slowly added pyridine (0.158 g, 2.00 mmol), and the resulting solution was stirred at −78 °C for 10 min. A solution of (3a*R*,5*r*,6a*S*)-5-(2-(trifluoromethyl)-phenyl)octahydrocyclopenta[*c*]pyrrole hydrochloride (**42**, 0.292 g, 1.00 mmol) in CH_2Cl_2 (2.0 mL) was added, and the resulting solution was stirred at −78 °C for 30 min. The solution was warmed to rt and stirred for 2 h. The mixture was diluted with 1 N HCl (8 mL) and extracted with CH_2Cl_2 (3 × 30 mL). The combined organic extracts were washed with saturated $NaHCO_3$ solution (40 mL) and concentrated under reduced pressure. The resulting residue was chromatographed over silica gel (0−30% EtOAc in hexanes) to give (3a*R*,5*r*,6a*S*)-5-(2-(trifluoromethyl)-phenyl)hexahydrocyclopenta[*c*]pyrrole-2(1*H*)-carbonyl chloride (**49**) as a light yellow solid (170 mg, 53%): ^{1}H NMR (300 MHz, DMSO-d_6) δ 7.81 (d, J = 8.4 Hz, 1H), 7.69−7.60 (m, 2H), 7.44−7.35 (m, 1H), 3.85−3.75 (m, 1H), 3.71−3.54 (m, 2H), 3.51−3.43 (m, 1H), 3.42−3.36 (m, 1H), 2.91−2.75 (m, 2H), 2.25−2.12 (m, 2H), 1.70−1.55 (m, 2H); ESI MS m/z 318 $[M+H]^+$.

Step B. To a solution of give (3a*R*,5*r*,6a*S*)-5-(2-(trifluoromethyl)-phenyl)hexahydrocyclopenta[*c*]pyrrole-2(1*H*)-carbonyl chloride (**49**, 0.100 g, 0.31 mmol) in THF (1.8 mL) were added *i*-Pr_2NEt (0.041 g, 0.31 mmol) and methyl 2-amino-5-fluorobenzoate (0.064 g, 0.37 mmol). The resulting solution was heated at reflux for 5 h. The mixture was diluted with H_2O (30 mL) and extracted with EtOAc (4 × 30 mL). The combined organic extracts were concentrated under reduced pressure. The resulting residue was chromatographed over silica gel (0−10% EtOAc in hexanes) to give methyl 5-fluoro-2-((3a*R*,5*r*,6a*S*)-5-(2-(trifluoromethyl)phenyl)octahydrocyclopenta[*c*]pyrrole-2-carboxamido)benzoate as a light orange film (101 mg, crude): ESI MS m/z 451 $[M+H]^+$.

Step C. To a solution of methyl 5-fluoro-2-((3a*R*,5*r*,6a*S*)-5-(2-(trifluoromethyl)phenyl)octahydrocyclopenta[*c*]pyrrole-2-carboxamido)benzoate (0.101 g, 0.22 mmol) in THF (4.4 mL) and CH_3OH (2.3 mL) was added a solution of LiOH·H_2O (0.094 g, 2.24 mmol) in H_2O (1.2 mL). The mixture was stirred at rt for 18 h, was then acidified to pH 5 with 2 N HCl, and was diluted with H_2O (20 mL). The aqueous mixture was extracted with EtOAc (3 × 30 mL), and the combined organic extracts were concentrated under reduced pressure. The resulting residue was chromatographed by reverse phase column (Isco RediSep 12 g Gold C18 reverse phase column, 0−100% CH_3CN in H_2O) to provide 5-fluoro-2-((3a*R*,5*r*,6a*S*)-5-(2-(trifluoromethyl)-phenyl)octahydrocyclopenta[*c*]pyrrole-2-carboxamido)benzoic acid (**50**) as a white solid (0.011 g, 12%): mp 176−180 °C; ^{1}H NMR (500 MHz, DMSO-d_6) δ 13.83 (br s, 1H), 10.65 (br s, 1H), 8.57−8.51 (m, 1H), 7.75 (d, J = 8.5 Hz, 1H), 7.69−7.59 (m, 3H), 7.46−7.36 (m, 2H), 3.67−3.58 (m, 2H), 3.47−3.36 (m, 3H), 2.90−2.81 (m, 2H), 2.28−2.20 (m, 2H), 1.68−1.58 (m, 2H); ESI MS m/z 437 $[M+H]^+$; HPLC >99% purity (AUC), t_R = 11.3 min (method B).

5-Methoxy-2-((3a*R*,5*r*,6a*S*)-5-(2-(trifluoromethyl)phenyl)-octahydrocyclopenta[*c*]pyrrole-2-carboxamido)benzoic Acid (51). Compound **51** was prepared according to a similar procedure described for the synthesis of **50**. Mp 176−179 °C; ^{1}H NMR (500 MHz, DMSO-d_6) δ 13.56 (s, 1H), 10.42 (br s, 1H), 8.43 (d, J = 9.0 Hz, 1H), 7.75 (d, J = 8.0 Hz, 1H), 7.67−7.59 (m, 2H), 7.43 (d, J = 3.0 Hz, 1H), 7.42−7.36 (m, 1H), 7.18 (dd, J = 9.5, 3.0 Hz, 1H), 3.75 (s, 3H), 3.65−3.58 (m, 2H), 3.46−3.36 (m, 3H), 2.90−2.79 (m, 2H), 2.28−2.19 (m, 2H), 1.66−1.57 (m, 2H); ESI MS m/z 449 $[M+H]^+$; HPLC >99% purity (AUC), t_R = 11.2 min (method B).

5-Chloro-2-((3a*R*,5*r*,6a*S*)-5-(2-(trifluoromethyl)phenyl)-octahydrocyclopenta[*c*]pyrrole-2-carboxamido)benzoic Acid (52). To a solution of methyl 2-amino-5-chlorobenzoate (0.058 g, 0.31 mmol) in DMF (2.7 mL) cooled to −10 °C under N_2 was added NaH (60% in mineral oil, 0.019 g, 0.47 mmol), and the resulting solution was stirred at −10 °C for 20 min. A solution of (3a*R*,5*r*,6a*S*)-5-(2-(trifluoromethyl)phenyl)hexahydrocyclopenta[*c*]pyrrole-2(1*H*)-carbonyl chloride (**49**, 0.100 g, 0.315 mmol) in DMF (0.55 mL) was added and the mixture stirred at rt for 2 h. The mixture was carefully diluted with H_2O (30 mL), made acidic to pH 2 with 2 N HCl, and was extracted with EtOAc (4 × 30 mL). The combined organic extracts were washed with brine (4 × 30 mL) and concentrated under reduced pressure. The resulting residue was chromatographed over silica gel (0−10% CH_3OH in CH_2Cl_2 with 0.1% HOAc) followed by reverse phase column chromatography (Isco Gold RediSep 12 g C18 reverse phase column, 0−100% CH_3CN in H_2O) to give 5-chloro-2-((3a*R*,5*r*,6a*S*)-5-(2-(trifluoromethyl)phenyl)octahydrocyclopenta[*c*]pyrrole-2-carboxamido)benzoic acid (**52**) as a white solid (21 mg, 23%): mp 188−193 °C; ^{1}H NMR (500 MHz, DMSO-d_6) δ 13.92 (bs, 1H), 10.85 (bs, 1H), 8.56 (d, J = 9.5 Hz, 1H), 7.90 (s, 1H), 7.76 (d, J = 8.0 Hz, 1H), 7.68−7.54 (m, 3H), 7.42−7.35 (m, 1H), 3.67−3.58 (m, 2H), 3.48−3.35 (m, 3H), 2.90−2.80 (m, 2H), 2.28−2.19 (m, 2H), 1.67−1.53 (m, 2H); ESI MS m/z 453 $[M+H]^+$; HPLC >99% purity (AUC), t_R = 12.0 min (method B).

5-(Methylsulfonyl)-2-((3a*R*,5*r*,6a*S*)-5-(2-(trifluoromethyl)-phenyl)octahydrocyclopenta[*c*]pyrrole-2-carboxamido)-benzoic Acid (53). Compound **53** was prepared according to a similar procedure described for the synthesis of **52**. Mp 175−181 °C; ^{1}H NMR (500 MHz, DMSO-d_6) δ 14.09 (bs, 1H), 11.09 (bs, 1H), 8.77 (d, J = 9.0 Hz, 1H), 8.42 (d, J = 2.5 Hz, 1H), 8.04 (dd, J = 9.0, 2.5 Hz, 1H), 7.77 (d, J = 8.0 Hz, 1H), 7.67−7.60 (m, 2H), 7.42−7.37 (m, 1H), 3.72−3.64 (m, 2H), 3.52−3.46 (m, 2H), 3.45−3.32 (m, 1H), 3.20 (s, 3H), 2.92−2.84

dx.doi.org/10.1021/jm5010013 | J. Med. Chem. 2014, 57, 7731−7757

(m, 2H), 2.28−2.20 (m, 2H), 1.69−1.59 (m, 2H); ESI MS m/z 497 $[M + H]^+$; HPLC >99% purity (AUC), t_R = 10.6 min (method B).

2-((3a*R*,5*R*,6a*S*)-5-(2-(Trifluoromethyl)phenyl)octahydrocyclopenta[*c*]pyrrole-2-carboxamido)nicotinic Acid (54). *Step A.* A solution of (3a*R*,5*r*,6a*S*)-5-(2-(trifluoromethyl)phenyl)[*c*]pyrrole-2(1*H*)-carbonyl chloride (**49**, 0.300 g, 0.94 mmol) in 7 N NH_3 in CH_3OH (4.0 mL) was stirred at rt for 1 h. The mixture was concentrated under reduced pressure to provide (3a*R*,5*r*,6a*S*)-5-(2-(trifluoromethyl)-phenyl)hexahydrocyclopenta[*c*]pyrrole-2(1*H*)-carboxamide as a white solid (0.323 g, >99%): ESI MS m/z 299 $[M + H]^+$.

Step B. A mixture of (3a*R*,5*r*,6a*S*)-5-(2-(trifluoromethyl)phenyl)-hexahydrocyclopenta[*c*]pyrrole-2(1*H*)-carboxamide (0.100 g, 0.33 mmol), methyl 2-chloronicotinate (0.087 g, 0.50 mmol), Cs_2CO_3 (0.134 g, 0.47 mmol), $Pd(OAc)_2$ (0.022 g, 0.033 mmol), and racemic BINAP (0.042 g, 0.067 mmol) in toluene (4 mL) was heated at reflux for 2 h. The mixture cooled to rt and was filtered through Celite. The filtrate was washed with brine (3 × 30 mL) and concentrated under reduced pressure. The resulting residue was chromatographed over silica gel (0−5% CH_3OH in CH_2Cl_2 with 0.01% NH_4OH) to give methyl 2-((3a*R*,5*r*,6a*S*)-5-(2-(trifluoromethyl)phenyl)octahydrocyclopenta[*c*]-pyrrole-2-carboxamido)nicotinate as a light orange film (0.047 g, 31%): ^1H NMR (300 MHz, DMSO-d_6) δ 10.41 (br s, 1H), 8.69 (dd, J = 4.8, 1.8 Hz, 1H), 8.32 (dd, J = 7.8, 1.8 Hz, 1H), 7.61 (d, J = 7.8 Hz, 1H), 7.57−7.47 (m, 2H), 7.31−7.27 (m, 1H), 7.00 (dd, J = 7.8, 4.8 Hz, 1H), 3.95 (s, 3H), 3.84−3.74 (m, 2H), 3.68−3.60 (m, 2H), 3.58−3.43 (m, 1H), 2.95−2.83 (m, 2H), 2.43−2.32 (m, 2H), 1.72−1.57 (m, 2H); ESI MS m/z 434 $[M + H]^+$.

Step C. To a solution of methyl 2-((3a*R*,5*r*,6a*S*)-5-(2-(trifluoromethyl)phenyl)octahydrocyclopenta[*c*]pyrrole-2-carboxamido)nicotinate (0.039 g, 0.090 mmol) in THF (4.0 mL) and CH_3OH (1.9 mL) was added a solution of $LiOH·H_2O$ (0.037 g, 0.90 mmol) in H_2O (1.1 mL). The mixture was stirred at rt for 3 h, was then neutralized with 2 N HCl, and was extracted with CH_2Cl_2 (4 × 20 mL). The combined organic extracts were concentrated under reduced pressure and the resulting residue was chromatographed by reverse phase column chromatography (Isco RediSep Gold 12 g C18 reverse phase column, 0−60% CH_3CN in H_2O) to give 2-((3a*R*,5*r*,6a*S*)-5-(2-(trifluoromethyl)phenyl)octahydrocyclopenta[*c*]pyrrole-2-carboxamido)nicotinic acid (**54**) as a white solid (0.021 mg, 55%): mp 129−133 °C; ^1H NMR (300 MHz, DMSO-d_6) δ 8.45−8.30 (m, 2H), 7.76 (d, J = 7.8 Hz, 1H), 7.70−7.60 (m, 2H), 7.45−7.34 (m, 1H), 7.17−7.09 (m, 1H), 3.67−3.61 (m, 2H), 3.52−3.46 (m, 2H), 3.45−3.35 (m, 2H), 2.84 (m, 2H), 2.26 (m, 2H), 1.67 (m, 2H); ESI MS m/z 420 $[M + H]^+$. HPLC >99% purity (AUC), t_R = 13.6 min (method C).

4-((3a*R*,5*r*,6a*S*)-5-(2-(Trifluoromethyl)phenyl)octahydrocyclopenta[*c*]pyrrole-2-carboxamido)nicotinic Acid (55). *Step A.* To a solution of (3a*R*,5*R*,6a*S*)-5-(2-(trifluoromethyl)phenyl)-hexahydrocyclopenta[*c*]pyrrole-2(1*H*)-carbonyl chloride (**49**, 0.170 g, 0.53 mmol) in THF (3.0 mL) were added *i*-Pr_2NEt (0.064 g, 0.53 mmol) and methyl 4-aminonicotinate (0.081 g, 0.53 mmol), and the resulting mixture was heated at reflux for 4 h. The mixture was cooled to rt, was diluted with H_2O (20 mL), and was extracted with EtOAc (3 × 30 mL). The combined organic extracts were concentrated under reduced pressure. The resulting residue was chromatographed over silica gel (0−5% CH_3OH in CH_2Cl_2 with 0.1% NH_4OH) to give methyl 4-((3a*R*,5*r*,6a*S*)-5-(2-(trifluoromethyl)phenyl)octahydrocyclopenta[*c*]-pyrrole-2-carboxamido)nicotinate as a white solid (0.140 g, 60%): ^1H NMR (300 MHz, DMSO-d_6) δ 10.46 (br s, 1H), 8.98 (d, J = 0.3 Hz, 1H), 8.53 (d, J = 6.0 Hz, 1H), 8.46 (d, J = 6.3 Hz, 1H), 7.79 (d, J = 8.1 Hz, 1H), 7.68−7.59 (m, 2H), 7.43−7.35 (m, 1H), 3.91 (s, 3H), 3.75−3.61 (m, 2H), 3.52−3.35 (m, 3H), 2.94−2.81 (m, 2H), 2.31−2.17 (m, 2H), 1.72−1.56 (m, 2H); ESI MS m/z 434 $[M + H]^+$.

Step B. To a mixture of methyl 4-((3a*R*,5*r*,6a*S*)-5-(2-(trifluoromethyl)phenyl)octahydrocyclopenta[*c*]pyrrole-2-carboxamido)nicotinate (0.138 g, 0.31 mmol) in THF (6.2 mL) and CH_3OH (3.2 mL) was added a solution of $LiOH·H_2O$ (0.130 g, 3.11 mmol) in H_2O (1.6 mL). The mixture was stirred at rt for 3 h, was then acidified to pH 4 with 2 N HCl, and was diluted with H_2O (50 mL). The resulting solids were collected by filtration and dried to provide 4-((3a*R*,5*r*,6a*S*)-5-(2-(trifluoromethyl)phenyl)octahydrocyclopenta[*c*]-pyrrole-2-carboxamido)nicotinic acid (**55**) as a light yellow solid (0.130 g, >99%): mp 245−255 °C dec; ^1H NMR (500 MHz, DMSO-d_6) δ 8.92 (m, 1H), 8.53 (d, J = 6.5 Hz, 1H), 8.44 (d, J = 7.5 Hz, 1H), 7.76 (d, J = 8.0 Hz, 1H), 7.67−7.59 (m, 2H), 7.42−7.36 (m, 1H), 3.75−3.62 (m, 2H), 3.53−2.79 (m, 4H), 2.87 (m, 2H), 2.27 (m, 2H), 1.67 (m, 2H); ESI MS m/z 420 $[M + H]^+$; HPLC >99% purity (AUC), t_R = 12.5 min (method G).

6-Methyl-4-((3a*R*,5*r*,6a*S*)-5-(2-(trifluoromethyl)phenyl)-octahydrocyclopenta[*c*]pyrrole-2-carboxamido)nicotinic Acid (56). *Step A.* To a 0 °C cooled solution of H_2SO_4 (0.5 mL) in CH_3OH (5 mL) was slowly added 4-amino-6-methylnicotinic acid (0.200 g, 1.31 mmol), and the mixture was heated at reflux for 16 h. The mixture was cooled to rt and was poured into ice−water and neutralized with solid Na_2CO_3. The aqueous mixture was extracted with CH_2Cl_2 (3 × 30 mL) and the organic extracts were dried over Na_2SO_4, filtered, and concentrated to give methyl 4-amino-6-methylnicotinate as an off-white solid (0.120 g, 54%), which was used as is in the next step.

Step B. To a solution of methyl 4-amino-6-methylnicotinate (0.120 g, 0.72 mmol) in DMF (10 mL) cooled to 0 °C was added NaH (60% in mineral oil, 0.035 g, 0.86 mmol) and the resulting solution was stirred at 0 °C for 30 min. A solution of (3a*R*,5*R*,6a*S*)-5-(2-(trifluoromethyl)-phenyl)hexahydrocyclopenta[*c*]pyrrole-2(1*H*)-carbonyl chloride (**2**, 0.229 g, 0.72 mmol) in DMF (2 mL) was added and the mixture stirred at rt for 2 h. The mixture was carefully diluted with H_2O (30 mL) and extracted with EtOAc (4 × 30 mL). The combined organic extracts were washed with brine (4 × 30 mL) and concentrated under reduced pressure. The resulting residue was chromatographed over silica gel (0−10% CH_3OH in CH_2Cl_2) to give methyl 2-(6-methyl-4-((3a*R*,5*r*,6a*S*)-5-(2-(trifluoromethyl)phenyl)octahydrocyclopenta[*c*]pyrrole-2-carboxamido)pyridin-3-yl)-2-oxoacetate as a white solid (0.043 g, 13%).

Step C. To a solution of methyl 2-(6-methyl-4-((3a*R*,5*r*,6a*S*)-5-(2-(trifluoromethyl)phenyl)octahydrocyclopenta[*c*]pyrrole-2-carboxamido)pyridin-3-yl)-2-oxoacetate (0.040 g, 0.080 mmol) in THF (3 mL) was added a solution of $LiOH·H_2O$ (0.010 g, 0.24 mmol) in H_2O (2 mL). The mixture was stirred at rt for 24 h, was then carefully neutralized with 2 N HCl, and was extracted with CH_2Cl_2 (3 × 30 mL). The combined organic extracts were concentrated under reduced pressure and the resulting residue was chromatographed over silica gel (0−10% CH_3OH in CH_2Cl_2) to give 2-(6-methyl-4-((3a*R*,5*r*,6a*S*)-5-(2-(trifluoromethyl)phenyl)octahydrocyclopenta[*c*]pyrrole-2-carboxamido)pyridin-3-yl)-2-oxoacetic acid (**56**) as a light-yellow solid (0.020 g, 52%): ^1H NMR (300 MHz, DMSO-d_6) δ 8.78 (m, 1H), 8.35 (m, 1H), 7.77 (m, 3H), 7.36 (m, 1H), 3.68 (m, 2H), 3.48−3.29 (m, 7H), 2.56 (m, 3H), 2.26 (m, 2H), 1.55 (m, 2H); ESI MS m/z 434 $[M + H]^+$; HPLC 97.2% purity (AUC), t_R = 13.9 min (method C).

5-((3a*R*,5*r*,6a*S*)-5-(2-(Trifluoromethyl)phenyl)octahydrocyclopenta[*c*]pyrrole-2-carboxamido)pyridazine-4-carboxylic Acid (57). Compound **57** was prepared according to a similar procedure described for the synthesis of **56**. Mp 175−181 °C; ^1H NMR (300 MHz, DMSO-d_6) δ 10.30 (bs, 1H), 9.27 (bs, 1H), 7.79 (m, 1H), 7.64 (m, 2H), 7.39 (m, 2H), 3.72 (m, 2H), 3.69 (m, 2H), 2.89 (m, 2H), 2.26 (m, 2H), 1.62 (m, 2H), 1.26 (m, 2H); ESI MS m/z 421 $[M + H]^+$; HPLC 95.2% purity (AUC), t_R = 14.9 min (method C).

((3a*R*,5*r*,6a*S*)-5-(2-(Trifluoromethyl)phenyl)octahydrocyclopenta[*c*]pyrrole-2-carbonyl)carbamic Acid (58). *Step A.* To mixture of (3a*R*,5*r*,6a*S*)-5-(2-(trifluoromethyl)phenyl)hexahydrocyclopenta[*c*]pyrrole-2(1*H*)-carbonyl chloride (**49**, 50 mg, 0.15 mmol) and Et_3N (60 μL, 0.56 mmol) in DMF (4 mL) was added methyl 2-aminoacetate hydrochloride (24 mg, 0.189 mmol). The resulting mixture was stirred at rt for 18 h and then concentrated under reduced pressure to give crude methyl 2-((3a*R*,5*r*,6a*S*)-5-(2-(trifluoromethyl)phenyl)octahydrocyclopenta[*c*]pyrrole-2-carboxamido)acetate (0.055 g), which was used as is in the next step: ESI MS m/z 371 $[M + H]^+$.

Step B. To a mixture of crude methyl 2-((3a*R*,5*r*,6a*S*)-5-(2-(trifluoromethyl)phenyl)octahydrocyclopenta[*c*]pyrrole-2-carboxamido)acetate (0.055 g, 0.14 mmol) in THF (2 mL) was added a solution of $LiOH·H_2O$ (57 mg, 1.35 mmol) in H_2O (2 mL), and the resulting mixture was stirred at rt for 2 h. The mixture was acidified to pH 6 with 2 N HCl and extracted with CH_2Cl_2 (3 × 50 mL). The

dx.doi.org/10.1021/jm5010013 | J. Med. Chem. 2014, 57, 7731−7757

combined organic extracts were dried over Na_2SO_4, filtered, and concentrated under reduced pressure. The resulting residue was chromatographed over silica gel (12 g RediSep column, 0−10% CH_3OH in CH_2Cl_2 with 0.1% NH_4OH) to give 2-((3a*R*,5*r*,6a*S*)-5-(2-(trifluoromethyl)phenyl)octahydrocyclopenta[*c*]pyrrole-2-carboxamido)acetic acid (**58**) as a white solid (0.028 g, 55%): 173−176 °C; ^{1}H NMR (300 MHz, DMSO-d_6) δ 7.74−7.59 (m, 3H), 7.44−7.35 (m, 1H), 6.29 (m, 1H), 3.61−3.00 (m, 7H), 2.74 (m, 2H), 2.23 (m, 2H), 1.53 (m, 2H); ESI MS m/z 357 $[M + H]^+$; HPLC >99% purity (AUC), t_R = 16.4 min (method B).

(*S*)-2-((3a*R*,5*S*,6a*S*)-5-(2-(Trifluoromethyl)phenyl)octahydrocyclopenta[*c*]pyrrole-2-carboxamido)propanoic Acid ((*S*)-59). Compound (*S*)-**59** was prepared according to a similar procedure described for the synthesis of **58**. Mp 138−141 °C; ^{1}H NMR (300 MHz, DMSO-d_6) δ 7.78−7.56 (m, 3H), 7.49−7.28 (m, 1H), 6.22 (m, 1H), 3.93 (m, 1H), 3.50−3.23 (m, 5H), 2.86 (m, 2H), 2.20 (m, 2H), 1.56 (m, 2H), 1.34−1.13 (m, 3H); ESI MS m/z 371 $[M + H]^+$; HPLC 98.5% purity (AUC), t_R = 12.0 min (method B).

(*R*)-2-((3a*R*,5*R*,6a*S*)-5-(2-(Trifluoromethyl)phenyl)octahydrocyclopenta[*c*]pyrrole-2-carboxamido)propanoic Acid ((*R*)-60). Compound (*R*)-**60** was prepared according to a similar procedure described for the synthesis of **58**. Mp 141−145 °C; ^{1}H NMR (300 MHz, DMSO-d_6) δ 7.78−7.56 (m, 3H), 7.49−7.28 (m, 1H), 6.17 (m, 1H), 389 (m, 1H), 3.50−3.20 (m, 5H), 2.79 (m, 2H), 2.21 (m, 2H), 1.56 (m, 2H), 1.27 (m, 3H); ESI MS m/z 371 $[M + H]^+$; HPLC 97.0% purity (AUC), t_R = 11.9 min (method B).

(*S*)-2-Phenyl-2-((3a*R*,5*S*,6a*S*)-5-(2-(Trifluoromethyl)phenyl)-octahydrocyclopenta[*c*]pyrrole-2-carboxamido)acetic Acid ((*S*)-61). Compound (*S*)-**61** was prepared according to a similar procedure described for the synthesis of **58**. Mp 109−114 °C; ^{1}H NMR (300 MHz, DMSO-d_6) δ 7.67 (m, 3H), 7.49 (m, 3H), 7.34 (m, 3H), 6.55 (m, 1H), 5.06 (m, 1H), 3.50−3.20 (m, 5H), 2.78 (m, 2H), 2.34 (m, 2H), 1.62 (m, 2H); ESI MS m/z 433 $[M + H]^+$; HPLC 98.6% purity (AUC), t_R = 16.3 min (method B).

(*R*)-2-Phenyl-2-((3a*R*,5*S*,6a*S*)-5-(2-(Trifluoromethyl)phenyl)-octahydrocyclopenta[*c*]pyrrole-2-carboxamido)acetic Acid ((*R*)-62). Compound (*R*)-**62** was prepared according to a similar procedure described for the synthesis of **58**. Mp 109−112 °C; ^{1}H NMR (300 MHz, DMSO-d_6) δ 7.68 (m, 3H), 7.42 (m, 3H), 7.29−7.16 (m, 3H), 6.40 (m, 1H), 4.90 (m, 1H), 3.52−3.21 (m, 5H), 2.75 (m, 2H), 2.27 (m, 2H), 1.56 (m, 2H); ESI MS m/z 433 $[M + H]^+$; HPLC 98.3% purity (AUC), t_R = 16.3 min (method B).

In Vitro Assays. In Vitro Scintillation Proximity Binding Assay (SPA) for RBP4. Analogue binding affinities for RBP4 were measured using our previously reported scintillation proximity assay (SPA), which measured competitive displacement of radiolabeled retinol.[25] Briefly, human RBP4 was biotinylated using the EZ-link Sulfo-NHS-LC-Biotinylation kit from Pierce (Rockford, IL) following the manufacturer's recommendations. Binding experiments were performed in a final assay volume of 100 μL per well in SPA buffer (1× PBS, pH 7.4, 1 mM EDTA, 0.1% BSA, 0.5% CHAPS). The reaction mix contained 10 nM ^{3}H-retinol (48.7 Ci/mmol; PerkinElmer, Waltham, MA), 0.3 mg/well streptavidin-PVT beads, 50 nM biotinylated RBP4. Nonspecific binding was determined in the presence of 20 μM unlabeled retinol. Radio counts were measured using CHAMELEON plate reader (Hidex Oy, Turku, Finland) following overnight incubation at 4 °C.

In Vitro HTRF Assay for Antagonists of Retinol-Induced RBP4-TTR Interaction. The ability of compounds to antagonize the retinol-dependent RBP4-TTR interaction was measured using the HTRF assay.[25] Maltose binding protein-tagged RBP4 expressed in *E. coli* and untagged TTR were used in this assay. TTR was directly labeled with Eu^{3+} cryptate-NHS using the HTRF cryptate labeling kit from CisBio (Bedfored, MA) following the manufacturer's recommendations. The HTRF assay was performed in a final assay volume of 16 μL per well. The reaction buffer contained 10 mM Tris-HCl, pH 7.5, 1 mM DTT, 0.05% NP-40, 0.05% Prionex, 6% glycerol, and 400 mM KF. Each reaction contained 60 nM MBP-RBP4 and 2 nM TTR-Eu along with 26.7 nM anti-MBP antibody conjugated with d2 (CisBio). The RBP4-TTR interaction was stimulated by the addition of 1 μM *all-trans* retinol. HTRF signal was measured in the SpectraMax M5e multimode plate reader (Molecular Devices, Sunnyvale, CA) following the overnight 4 °C incubation. Fluorescence was excited at 337 nm; emission was measured at 668 and 620 nm with 75 μs counting delay. The TR-FRET signal was expressed as the ratio of fluorescence intensity: (Flu_{668}/Flu_{620}) × 10 000.

■ ASSOCIATED CONTENT

Ⓢ Supporting Information

In vitro biological assays, in vivo protocols, computational modeling methods and data (Glide scores, solvation energies, and F96 interaction scores), and ^{1}H NMR spectral data. This material is available free of charge via the Internet at http://pubs.acs.org.

■ AUTHOR INFORMATION

Corresponding Authors

*C.L.C.: phone, 518-512-2955; e-mail, christopher.cioffi@amriglobal.com.

*K.P.: phone, 212-305-9040; e-mail, kep4@cumc.columbia.edu.

Present Address

$^{\bigcirc}$Q.Q.: Capital Medical University, Beijing, 100069, P. R. China.

Notes

The authors declare the following competing financial interest(s): Patents protecting the classes of compounds disclosed in this paper were filed by The Trustees of Columbia University in the City of New York. C.L.C., N.D., E.E.F., M.P.C., P.C., L.Z., G.J., and K.P. are inventors on the patent applications for compounds disclosed in this paper that are assigned to The Trustees of Columbia University in the City of New York.

■ ACKNOWLEDGMENTS

This study was supported by NIH Grants U01 NS074476 (to K.P.) and P30 EY019007 (Core Support for Vision Research) and unrestricted funds from Research To Prevent Blindness (New York, NY) to the Department of Ophthalmology, Columbia University, NY. The authors thank The Burch Family Foundation, the Mary Jaharis-John Catsimatidis Scholarship Fund, the Kaplen Foundation, and the Eye Surgery Fund for gifts supporting this study. This project has also been funded in whole or in part with federal funds from the National Institute of Neurological Disorders and Stroke, Neurosciences Blueprint Program, National Institutes of Health, Department of Health and Human Services, under Contract No. HHSN271201100013C.

■ ABBREVIATIONS USED

AMD, age-related macular degeneration; A2E, *N*-retinide-*N*-retinylidene ethanolamine; SPA, scintillation proximity assay; HTRF, homogeneous time-resolved fluorescence assay; HLM, human liver microsome; HATU, (1-[bis(dimethylamino)-methylene]-1*H*-1,2,3-triazolo[4,5-*b*]pyridinium 3-oxide hexafluorophosphate); *n*-BuLi, *n*-butyllithium; THF, tetrahydrofuran; DMF, *N*,*N*-dimethylformamide; DME, dimethoxyethane; Et_2O, diethyl ether; Boc_2O, di-*tert*-butyl dicarbonate; TFA, trifluoroacetic acid; $Pd(OAc)_2$, palladium(II) acetate; BINAP, 2,2′-bis(diphenylphosphino)-1,1′-binaphthalene; Ac_2O, acetic anhydride; NaOAc, sodium acetate; LiHMDS, lithium bis(trimethylsilyl)amide; *i*-Pr_2NEt, *N*,*N*-diisopropylethylamine; Et_3N, triethylamine; $Pd(PPh_3)_4$, tetrakis(triphenylphosphine)-palladium(0); $PhN(SO_2CF_3)_2$, *N*-phenyl-bis(trifluoromethanesulfonimide); NOE, nuclear Overhauser effect; Gly, glycine; Tyr, tyrosine; Arg, arginine; Gln, glutamine; Leu, leucine; Phe, phenylalanine; MO, molecular orbital; CYP,

cytochrome P450; CYP2C9, cytochrome P450 2C9; CYP2C19, cytochrome P450 2C19; CYP2D6, cytochrome P450 2D6; CYP3A4, cytochrome P450 3A4; GPCR, G-protein-coupled receptor; hERG, human ether-a-go-go-related gene; PK, pharmacokinetics; PD, pharmacodynamics; iv, intravenous; po, oral administration; q.d., once daily; Cl, clearance; V_{ss}, volume of distribution at steady state; AUC, area under the curve; *F*, % bioavailability

REFERENCES

(1) Hubschman, J. P.; Reddy, S.; Schwartz, S. D. Age-related macular degeneration: current treatments. *Clin. Ophthalmol.* **2009**, *3*, 155−166.

(2) Macular Degeneration Facts & Statistics. http://www.brightfocus.org/macular/about/understanding/facts.html (accessed June 10, 2014).

(3) Petrukhin, K. New therapeutic targets in atrophic age-related macular degeneration. *Expert Opin. Ther. Targets* **2007**, *11* (5), 625−639.

(4) (a) Young, R. W. Pathophysiology of age-related macular degeneration. *Surv. Ophthalmol.* **1987**, *31* (5), 291−306. (b) Dorey, C. K.; Wu, G.; Ebenstein, D.; Garsd, A.; Weiter, J. J. Cell loss in the aging retina. Relationship to lipofuscin accumulation and macular degeneration. *Invest. Ophthalmol. Visual Sci.* **1989**, *30* (8), 1691−1699. (c) Holz, F. G.; Bellmann, C.; Margaritidis, M.; Schutt, F.; Otto, T. P.; Volcker, H. E. Patterns of increased in vivo fundus autofluorescence in the junctional zone of geographic atrophy of the retinal pigment epithelium associated with age-related macular degeneration. *Graefe's Arch. Clin. Exp. Ophthalmol.* **1999**, *237* (2), 145−152. (d) Holz, F. G.; Bindewald-Wittich, A.; Fleckenstein, M.; Dreyhaupt, J.; Scholl, H. P.; Schmitz-Valckenberg, S. Progression of geographic atrophy and impact of fundus autofluorescence patterns in age-related macular degeneration. *Am. J. Ophthalmol* **2007**, *143* (3), 463−472. (e) Schmitz-Valckenberg, S.; Fleckenstein, M.; Scholl, H. P.; Holz, F. G. Fundus autofluorescence and progression of age-related macular degeneration. *Surv. Ophthalmol.* **2009**, *54* (1), 96−117.

(5) (a) Finnemann, S. C.; Leung, L. W.; Rodriguez-Boulan, E. The lipofuscin component A2E selectively inhibits phagolysosomal degradation of photoreceptor phospholipid by the retinal pigment epithelium. *Proc. Natl. Acad. Sci. U.S.A.* **2002**, *99* (6), 3842−3847. (b) Suter, M.; Reme, C.; Grimm, C.; Wenzel, A.; Jaattela, M.; Esser, P.; Kociok, N.; Leist, M.; Richter, C. Age-related macular degeneration. The lipofusion component *N*-retinyl-*N*-retinylidene ethanolamine detaches proapoptotic proteins from mitochondria and induces apoptosis in mammalian retinal pigment epithelial cells. *J. Biol. Chem.* **2000**, *275* (50), 39625−39630. (c) Sparrow, J. R.; Fishkin, N.; Zhou, J.; Cai, B.; Jang, Y. P.; Krane, S.; Itagaki, Y.; Nakanishi, K. A2E, a byproduct of the visual cycle. *Vision Res.* **2003**, *43* (28), 2983−2990. (d) Delori, F. C. RPE lipofuscin in ageing and age-related macular degeneration. In *Retinal Pigment Epithelium and Macular Disease (Documenta Ophthalmologica)*; Coscas, G., Piccolino, F. C., Eds.; Kluwer Academic Publishers: Dordrecht, The Netherlands, 1995; Vol. *62*, pp 37−45.

(6) Sparrow, J. R.; Gregory-Roberts, E.; Yamamoto, K.; Blonska, A.; Ghosh, S. K.; Ueda, K.; Zhou, J. The bisretinoids of retinal pigment epithelium. *Prog. Retinal Eye Res.* **2012**, *31* (2), 121−135.

(7) Sparrow, J. R.; Cai, B. Blue light-induced apoptosis of A2E-containing RPE: involvement of caspase-3 and protection by Bcl-2. *Invest. Ophthalmol. Visual Sci.* **2001**, *42* (6), 1356−1362.

(8) Bergmann, M.; Schutt, F.; Holz, F. G.; Kopitz, J. Inhibition of the ATP-driven proton pump in RPE lysosomes by the major lipofuscin fluorophore A2-E may contribute to the pathogenesis of age-related macular degeneration. *FASEB J.* **2004**, *18* (3), 562−564.

(9) (a) Sparrow, J. R.; Parish, C. A.; Hashimoto, M.; Nakanishi, K. A2E, a lipofuscin fluorophore, in human retinal pigmented epithelial cells in culture. *Invest. Ophthalmol. Visual Sci.* **1999**, *40* (12), 2988−2895. (b) De, S.; Sakmar, T. P. Interaction of A2E with model membranes. Implications to the pathogenesis of age-related macular degeneration. *J. Gen. Physiol.* **2002**, *120* (2), 147−157.

(10) Vives-Bauza, C.; Anand, M.; Shirazi, A. K.; Magrane, J.; Gao, J.; Vollmer-Snarr, H. R.; Manfredi, G.; Finnemann, S. C. The age lipid A2E and mitochondrial dysfunction synergistically impair phagocytosis by retinal pigment epithelial cells. *J. Biol. Chem.* **2008**, *283* (36), 24770−24780.

(11) (a) Zhou, J.; Jang, Y. P.; Kim, S. R.; Sparrow, J. R. Complement activation by photooxidation products of A2E, a lipofuscin constituent of the retinal pigment epithelium. *Proc. Natl. Acad. Sci. U.S.A.* **2006**, *103* (44), 16182−16187. (b) Radu, R. A.; Hu, J.; Yuan, Q.; Welch, D. L.; Makshanoff, J.; Lloyd, M.; McMullen, S.; Travis, G. H.; Bok, D. Complement system dysregulation and inflammation in the retinal pigment epithelium of a mouse model for Stargardt macular degeneration. *J. Biol. Chem.* **2011**, *286* (21), 18593−18601.

(12) (a) Ben-Shabat, S.; Parish, C. A.; Vollmer, H. R.; Itagaki, Y.; Fishkin, N.; Nakanishi, K.; Sparrow, J. R. Biosynthetic studies of A2E, a major fluorophore of retinal pigment epithelial lipofuscin. *J. Biol. Chem.* **2002**, *277* (9), 7183−7190. (b) Rozanowska, M.; Jarvis-Evans, J.; Korytowski, W.; Boulton, M. E.; Burke, J. M.; Sarna, T. Blue light-induced reactivity of retinal age pigment. In vitro generation of oxygen-reactive species. *J. Biol. Chem.* **1995**, *270* (32), 18825−18830. (c) Sparrow, J. R.; Zhou, J.; Ben-Shabat, S.; Vollmer, H.; Itagaki, Y.; Nakanishi, K. Involvement of oxidative mechanisms in blue-light-induced damage to A2E-laden RPE. *Invest. Ophthalmol. Visual Sci.* **2002**, *43* (4), 1222−1227. (d) Dontsov, A. E.; Sakina, N. L.; Golubkov, A. M.; Ostrovsky, M. A. Light-induced release of A2E photooxidation toxic products from lipofuscin granules of human retinal pigment epithelium. *Dokl. Biochem. Biophys.* **2009**, *425*, 98−101.

(13) (a) Radu, R. A.; Han, Y.; Bui, T. V.; Nusinowitz, S.; Bok, D.; Lichter, J.; Widder, K.; Travis, G. H.; Mata, N. L. Reductions in serum vitamin A arrest accumulation of toxic retinal fluorophores: a potential therapy for treatment of lipofuscin-based retinal diseases. *Invest. Ophthalmol. Visual Sci.* **2005**, *46* (12), 4393−4401. (b) Radu, R. A.; Mata, N. L.; Nusinowitz, S.; Liu, X.; Sieving, P. A.; Travis, G. H. Treatment with isotretinoin inhibits lipofuscin accumulation in a mouse model of recessive Stargardt's macular degeneration. *Proc. Natl. Acad. Sci. U.S.A.* **2003**, *100* (8), 4742−4747. (c) Maeda, A.; Maeda, T.; Golczak, M.; Imanishi, Y.; Leahy, P.; Kubota, R.; Palczewski, K. Effects of potent inhibitors of the retinoid cycle on visual function and photoreceptor protection from light damage in mice. *Mol. Pharmacol.* **2006**, *70* (4), 1220−1229. (d) Palczewski, K. Retinoids for treatment of retinal diseases. *Trends Pharmacol. Sci.* **2010**, *31* (6), 284−295.

(14) Petrukhin, K. Pharmacological inhibition of lipofuscin accumulation in the retina as a therapeutic strategy for dry AMD treatment. *Drug Discovery Today: Ther. Strategies* **2013**, *10*, e11−e20.

(15) Wolf, G. Multiple functions of vitamin A. *Physiol. Rev.* **1984**, *64* (3), 873−937.

(16) (a) Kanai, M.; Raz, A.; Goodman, D. S. Retinol-binding protein: the transport protein for vitamin A in human plasma. *J. Clin. Invest.* **1968**, *47* (9), 2025−2044. (b) Naylor, H. M.; Newcomer, M. E. The structure of human retinol-binding protein (RBP) with its carrier protein transthyretin reveals an interaction with the carboxy terminus of RBP. *Biochemistry* **1999**, *38* (9), 2647−2653. (c) Noy, N.; Slosberg, E.; Scarlata, S. Interactions of retinol with binding proteins: studies with retinol-binding protein and with transthyretin. *Biochemistry* **1992**, *31* (45), 11118−11124. (d) Noy, N.; Xu, Z. J. Interactions of retinol with binding proteins: implications for the mechanism of uptake by cells. *Biochemistry* **1990**, *29* (16), 3878−3883. (e) Monaco, H. L. The transthyretin-retinol-binding protein complex. *Biochim. Biophys. Acta* **2000**, *1482* (1−2), 65−72. (f) Monaco, H. L. Three-dimensional structure of the transthyretin-retinol-binding protein complex. *Clin. Chem. Lab. Med.* **2002**, *40* (12), 1229−1236. (g) Monaco, H. L.; Rizzi, M.; Coda, A. Structure of a complex of two plasma proteins: transthyretin and retinol-binding protein. *Science* **1995**, *268* (5213), 1039−1041.

(17) Schlehuber, S.; Skerra, A. Lipocalins in drug discovery: from natural ligand-binding proteins to "anticalins". *Drug Discovery Today* **2005**, *10* (1), 23−33.

(18) Sporn, M. B.; Roberts, A. B.; Goodman, D. S. *The Retinoids*; Academic Press: New York, 1984; pp 41−88.

(19) (a) Blomhoff, R.; Green, M. H.; Green, J. B.; Berg, T.; Norum, K. R. Vitamin A metabolism: new perspectives on absorption, transport, and storage. *Physiol. Rev.* **1991**, *71* (4), 951−990. (b) Yang, Q.; Graham, T. E.; Mody, N.; Preitner, F.; Peroni, O. D.; Zabolotny, J. M.; Kotani, K.; Quadro, L.; Kahn, B. B. Serum retinol binding protein 4 contributes to insulin resistance in obesity and type 2 diabetes. *Nature* **2005**, *436* (7049), 356−362. (c) Kotnik, P.; Fischer-Posovszky, P.; Wabitsch, M. RBP4: a controversial adipokine. *Eur. J. Endocrinol.* **2011**, *165* (5), 703−711.

(20) Berni, R.; Formelli, F. In vitro interaction of fenretinide with plasma retinol-binding protein and its functional consequences. *FEBS Lett.* **1992**, *308* (1), 43−45.

(21) Adams, W. R.; Smith, J. E.; Green, M. H. Effects of *N*-(4-hydroxyphenyl)retinamide on vitamin A metabolism in rats. *Proc. Soc. Exp. Biol. Med.* **1995**, *208* (2), 178−185.

(22) Mata, N. L.; Lichter, J. B.; Vogel, R.; Han, Y.; Bui, T. V.; Singerman, L. J. Investigation of oral fenretinide for treatment of geographic atrophy in age-related macular degeneration. *Retina* **2013**, *33* (3), 498−507.

(23) (a) Graham, T. E.; Yang, Q.; Bluher, M.; Hammarstedt, A.; Ciaraldi, T. P.; Henry, R. R.; Wason, C. J.; Oberbach, A.; Jansson, P. A.; Smith, U.; Kahn, B. B. Retinol-binding protein 4 and insulin resistance in lean, obese, and diabetic subjects. *N. Engl. J. Med.* **2006**, *354* (24), 2552−2563. (b) Balagopal, P.; Graham, T. E.; Kahn, B. B.; Altomare, A.; Funanage, V.; George, D. Reduction of elevated serum retinol binding protein in obese children by lifestyle intervention: association with subclinical inflammation. *J. Clin. Endocrinol. Metab.* **2007**, *92* (5), 1971−1974. (c) Cho, Y. M.; Youn, B. S.; Lee, H.; Lee, N.; Min, S. S.; Kwak, S. H.; Lee, H. K.; Park, K. S. Plasma retinol-binding protein-4 concentrations are elevated in human subjects with impaired glucose tolerance and type 2 diabetes. *Diabetes Care* **2006**, *29* (11), 2457−2461. (d) Stefan, N.; Hennige, A. M.; Staiger, H.; Machann, J.; Schick, F.; Schleicher, E.; Fritsche, A.; Haring, H.-U. High circulating retinol-binding protein 4 is associated with elevated liver fat but not with total, subcutaneous, visceral, or intramyocellular fat in humans. *Diabetes Care* **2007**, *30* (5), 1173−1178. (e) Qi, Q.; Yu, Z.; Ye, X.; Zhao, F.; Huang, P.; Hu, F. B.; Franco, O. H.; Wang, J.; Li, H.; Liu, Y.; Lin, X. Elevated retinol-binding protein 4 levels are associated with metabolic syndrome in Chinese people. *J. Clin. Endocrinol. Metab.* **2007**, *92* (12), 4827−4834.

(24) Motani, A.; Wang, Z.; Conn, M.; Siegler, K.; Zhang, Y.; Liu, Q.; Johnstone, S.; Xu, H.; Thibault, S.; Wang, Y.; Fan, P.; Connors, R.; Le, H.; Xu, G.; Walker, N.; Shan, B.; Coward, P. Identification and characterization of a non-retinoid ligand for retinol-binding protein 4 which lowers serum retinol-binding protein 4 levels in vivo. *J. Biol. Chem.* **2009**, *284* (12), 7673−7680.

(25) Dobri, N.; Qin, Q.; Kong, J.; Yamamoto, K.; Liu, Z.; Moiseyev, G.; Ma, J.-X.; Allikmets, R.; Sparrow, J. R.; Petrukhin, K. A1120, a nonretinoid RBP4 antagonist, inhibits formation of cytotoxic bisretinoids in the animal model of enhanced retinal lipofuscinogenesis. *Invest. Ophthalmol. Visual Sci.* **2013**, *54* (1), 85−95.

(26) Bui, T. V.; Haddach, M.; Mata, N. L.; Phan, K. B. Methods and compounds for treating retinol-related diseases. PCT Int. Appl. WO2009042444 A2. 2009.

(27) Swanson, D. M.; Dubin, A. E.; Shah, C.; Nasser, N.; Chang, L.; Dax, S. L.; Jetter, M.; Breitenbucher, J. G.; Liu, C.; Mazur, C.; Lord, B.; Gonzales, L.; Hoey, K.; Rizzolio, M.; Bogenstaetter, M.; Codd, E. E.; Lee, D. H.; Zhang, S. P.; Chaplan, S. R.; Carruthers, N. I. Identification and biological evaluation of 4-(3-trifluoromethylpyridin-2-yl)-piperazine-1-carboxylic acid (5-trifluoromethylpyridin-2-yl)amide, a high affinity TRPV1 (VR1) vanilloid receptor antagonist. *J. Med. Chem.* **2005**, *48* (6), 1857−1872.

(28) Heck, S. D.; Liras, S.; Mchardy, S. F. 3-Azabicyclo (3.1.0) hexane derivatives as opioid receptor antagonists. PCT Int. Appl. WO2003035622 A1, 2003.

(29) Burkhard, J.; Carreira, E. M. 2,6-Diazaspiro[3.3]heptanes: synthesis and application in Pd-catalyzed aryl amination reactions. *Org. Lett.* **2008**, *10* (16), 3525−3526.

(30) Pettersson, M.; Campbell, B. M.; Dounay, A. B.; Gray, D. L.; Xie, L.; O'Donnell, C. J.; Stratman, N. C.; Zoski, K.; Drummond, E.; Bora, G.; Probert, A.; Whisman, T. Design, synthesis, and pharmacological evaluation of azetedine and pyrrolidine derivatives as dual norepinephrine reuptake inhibitors and 5-HT(1A) partial agonists. *Bioorg. Med. Chem. Lett.* **2011**, *21* (2), 865−868.

(31) Dart, M. J.; Searle, X. B.; Tietje, K. R.; Toupence, R. B. Azabicyclic compounds are central nervous system active agents. PCT Int. Appl. WO2004016604 A2, 2004.

(32) Lauffer, D.; Li, P.; Waal, N.; Mcginty, K.; Tang, Q.; Ronkin, S.; Farmer, L.; Shannon, D.; Jacobs, D. C-met protein kinase inhibitors. PCT Int. Appl. WO2009045992 A2, 2009.

(33) Guillemont, J. E. G.; Lançois, D. F. A.; Motte, M. M. S.; Koul, A.; Balemans, W. M. A.; Arnoult, E. P. A. Antibacterial cyclopenta[*c*]pyrrole substituted 3,4-dihydro-1*H*-[1,8]naphthyridinones. PCT Int. Appl. WO2013021054 A1, 2013.

(34) (a) Newcomer, M. E.; Jones, T. A.; Aqvist, J.; Sundelin, J.; Eriksson, U.; Rask, L.; Peterson, P. A. The three-dimensional structure of retinol-binding protein. *EMBO J.* **1984**, *3* (7), 1451−1454. (b) Cowan, S. W.; Newcomer, M. E.; Jones, T. A. Crystallographic refinement of human serum retinol binding protein at 2A resolution. *Proteins* **1990**, *8* (1), 44−61.

(35) Zanotti, G.; Folli, C.; Cendron, L.; Alfieri, B.; Nishida, S. K.; Gliubich, F.; Pasquato, N.; Negro, A.; Berni, R. Structural and mutational analyses of protein−protein interactions between transthyretin and retinol-binding protein. *FEBS J.* **2008**, *275* (23), 5841−5854.

(36) Zanotti, G.; Marcello, M.; Malpeli, G.; Folli, C.; Sartori, G.; Berni, R. Crystallographic studies on complexes between retinoids and plasma retinol-binding protein. *J. Biol. Chem.* **1994**, *269* (47), 29613−29620.

(37) Campos-Sandoval, J. A.; Redondo, C.; Kinsella, G. K.; Pal, A.; Jones, G.; Eyre, G. S.; Hirst, S. C.; Findlay, J. B. C. Fenretinide derivatives act as disrupters of interactions of serum retinol binding protein (sRBP) with transthyretin and the sRBP receptor. *J. Med. Chem.* **2011**, *54* (13), 4378−4387.

(38) Cogan, U.; Kopelman, M.; Mokady, S.; Shinitzky, M. Binding affinities of retinol and related compounds to retinol binding proteins. *Eur. J. Biochem.* **1976**, *65* (1), 71−78.

(39) Meyer, E. A.; Castellano, R. K.; Diederich, F. Interactions with aromatic rings in chemical and biological recognition. *Angew. Chem.* **2003**, *42* (11), 1210−1250.